University of Alberta

Hydrogen Behavior in Three Grades of Pipeline Steel

by

Naimesh M Vadhwana

A thesis submitted to the Faculty of Graduate Studies and Research in partial fulfillment of the

requirements for the degree of *Master of Science*

in

Materials Engineering

Department of *Chemical and Materials Engineering*

Edmonton, Alberta

Spring 2004

Your file Votre référence
ISBN: 0-612-96559-7
Our file Notre référence
ISBN: 0-612-96559-7

Abstract

This research studied the hydrogen behavior of three grades of pipeline steel, focusing on a new X100 grade. First the microstructure was investigated, and then various mechanical and environmental tests were performed to determine how the various grades would react when in contact with hydrogen. From the appearance of the microstructure, it was proposed that the X100 would be most susceptible to hydrogen embrittlement. In all cases, the X100 steel had higher hydrogen content, both diffusible and trapped, than the lower grades that were tested. In addition, the X100 had the lowest diffusivity for hydrogen, as would be expected. The hydrogen behavior of the X100 was primarily dependant on the microstructure. Its microstructure had more interfacial area than the other grades, and therefore more locations for hydrogen to migrate during the various testing regimes.

Acknowledgements

I am extremely grateful to Dr Weixing Chen for his supervision, guidance and encouragement throughout the course of my thesis work. I am impressed by his knowledge in various aspects of Materials Engineering research and methods, as well as his friendly attitude.

I wish to thank A Glover, D Dorling, R Sutherby of TransCanada Pipelines, T Jack, K Fraser of NOVA, K Keith and J Beattie of Foothills Pipelines for useful feedback and guidance in the early stages of the research. I would also like to acknowledge TransCanada Pipelines Ltd, NOVA Research and Technology Corp, Foothills Pipelines Ltd, as well as NSERC for funding this research.

I am also thankful to T Barker, B Scott, B Konzuk, W Boddez, and A C Bicknell from the University of Alberta for their technical support and advice throughout the progress of the work.

Naimesh M Vadhwana

4 November 2003

Table of Contents

List of Tables

List of Figures

1 Introduction

Buried pipelines for oil and gas transmission have long been made from steel, and there has been a constant movement to higher strength steels. However, with increased tensile properties, there is also an increased susceptibility to brittle failure due to lost ductility and hydrogen embrittlement. Ductility losses are often due to increased work-hardening from controlled rolling of the steel in order to achieve the desired strength.

Controlled rolling during pipe fabrication can also induce a highly directional banded structure in the steel. These two effects of work-hardening can act concurrently with other micro structural feature such as second phases and their interfaces with the matrix in pipeline steel to increase the embrittling effect of hydrogen.

Most of the environmental attack comes as stress corrosion cracking (SCC) both at high and near-neutral pH. Near-neutral pH has often been found to occur concurrently with hydrogen attack. The mechanism for hydrogen attack requires solution, usually groundwater, to come into contact with the pipe surface, as well as a mechanism for hydrogen to be liberated at the pipe surface. This takes place at coating disbonded areas where groundwater can now come into contact with the surface, and the impressed current (to prevent corrosion) is diminished due to high electrical resistance of ground water. Atomic hydrogen is produced as a result of dissolution of iron at coating disbonded area.

The action of hydrogen on reducing the toughness and the breaking strain of steels has been known for well over 100 years. Even early on, it was noticed that the effect of hydrogen was more noticeable for higher strength steels than for softer steels. Since the time of the earliest papers, much work has been done on trying to explain the phenomenon of hydrogen and its interactions with steel that reduce the breaking strain of steel.

While there is a synergistic effect between corrosion and hydrogen assisted cracking (HAC), the present research involves isolating the hydrogen behavior of various pipeline steels, and to relate the behavior to the various mechanical properties. In addition, the effects of previous mechanical history of the steels are examined with respect to the hydrogen uptake behavior. First, the steels were tested in the as received from the suppliers, then they were tested after undergoing various mechanical testing. The final testing on mechanical specimens was carried out after they were saturated with hydrogen, without removing the hydrogen source. The last testing was performed, again on the "as received" materials in order to observe permeation behavior. The goal of this research was to determine the mechanical behavior of the X100 steel in the presence of hydrogen, and compare it to lower grades which are currently in use.

This thesis is presented with a Literature Review first, followed by Materials and Experimental Details, followed by Results and Discussion. The final sections provide a Summary and Suggestions for further work.

2 Literature review

The role of hydrogen on the mechanical properties of steel has been the subject of much study in past years, yet there remains no single unifying theory which can explain all situations and reaction of the metals of interest. On the industrial scale, especially in pipelines, interactions of hydrogen with the metal has been found to be responsible for billions of dollars in damage over the years, yet there remains no method to predict and thereby prevent failures due to hydrogen. It has been found that hydrogen serves to reduce the ductility and thus embrittle steel. The role of hydrogen on the through thickness properties of steel is governed by the interaction with the microstructural features that may be present in the steel. The features may serve to allow for easy diffusion or may trap hydrogen. In this way the mechanical properties, such as ductility and strength can be changed due to the presence of hydrogen. As the mechanical and microstructural features are affected by hydrogen, so too is the fracture behavior. The following sections will summarize some of the work that has been carried out to date on the interaction of hydrogen with the mechanical properties of steel. The final section of this chapter will discuss some of the methods used for testing various interactions of hydrogen with steel.

2.1 Some historical perspective

As early as the 1860's it was recognized that hydrogen interacted with other metals to reduce their mechanical properties. This was recognized even before much of the current understanding on the fundamental reasons for metals to gain strength. In the 1940's

Zappfe and Sims were putting forward that steels had a "block" structure. Years later, with advances in electron microscopy, this "block" structure was the foundation for the current understanding of the grains structure of steels. At that time they had found that there were many hundreds of papers on the subject of hydrogen in iron and steels that were published since the 1860's.[1]

One such paper from 1868 stated that the best way to charge metals with hydrogen is to make the metal an electrode in acidulated water.[2] During this time, in the late 1800's it was recognized that iron wire, when put in acidic solutions which liberate hydrogen, become brittle and lose their toughness. It was also recognized that heating the sample after exposure to hydrogen effectively removed enough of the hydrogen that was in the iron such that the wire would regain its original toughness. The change in the mechanical properties was measured by monitoring the fracture strain of the samples. Much of the subsequent work that was done on the interaction of hydrogen with iron and steel used these findings as fundamental parts of their experiments. Currently, many studies use this early method of electrolytic charging in acid solutions as the hydrogen source. As well, the property of steel that is found to be most affected by hydrogen is the ductility, often measured as a change in elongation to failure.

2.2 Mechanical properties

As mentioned, hydrogen generally tends to decrease the mechanical properties of steel. The most noticeable change is in the ductility of the steel, whereas the changes in the yield strength (YS) and the ultimate tensile strength (UTS) are comparatively minor.

2.2.1 Ductility

As early as the 1800's it was recognized that the most reduced mechanical property of steel in the presence of hydrogen is the ductility. The loss in ductility was found to occur regardless of the source of hydrogen, whether internal, from cathodic charging, or external hydrogen due to gas pressure. The two most popular methods for measuring the loss in ductility due to hydrogen charging are the elongation to failure, ε_f, and the percent reduction in area, RA%. It was recognized that these are the first properties to show any decrease with increasing hydrogen in unalloyed steel.[3] In an X50 steel cathodically charged at 100 mA/cm^2 for 30 minutes, it was found that the RA% dropped from 60% in the uncharged specimen to 25% in the charged.[4] In another study, it was shown that RA% moved from 50% without hydrogen, but was up to 80% lower after hydrogen charging.[5] In a pearlitic steel, it was found that the ductility suffered a loss of 82%.[6] Sensitivity to testing strain rate was observed when a reducing potential was used in conjunction with a slow strain rate, it was seen that the RA% went from 75% to 15% as the charging potential was more negative (more hydrogen generated).[7]

Sensitivity to strain rate was earlier seen when it was put forward that the hydrogen embrittlement was a diffusion controlled process. It was observed that there are two competing processes: straining the metal versus the embritting process. If the strain rate predominates, the metal was found ductile, whereas if the embrittling process predominates, the metal was found to be brittle.[8] However, if the RA% criterion is used as the ductility measurement, the results would differ from a study where the ε_f criterion is used.[9] It was established that small concentrations of hydrogen (~1 ppm by weight) in

cathodically charged steel have no significant influence on the fracture toughness, as measured by conventional strain rate (crosshead speed 1mm/min). However, low strain rate testing (crosshead speed 0.1 mm/min) of hydrogen charged high strength steel decreases the fracture ductility.[10]

As will be discussed below, the appearance of the fracture surface is not always characteristically brittle, rather, microscopically there are still many dimples on the fracture surface. Also to be discussed is the effect of microstructure and chemical composition on the embrittling effect of hydrogen.

2.2.2 Yield strength

Zappfe and Sims noted that hydrogen, much like cold work, could remove the yield point phenomenon in steel, however, on recrystallization, or on removal of the hydrogen, the phenomenon would return.[1] It was later confirmed by Bastien and Azou, who showed that there was not a drop in yield strength, but that there was a difference of the order of 4 ksi in the presence of hydrogen.[11] However, de Kazinczy found that the lowering of the yield point only happened in some exceptional cases.[3] One such an exceptional case was fracture at 75% of the yield stress.[12]

Christenson et al. showed that the strengths did not vary much with internal or external hydrogen. In these tests, no matter the charging condition, the strength change was scarcely noticeable.[5]

For Hanninen's hydrogen charged AISI 316 steel specimen the fracture stress was 79 MPa with no elongation, as mentioned above, but a similar uncharged reference specimen the yield strength was 300 MPa. The lower fracture stress in this case is more likely due to decohesion or due to formation of voids due to internal hydrogen pressure, as will be discussed, rather than by embrittling.[13]

Ule et al found that hydrogen does not significantly affect the yield strength. The three classes of yield stress in these tests were 1220, 1020, 900 MPa. The low strain rate tension of uncharged steel does not produce any noticeable changes, and the hydrogen charging of the steel had almost no effect on the yield strength. It was seen that hydrogen only changes the shape of the load-displacement curve after the onset of plasticity.[10]

Again, with these different steels, there was uniformly little effect of hydrogen on the yield strength of the steels. The various effects that were sometimes shown on the yield could be explained by hydrogen dissolved in the ferrite matrix aiding in the deformation of the matrix.[14]

2.2.3 Ultimate tensile strength

Some of the early work on hydrogen embrittlement of steels found that the ultimate tensile strength (UTS) of a whole test bar would be somewhat reduced. This is because hydrogen can be discharged into cavities, forming hydrogen gas and thus causing regions of high triaxial stress.[3]

From mechanical tests done by Lukito et al. it was apparent that the hydrogen did not produce any significant effect on the maximum strength (i.e. UTS) of 1022 quench and tempered, 1022 carbonitrided, 4037 quench and tempered or BHS-1 steels.[15] Other work on a pearlitic steel found that there was no effect of hydrogen on the UTS.[6]

It should be noted that experiments carried out by Sasmal et al. showed an apparently anomalous behavior of cathodically charged steel under tension. They found that the mechanical properties of a high-strength low-alloy steel could either be worsen or improve for the same hydrogen content, dependant on charging conditions, at short charging times. Specimens having different amounts of hydrogen can have the same YS depending on the electrolyte used to charge the sample for short times. But for longer times (16-24 hours) the change in yield strength is dependant on the hydrogen content irrespective of the electrolyte. The anomalous behavior at short times is due to a hydrogen gradient in the sample, as determined by a hardness gradient. The gradient was due to a higher rate of absorption in the subsurface layers compared to the diffusion into the interior and preferential trapping of H at the carbide-matrix interface, ferrite GB's and lattice defects.[16]

From these few results, it is clear that there needs to be a large charging time before any conclusions on the effect of hydrogen on the mechanical properties. The apparently anomalous behavior of hydrogen with respect to the UTS might be due to the very different charging conditions that the various investigators used. As well, on careful examination of testing methods, it was evident that this would play a major role in all the

results. For example, in tensile testing, some researchers would remove the sample from the hydrogen source before mechanical testing, while others would keep the sample in a hydrogen atmosphere, whether gaseous or electrolytic, while performing mechanical tests. As will be evident from the diffusion behavior of hydrogen in steel, this time required to remove the sample from the charging condition and set up the tensile test would have a profound impact on the amount of hydrogen still in the sample. This time effect would be most noticeable on the UTS as this strength is the last one to be found during mechanical testing.

2.3 Diffusion and trapping

Callister defines diffusion as mass transport by atomic motion.[17] The crystal structure of steel is body-centered cubic (BCC) so it has a low atomic packing factor with many interstitial sites. Hydrogen atoms, having a much smaller diameter than iron atoms can move quickly through the interstitial spaces, however, if there is an impediment in the path, there will be a competition between the driving force for diffusion, and the stopping force of the impediment. If the stopping force is greater than the driving force, diffusion will be stopped and hydrogen will remain in the steel. If two hydrogen atoms come into contact at an impediment, they can recombine to form hydrogen gas, which, with a much larger radius than atomic hydrogen, cannot escape the steel sample, and is thus trapped.

However, before considering bulk diffusion in steel, hydrogen atoms must first get through the surface layers of steel, which have their own interactions with hydrogen entering steel. Once it is past the surface layers, there are interactions at various places in

the bulk of the material which are to be considered in the diffusion and trapping processes. At a crack on the surface, there are other variables to hydrogen transport which much again be considered. Therefore, it is important to consider both macrostructure and microstructure when dealing with hydrogen diffusion and trapping in steel.

2.3.1 Macrostructure

2.3.1.1 Surface

To understand the surface effects of hydrogen entry into steel, it is best to consider the mechanism by with hydrogen enters into a metal from the environment. In the case of gaseous hydrogen, to enter into the bulk of the metals, the adsorbed gas at the surface must first dissociate.[18],[19] Once it is dissociated into H atoms, it can then be absorbed into the sample. In the case of electrolytic charging, there is a layer of H^+ ions at the surface which can easily combine with the cathodically provided electrons then be readily absorbed into the metal; this is especially true when poisons are used in the charging solution. The hydrogen can then diffuse into the bulk of the steel, where the embrittlement reaction can take place. This process is shown schematically in Figure 2-1 at a crack tip.

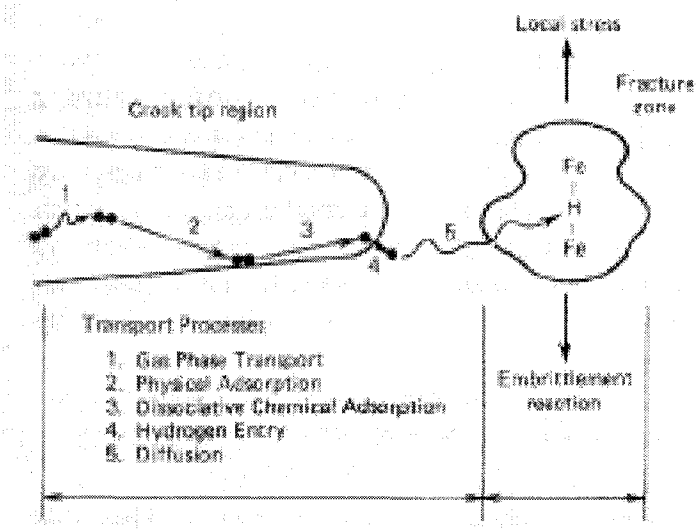

Figure 2-1 Various processes involved in the hydrogen embrittlement of ferrous alloys [Hertzberg, 1995]

Many researchers have found that the specific surface conditions of a steel sample can influence the hydrogen uptake, and therefore the hydrogen embrittlement behavior.[20],[21],[22] When copper is present in the steel, as is often the case in pipelines from electric arc furnace mini-mill operations, a copper rich film is formed at the surface. Even as little as 1% copper in an X70 pipeline steel was found to form the beneficial copper film on the surface, thus making the steel hydrogen induced cracking (HIC) resistant.[23] If there is sulfur in the surrounding environment, CuS can form which acts as a seed for FeS formation; however, the FeS film is only protective in some pH ranges.[24] These kinds of surface films impede hydrogen entry into the steel, and thus reduce hydrogen embrittlement. In cases where stress corrosion cracking (SCC) is present, cracking or disruption of the surface film allows bare steel to be exposed to the hydrogen from the environment.[25] In his recent work, He found that on cathodically charging pipeline steel in a near-neutral pH groundwater solution, a carbonate film would form and lower the

hydrogen uptake of the steel.[21] Thus it can be seen that there is a beneficial effect in terms of resistance to hydrogen attack, if there is a coherent surface film on the steel.

The surface roughness also has a large effect on the hydrogen uptake of steel. One such investigation created three different surfaces by mechanically grinding, sandblasting and shot-peening before electrolytically charging with hydrogen. Before starting the investigations it was expected shot-peening to be the most effective way to reduce hydrogen-embrittlement during electrolytical plating; however, it was surprising to find sand-blasting as the most favorable surface-treatment of high-strength low-alloy steel. This was the most favorable because the increased surface area, due to a needle effect* promoted hydrogen recombination before the atomic hydrogen could diffuse into the bulk of the material.[26] Therefore, it could be assumed that a smooth surface would promote hydrogen entry before the recombination reaction could occur.

Another surface phenomenon is the residual stress at the surface. These stresses can arise during the fabrication, especially in the case of control-rolled steels. Whether they are tensile or compressive, they can accelerate or delay failure, particularly in when hydrogen is present.[27] If the surface residual stress is compressive, it will delay hydrogen permeation, and therefore the failure due to hydrogen will be delayed.[28]

* Bombarding the steel with sand creates a rough surface on the sample. The bombardment causes small peaks in the steel which, on the microscopic level would seem like needles protruding from the surface of the sample.

The above discussion deals with hydrogen entry into steel. Blisters are a surface phenomenon which occurs when too much hydrogen has already entered the steel, and will be discussed later.

2.3.1.2 Bulk

Diffusion in the bulk of the material can be either in the gas phase if it occurs along adjoining voids and rifts already in the steel. Most hydrogen, however, diffuses in the atomic state through the lattice of steel.[1] As always, hydrogen diffusion is controlled by a potential energy gradient, and anything in the bulk of the steel will have an impact on the potential energy gradient.[3,29,30,31] Hence, diffusion through the bulk is then impacted by any discontinuity in the lattice, such as interstitial elements, inclusions, precipitates, voids, stress fields, etc.[10,15,32] The effects of inclusions and precipitates are related to the chemistry of the steel, therefore discussion of these effects will be left for later. Thus, the apparent diffusivity when measured by permeation testing, to be described later, is in fact much lower than the actual lattice diffusion due to buildup and trapping of hydrogen at the various sites listed above.[33] Lukito et al., found that this was overcome, and it was possible to measure the actual lattice diffusivity of hydrogen in steel by the steady-state hydrogen flux, since all the trap sites would be filled from earlier transients.[15]

The effect of stress on hydrogen diffusion is minimal, nevertheless, with an increased tensile stress, the hydrogen content will increase.[12,34] Work by Li et al. showed that the gradient in chemical potential of hydrogen within the metal lattice is caused by a stress gradient which produces a driving force for the diffusion of interstitially dissolved

hydrogen, so that hydrogen concentrates at regions of predominantly tensile stresses, whereas compressively strained regions become deficient in hydrogen. This work also showed that there is a strong interaction between hydrogen and the stress field at different discontinuities in the lattice.[35] Oriani's theory on hydrogen embrittlement showed how hydrogen decreased the strength of the lattice. This becomes more clear when it is realized that hydrogen as an interstitial acts to dilate the lattice thus decreasing the atomic cohesion.[33],[36],[37] There is a finite amount of energy that is required to break the lattice, and since hydrogen dilates the lattice, it would follow that with hydrogen in the lattice, decohesion, especially where the lattice may not be completely coherent, as is the case with grain boundaries, would follow. This was demonstrated by de Schiapparelli.[38]

Lukito and Szklarska-Smialowska showed that it was energetically less favorable for hydrogen to be at interstitial sites, and that it would be more favorable for hydrogen to be trapped.[15] As was mentioned earlier, these trap sites can be any imperfection or discontinuity in the lattice. Trapped hydrogen can lead to decohesion between phases, such as inclusions or precipitates, or between grains, and if enough hydrogen is in a trap site near the surface, blisters can form on the surface. The various sites where hydrogen gets trapped can start acting as cracks. At the tip of these cracks, or at already existing cracks, the behavior of hydrogen can be slightly different.

2.3.1.3 Crack tip

In one theory, hydrogen embrittlement is caused by lowering shear and cleavage strength. It is assuming that molecular hydrogen of high pressure is included in the crack which

initiates fracturing. As the crack spreads, hydrogen gas leaves the lattice and goes to the more energetically favorable crack, expanding and releasing energy, thus lowering the fracture stress. Thus hydrogen diffusion to the region near the crack tip is needed for crack expansion.[3] If the material contains hydrogen, a crack, initially present or opened under stress by deformation, will under equilibrium conditions be filled with hydrogen gas, the pressure of which is determined by the hydrogen content dissolved in the lattice.

From fracture mechanics it is known that the highest stress state is just ahead of the crack tip, and for sharper cracks the peak stress moves closer to the crack front. The hydrogen induced cracking (HIC) that is due to hydrogen concentration and stress state will occur at this point, and the crack will grow backwards into the main crack. This was illustrated by Troiano as shown in Figure 2-2 where the crack is initiating ahead of the notch in the region of the highest triaxial stress.[30] Once the crack ahead of the notch tip joins the notch, further crack growth must await diffusion of hydrogen to the new region of high stress. In this way crack growth occurs in a stepwise manner as is evidenced in Figure 2-3 by plotting the resistance to growth as a function of time for uniformly charged specimens.

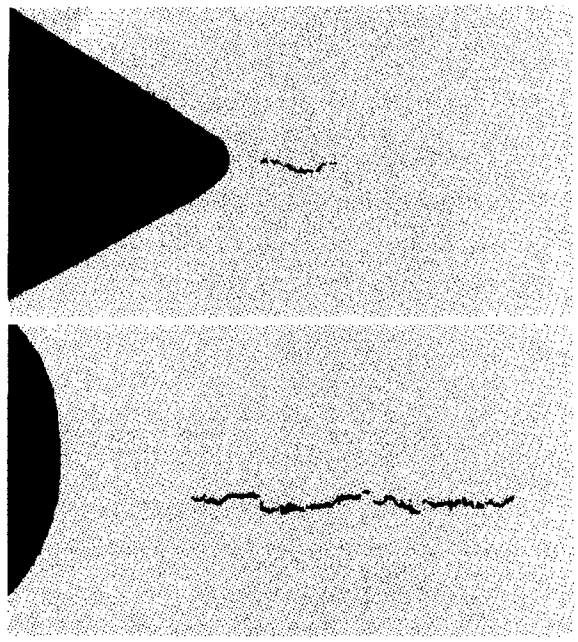

Figure 2-2 Cracks observed in a hydrogenated notched specimens sectioned after static loading. Top specimen has 0.001 inch notch radius and bottom specimen has 0.010 inch notch radius [Troiano, 1960]

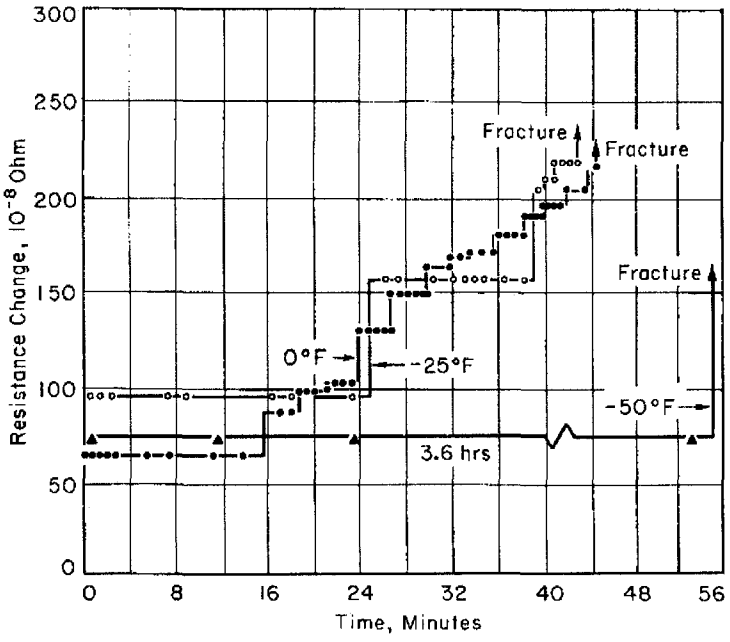

Figure 2-3 Resistance increase as a function of time for uniformly hydrongenated specimens tested in the stress range of delayed fracture. [Troiano, 1960]

It was found by Oriani that if the local hydrogen concentration is not sufficient to propagate a crack, it must wait for there to be a localized increase of hydrogen in front of the crack. The increase of hydrogen ahead of the crack tip can occur rapidly as the solution in the crack tip can be acidified,[39] as is the case during SCC,[40] or by diffusion or movement with dislocations[19],[41]. This merely means that the crack progresses at a rate controlled by hydrogen diffusion to a region near the crack tip, and here, the atomic bonds at the edge of the crack are stretched and broken.[31] Oriani's atomic bond model of a crack edge is shown in Figure 2-4.

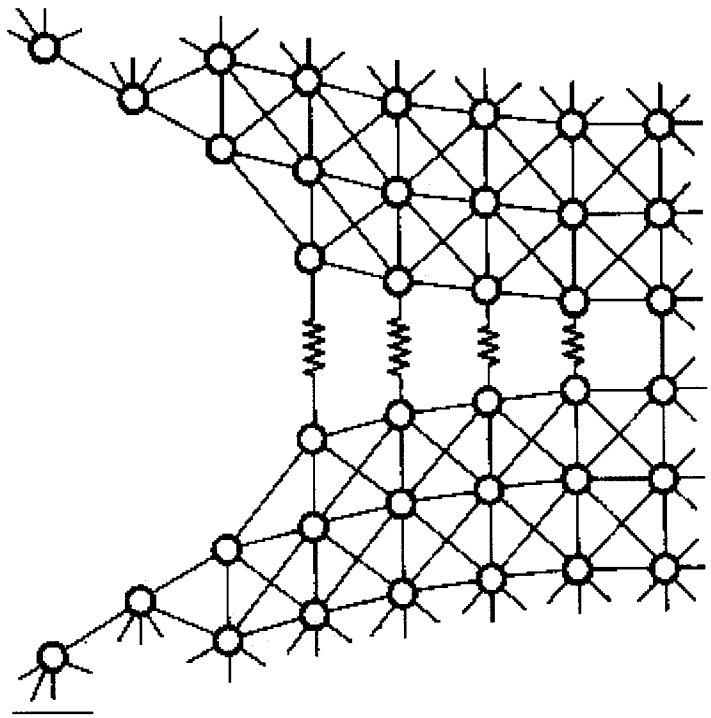

Figure 2-4 Atomic model of the crack edge. The straight lines represent bonds stretched in the linear stress-strain region. The zigzag lines represent bonds stretched in the non-linear region. [Oriani, 1972]

Liao et al.'s results with samples of bridge steel were in agreement with Oriani's view that hydrogen promotes local plastic deformation ahead of the crack tip and change the mode of crack propagation so that the crack propagated in a zigzag path. Hydrogen was found to bring about a strong tendency for localized plastic deformation. It was indicated that hydrogen decreased the stress required for plastic deformation.[42] The decreased stress required for plastic deformation was further explained by Wang et al. as a reaction to the hydrogen pinning dislocations and therefore reducing the plastic zone ahead of the crack tip.[19] As the zone size is smaller, the energy required to break through it would be less.

Tetelman and Robertson's experiments on Fe-Si single crystals also showed this phenomenon where there is some upper limit of pressure defined by the existing length of the crack, the yield strength of the crystal, and its strain-hardening capacity, the stress component normal to the plane of the crack reaches a sufficiently large value to cause the crack to move forward into the relatively undeformed volume of crystal ahead of the crack front.[29] Thus, when hydrogen is continuously supplied, both the lattice strain due to increased hydrogen concentration and the applied stress are additive and combine to propagate cracks, and crack growth is accelerated.

More recent work was carried out on hydrogen-assisted stable crack growth (H-SCG) in iron-3 wt% silicon steel concentrating on events at the crack tip. It was found that the kinetics of the crack growth are controlled by hydrogen diffusion through the area surrounding the crack tip. If trap sites such as dislocations are created ahead of the crack

tip, then the hydrogen diffusion ahead of the crack tip will be slowed.[43] Once the amount of trapped hydrogen reaches a critical value where the stress exerted by hydrogen atoms is higher than the cohesive strength of the atomic bonds, then a crack will form ahead of the crack tip. Addition of an external tensile stress at the crack tip will make this happen at a lower hydrogen gas pressure as was shown by varying stress intensities in Figure 2-2 by Troiano et al. If the external stress is compressive, there will be less driving force for hydrogen to accumulate,[44] as the atomic bonds at the crack tip would not be stretched as shown in Figure 2-4.

Much of the diffusion and trapping that was mentioned in this section is affected by microstructural features such as grain boundaries, precipitates, dislocations etc. It is therefore necessary to examine some of the interactions of these various features with hydrogen in more detail.

2.3.2 Microstructure

As was alluded to in the above, the damage that can occur to steel due to hydrogen will be influenced to a large degree by the microstructural features. Trapping sites are such microstructural defects as dislocations, internal cracks and voids, grain boundaries, impurity atoms, inclusions, and interfaces between the matrix and particles.[15,45,46,47,48] As the hydrogen is trapped at these various metallurgical defects, which can be mobile (dislocations) or stationary, there is a lag in the hydrogen flux through the metal.[49] With many traps, diffusion of hydrogen through the bulk can be slowed, until the trap sites are all filled. However, filling the trap sites can lead to catastrophic failure.

2.3.2.1 Dislocations

The application of external force moves dislocations that are present in steel. In cyclic loading, as is the case of fatigue that pipelines undergo due to pressure variations, each strain increment increases the internal stress thus decreasing the force on mobile dislocations.[25] With repeated cyclic loading, dislocations will pileup and form a cellular structure,[50,51] and modify the diffusion characteristics of hydrogen. As dislocations are generated, hydrogen can be transported by dislocation sweep-in or by piping; piping is more common when the dislocations form a cellular structure. [52] Thus, dislocation transport of hydrogen can be faster than pure lattice difusion,[4] but only when the dislocations are already filled with hydrogen.

During plastic deformation, dislocations can act as local hydrogen sinks, depending on the electrochemical properties of the atoms in the region,[3] thus attracting more hydrogen to the local area. Hydrogen being attracted to dislocations, and dislocations moving with external force, it can be seen that hydrogen can be transported through the material with the movement of dislocations.[3,9,11,20,29] As hydrogen is being transported with dislocation movement, it moves away from the hydrogen generating area, and can thus increase the uptake in a test where it is being supplied while dislocations are moving.[20] Beacham furthered this idea when he found that hydrogen interacting with the dislocations does not hinder the motion, rather it acts to unlock dislocations, and allows them to multiply at a lower applied stress,[14] thus leading to greater reduction in ductility.

If there is a crack present in the sample, dislocations can be generated at the crack tip. The presence of hydrogen near the crack tip will encourage the nucleation of dislocations from the tip.[53] At a crack tip, an increasing external load will emit dislocations, which react with hydrogen and are transported away. Hydrogen at the crack tip was also found to promote the generation of dislocations.[42] However, Matsui et al. found that there is a distinction between edge and screw dislocations; hydrogen tends to increase the mobility of screw dislocations leading to softening, but hinders mobility of edge dislocations leading to hardening.[54],[55] Therefore, it was likely edge dislocations that were encountered when various researchers found that hydrogen pinned dislocations.[10],[19]

In materials which are susceptible to planar slip at low temperature, such as pipeline steels, however, dislocation will pile up at obstacles that may be present. When they are moving with hydrogen, hydrogen will also pile up, and can precipitate out at these obstacles in the form of hydrogen gas. These obstacles can be microvoids, where released hydrogen will stabilize the microcrack,[20] or might just be regions of high dislocation density.[56]

Hydrogen is in this way trapped by dislocations, and will move with them through steels with the application of external force. When permeation testing is carried out, until any dislocations present in the sample are filled with hydrogen, the apparent diffusivity will be lower than the actual lattice diffusivity.[33] Nevertheless, dislocations are low energy trapping sites ($\leq$60kJ/mol) for hydrogen as the binding energy is less than 30 kJ/mol in

steel, and as such hydrogen is reversibly trapped here; in other words, at room temperature hydrogen trapped at dislocations will escape from the sample.[33],[45],[57],[58]

2.3.2.2 Inclusions

The incoherent interface between the matrix and inclusions in steel provide another trapping site for hydrogen.[29],[49] Inclusions present in steel can act to strengthen it by changing fracture paths of crack and hindering dislocation motion as steel is strained in service. Depending on the shape and type of the inclusion, the effect of hydrogen behavior can be quite different. The results of trapping can range from blistering near the surface, to fast fracture depending on the number, type and location of the inclusions.

In diffusion studies, it was found that inclusions near the surface acted as traps, lowering the diffusible hydrogen flux.[59],[60],[61] Once traps were filled, the diffusible hydrogen flux returns to normal. If the inclusions were near the surface of the steel, blisters would form on the surface of the steel as will be discussed later.[62]

However, depending on the shape of the inclusions the effect of hydrogen introduced may be different. Addition of calcium to pipeline steels leads to the formation of round CaS inclusions instead of MnS inclusions which deform into long stringers during controlled rolling. Sharp edges can form at the ends of the stringer during forming operations which can act as a stress raiser in service. If hydrogen is introduced and recombines at the interface between the inclusion and the matrix, the stress at the end will increase even more. Thus, the formation of round CaS inclusions were found to create a

more HIC resistant steel.[48],[63] In pipeline steels Nakagawa et al. found that there exists an optimum concentration of calcium for shape control, but this will be discussed later.[39] Whereas round inclusions created a more HIC resistant steel, angular inclusions lead to more hydrogen damage.[27]

Hard inclusions, such as alumina, do not deform during the controlled hot rolling that pipeline steels undergo. In general, blisters and voids from hydrogen damage initiate at hard inclusions such as alumina, or complex inclusions with alumina, mullite, magnesium oxide, and manganese sulfides.[32],[38],[64] HIC was also observed in steel that had inclusions which had the structure of Mn-O-Si-Al, as well as at inclusions with a structure of Mn-O-Si.[4],[65] Soft MnS inclusions were found to be a site for blister initiation,[63] but usually, it was found that hard inclusions such as alumina were preferred to MnS for blister initiation.[32],[38],[64] However, in the case when MnS segregates, there is a tendency for HIC.[65]

With respect to inclusions, the HIC mechanism is recombination of molecular hydrogen at the interface between the matrix and the inclusion.[4],[10],[66] When the steel is degassed, there is some permanent damage such as near-surface cracks.[67] Early work by Rice et al, found that the fracture path most sensitized by hydrogen are along the interfaces between phases.[68] This is because the interfaces provide irreversible trapping sites for hydrogen; the hydrogen is trapped as a gas instead of in the atomic form.[4],[57],[65] Hydrogen is more strongly trapped at interfaces between inclusions as the steel must be heated to at least 300°C in order to remove it,[69] whereas in the case of dislocations, room temperature was

sufficient. Thus, in cyclic loading, the synergy between hydrogen gas at the interfaces between the matrix and the inclusion is critical in superlong fatigue.[69]

Advances in secondary ion mass spectrometry (SIMS) were needed to directly verify the presence of hydrogen at the interfaces, though it was already suspected for a long time.[70,71]

Voids can also initiate at the ends of inclusions during rolling processes, especially hard inclusions, and hydrogen entering the steel during service would promote their growth.[63] Second phase particles are also initiation sites for mivroviods.[4,72] Hence, chemistry that promotes inclusions thus increases the amount of hydrogen damage that can occur in a steel sample. The specific effects of chemistry will be discussed later.

2.3.2.3 Microvoids

Microvoids in the steel provide strong, irreversible trapping sites for hydrogen in steel with binding energy in the order of 84 kJ/mol.[33] The reason that the trapping is much stronger than in dislocations is that hydrogen is trapped as molecular hydrogen, not atomic, and it would therefore have to dissociate in order to once again become mobile in the steel lattice. In fact, at microvoids, it has been observed by many researchers that hydrogen precipitates out.[3,8,20,56] Pathiraj et al. found that the gas pressure in these voids can reach several thousands of atmospheres, severely straining the material.[73] Of course, this only happens once the stresses introduced from the gas buildup in the void exceeds

the flow stress of the steel.[74] If the voids are near the surface, the strained steel was found to form blisters on the surface of the steel.[20,38]

Strong trapping at voids also lowers measured rates of diffusion as hydrogen, instead of diffusing, recombines inside the voids.[15,48,51,57,59] This is similar to the lowering of measured diffusion that happens when there are many dislocations present in the steel, as in the case of cold-worked steel. Cold-work can also increase the number of voids that are present in steel.[48] The voids that are introduced by cold-work are often associated with inclusions, as was discussed previously. These voids are generated due to low coherence between inclusions and the surrounding matrix.[38] Often, these are sulfide, or oxysulfide particles,[75] as was the case with the HSLA 100 steel that was tested by Densley et al.[76]

Tsuboi et al., following the decohesion model put forward by Zappfe, suggested that hydrogen created voids in their high-strength steel; this was because subsurface voids were not observed in their steel before charging, but were there after charging with hydrogen.[77] This is contrary to most other researcher who found that hydrogen was not responsibly for nucleation of voids, but rather, the pressure from the hydrogen gas buildup simply acted to assist expansion of existing microvoids.[10,78] The latter finding would correspond to microvoids or even nanovoids being present at the interface of second phase particles with the matrix as this was often found to be the nucleation site for voids,[38,72] though it is not always necessary to have second phase particles for voids to

form.[79] As hydrogen often fills voids, the fracture mode in the presence of hydrogen was often found to be microvoids coalescence (MVC), as will be discussed below.

2.3.2.4 Grain boundaries

As mentioned earlier, Zappfe and Sims, while unclear of the grain structure in steel that is now well known, were aware that this structure would easily be pulled apart in the presence of hydrogen.[1] Later, this was shown to be due to hydrogen trapping at ferrite grain boundaries.[15,16,37,47,51,59] As with other sites in diffusion testing, trapping at grain boundaries was found to lower the apparent diffusion of hydrogen through steel.[36,57,59,61] However, Beck et al. had found the steady-state diffusion was of the same order in a single crystal as in a polycrystalline metal, which further proves that there is only trapping along grain boundaries and that it does not contribute to the diffusible portion of hydrogen.[12] More recent studies by Maier et al. confirmed the negligible effect of grain boundaries on steady-state hydrogen diffusion in steel.[52]

While hydrogen is trapped at the grain boundary, the binding energy was found to be lower than at matrix/inclusion interfaces.[69] The trapping was found to be either low energy ($\leq$ 30 kJ/mol), or in the case of high angle grain boundaries, to be medium energy, in the range 53 – 59 kJ/mol, in steels.[58] Since they are low energy hydrogen trapping sites, grain boundaries have been described as being reversible traps.[57]

Uhlig had found that grain boundaries can act locally as a cathodic site, promoting hydrogen generation, or as an anodic site, promoting corrosion, depending on what types

of atoms segregated to these regions.[80] Later, the corrosion aspect was confirmed in pipeline steels exposed to a near-neutral pH solution.[40] Additional hydrogen formation as the result of becoming locally cathodic would conceivably increase hydrogen recombination at grain boundaries. This would result in loss of cohesion along the grain boundary,[10] or if cracks were growing along such grain boundaries, would create sufficient pressure to get dormant cracks restarted.[29] Pound found that there is an increased susceptibility with an increase in grain boundary segregation of elements.[58]

With respect to grain size, Christenson et al. found that in pipeline steels, there seems to be no effect on the hydrogen behavior.[5] There also seems to be no effect on the grain boundaries with cyclic loading as was found by Maier et al.[52]

2.3.2.5 Blisters

As was mentioned in the above discussion, blisters are a surface phenomenon which occurs with a gas pressure buildup near the surface. When the pressure of the gas at some discontinuity or at an interface exceeds the yield strength of the sample, a blister will form, or grow.[32] Thus, for similar microstructural features, such as inclusion etc., the steel with the higher yield strength will be more resistant to blistering. Also, for the same strength level in the steel, the steel with fewer interfaces will be more resistant.[60] Figure 2-5 shows how a blister can form near the surface of steel.

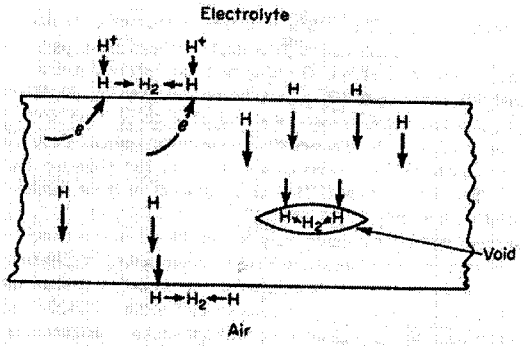

Figure 2-5 Schematic diagram of hydrogen migration and blister formation. [Jones Fig 10.3]

Blisters are most readily observed in the thin specimens used in hydrogen permeation testing. Steels with low diffusivity for hydrogen, or more importantly, low exit flux have been found to be more prone to blistering. The exit flux would be lowered due to excessive hydrogen recombination at blisters, allowing them to grow, and since there is less steel for hydrogen to migrate through, the hydrogen flux will naturally decline. These results were found when comparing a pipeline steel to a structural steel. It was also noted that after blistering there was a decline in the peak hydrogen flux.[12,62]

As was mentioned in the above sections, blisters are due to the recombination of atomic hydrogen to molecular hydrogen.[12] However, as was noted by Louthan et al., blisters can form as a result of any gas, such as methane, where carbon would be pulled out of solid solution in the steel and combine with hydrogen that is permeating through.[20] Most research on hydrogen damage agrees that this is rarely the case, but that the hydrogen recombination reaction is the predominant one, especially when the hydrogen charging time is high.[8,12,32]

In single crystal Fe-Si, the blisters were found to form on {100} cleavage planes, indicating that the pressure will create damage in the path of least resistance.[29] In pipeline steels, the path of least resistance is often at interfaces such as between the matrix and hard inclusions, thus blisters are mostly found at interfaces or some other hiatus in the matrix.[12],[32],[38] de Schiapparelli found that blisters were never associated with soft inclusions such as MnS, which deform during rolling.

Blistering is also a special case of HIC which only affects the surface layers. Thus, HIC-resistant pipe have been found to have some blistering at the surface, however, the hydrogen effects are only at the surface, and do not enter into the bulk of the steel. Accordingly, blistering may not be entirely dependant on the steel making process, but on the properties near the surface.[63] For example, the existence of underskin inclusions, or a two phase microstructure near the surface through which molecular hydrogen could propagate and here promote blistering.[60]

The Metals Handbook mentions blisters as embrittlement without the effects of residual stress or external load,[74] however, this definitions is not commonly used. As was seen from the above works, most researchers simple use the latter criterion of no external load.

2.3.3 Chemistry

Desired strength levels in steel can be achieved by microstructural control of the steel as well as by changing the chemical composition. Hardenability, and therefore yield strength can be improved by increasing contents of various elements in the steel which

will change the number and size of the precipitates and/or inclusions in the steel. These changes will also affect the behavior of hydrogen in steel. The example of copper bearing steels decreasing hydrogen entry were given in Section 2.3.1.1 dealing with surface effects.

Copper adds to the strength of pipeline steels by solid-solution as well as precipitation hardening.[23],[81],[82] Tamehiro et al. found the increase in strength to be as high as 70 MPa without decreasing the strength in the weld heat-affected zone (HAZ). Copper was also found to decrease the ferrite grain size, which again is a strengthening mechanism in steel. Decreasing the grain size would increase the grain boundary area, and could possibly increase hydrogen damage at grain boundaries, however, recalling that copper at the surface decreases the entry of hydrogen, this effect is negligible.

Small nickel additions to steel have been shown to increase strength and toughness such that X100 grades are now available.[76] In an alloy of iron and nickel, Beck et al. found that the maximum permeability was achieved at 5-wt% nickel in iron.[83] Nickel is known to increase the hydrogen absorbing capacity of iron.[9] However, the solubility of hydrogen decreases with increasing nickel content, therefore, hydrogen could come out of solution in the lattice and accelerate cracking.[33]

Carbon effects on hydrogen damage have been studied for some time. Since carbon occupies interstitial sites in iron, it follows that the absorption of hydrogen would decrease with increasing carbon content up to 0.02wt% (carbon solubility limit in iron).[9]

Hence, increasing carbon would also decrease the diffusivity of hydrogen in iron.[15,45,46,84] In addition, carbides form strong traps for hydrogen,[33] consequently, HIC resistant steels use low carbon level to decrease inclusions and hard microstructures.[62] If a steel is fixed at a strength level, lowering carbon while maintaining the strength the steel acts as if coupled with copper (anodic) but when the carbon content is increased, again at a fixed yield strength, it acts cathodic.[85]

Titanium is sometimes added to steel to aid in the weldability by refining the HAZ microstructure and forming fine titanium nitrides.[23] However, if titanium carbides form, they act as irreversible traps because they have high interaction energy of 0.98eV, and increase the residency time of hydrogen, especially when the carbides form as large precipitates. If a carbide does not form, and titanium acts as a substitutional atom in the iron lattice, the interaction energy is much smaller, 0.27eV, and the titanium acts as a reversible trap, similar to a dislocation. Increasing the titanium levels was found to decrease the permeability of hydrogen.[47]

Earlier, work by Galis and Guntz was mentioned in regards to inclusions. Their work showed the beneficial aspects of calcium additions. These tests were done in an assortment of 250 steels, and showed the benefits of lowering sulfur to less than 30 ppm, with a Ca/S ratio between 0.5 and 1.1. As well, the oxygen content should be kept low such that the sum of sulfur and oxygen is less than 60 or 70 ppm.[60] Nakagawa et al. found that calcium also shape-controlled MnS inclusion in X65 pipeline steel. They also showed that to create a steel resistant to HIC, care should be taken to ensure that

manganese and phosphorus do not segregate and carbon should be lowered to as low as 0.04%.[39]

2.4 Fracture

From the above discussion it is clear that there are many microstructural features to which hydrogen will migrate and cause damage. The microstructural features influence the macrostructural diffusion and trapping behavior, which can ultimately lead to fracture. This is summarized in Figure 2-6 which shows three fracture types. Figure 2-7 shows schematically all three mechanisms. Beacham found it is possible for all three to happen in the same steel tested at different stress levels.[86]

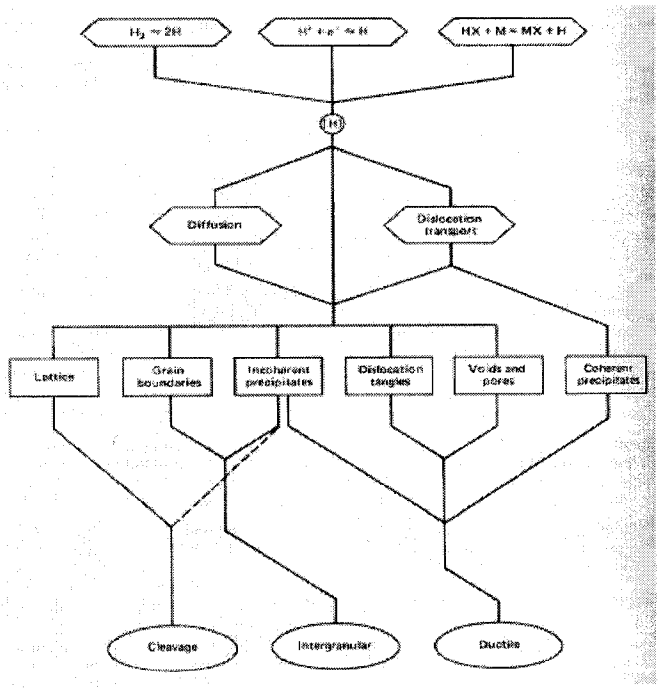

Figure 2-6 Flow diagram depicting hydrogen sources, transport paths, destinations and fracture micromechanisms [Hertzberg, 1996]

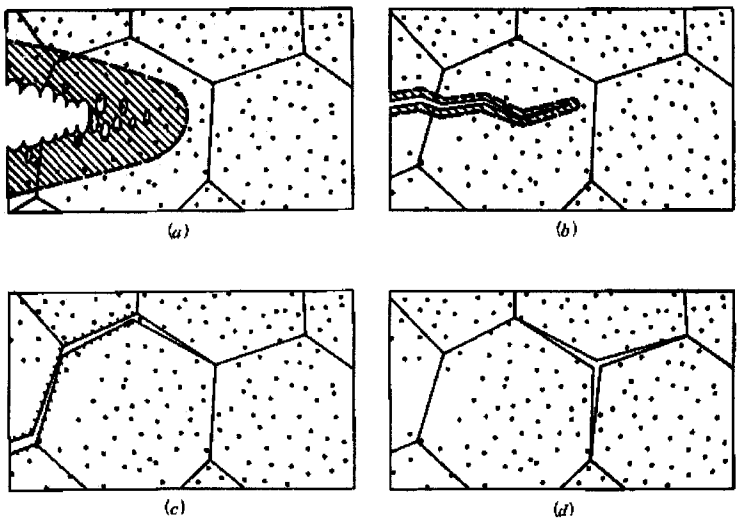

Figure 2-7 Schematic representation of different hydrogen-induced fracture paths as a function of stress level. (a) High K, microvoid coalescence fracture; (b) intermediate K, quasicleavage fracture; (c) low K, intergranular fracture; (d) intergranular cracking with an assist from hydrogen pressure. [Beacham, 1972]

2.4.1 Microvoid coalescence

As is clear from Figure 2-7, many small voids join together to create the dimples fracture surface that is microvoid coalescence. MVC is sometimes thought of as a ductile fracture mode with mild steel,[87] but if there is hydrogen present from the environment, dimples can be due to the linkup of gas filled microvoids. As well, in the study of crack tip SCC in combination with hydrogen-assisted cracking (HAC), it was found that part of the fracture surface was dimpled, hence crack tip dissolution could not be the only mechanism for crack growth. This tends to move HAC away from an embrittlement mechanism towards a microplasticity mechanism.[14] Figure 2-8 shows a replica of the

dimples left by HAC in a tempered 4340 steel. The dimples shown were caused by hydrogen voids linking together, or coalescing.

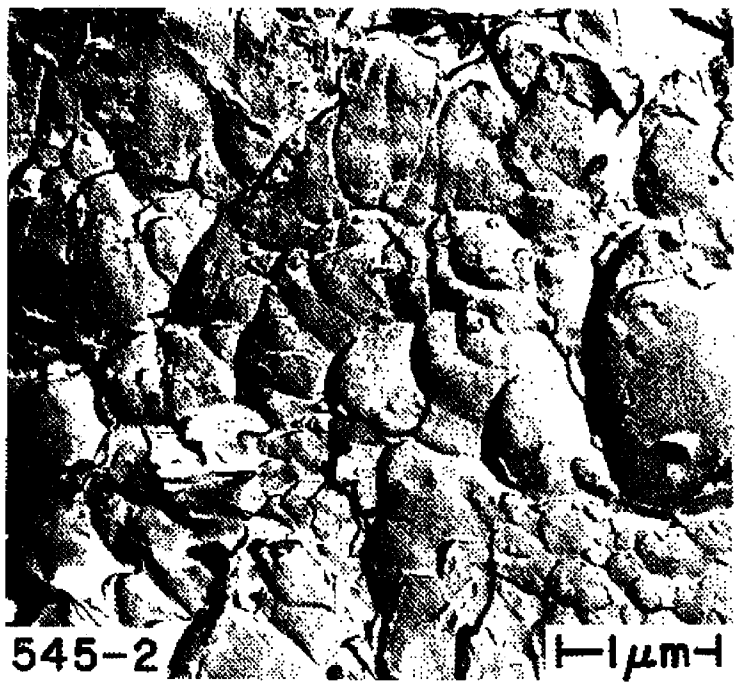

Figure 2-8 Dimples found in HAC regions formed in dry hydrogen gas at 1 atm. Two-stage replica. [Beacham, 1972]

Sandoz had found that the crack growth mode depends not on the source of hydrogen, but rather on the concentration and the yield strength of the metal.[85] With hydrogen charging, concentrations are increased at the edges of submicroscopic openings until high enough pressures of gas are built up to allow whatever the deformation mechanism the matrix will allow.[14] Thus, hydrogen does not change the fracture mode, but enhances it. Li et al. confirmed this in steel when they observed that the overall fracture mode did not change in the presence of hydrogen, the surface was simply flatter due to the presence of hydrogen.[75] In the case of MVC, hydrogen increases the growth rate of the voids, but

does not affect the initiation of the voids.[10,78] Li et al also observed that the MVC voids were distorted in shear due to plastic shear,[75] the joining and coalescing of the voids were probably assisted by pressure induced plasticity from the hydrogen charging.[74]

2.4.2 Quasicleavage

When assessing the effect of hydrogen on a pipeline steel with a ferrite-pearlite microstructure, Christenson et al. found that without hydrogen, the samples had a dimpled fracture surface, but in the presence of hydrogen, there was always quasicleavage.[5] Parkins et al. also found that quasicleavage in ferritic pipeline steels exposed to hydrogen.[88]

More recent studies of high strength steel in a hydrogen environment showed that quasicleavage cracks initiate at the beginning of the fracture process, and are followed by other types of cracking such as microvoid coalescence.[41] This is in agreement with earlier work by Beacham who established that quasicleavage would precede MVC as it is a lower energy form of HAC. He also put forward that in the presence of hydrogen, but the absence of external loading, crack initiation by MVC would not occur, but rather a lower energy form of cracking, such as quasicleavage would happen before MVC.[14]

High deformation rates at fracture in high strength steels tested by Ule et al. gave only a few ductile regions with the rest of the fracture surface being quasicleavage. Hydrogen at grain or subgrain boundaries could have enhanced the void growth by decreasing interfacial cohesion. This gave way to quasicleavage on the periphery of larger deeper

funnel type dimples.[10] Tsuboi et al. found that if hydrogen is the only contributor to quasicleavage in high strength steel, the rolling direction of the steel was the favored direction for fracture regardless of the loading axis.[77]

2.4.3 Cleavage

Hertzberg defines cleavage as involving transcrystalline fracture along specific crystallographic planes.[86] In Fe-Si single crystals, the cleavage plane was found to be along the {100} plane as blisters were found to grow along this plane due to hydrogen precipitating out of the matrix.[29] Tests on a Fe-3%Si steel found that cleavage striations had a spacing of 300 nm, with high dislocation density in the wake of the crack. It was also found that cleavage initiated when a critical atomic hydrogen concentration developed ahead of a crack tip, lowering the cohesive strength of the matrix until the crack moves ahead.[43]

Thus cleavage would be slow until the hydrogen gas pressure ahead of the crack tip reaches the critical level, then the crack proceeds rapidly.[66] In X65 pipeline steel, cleavage was found internally without contact with a corrosive or embrittling solution. In all cases, the cleavage was a result of the interaction of external stress with cathodically evolved hydrogen.[7] Cleavage is often found to be emanating from non-metallic inclusions, such as oxides, segregated regions of MnS and peralite colonies.[4,6,7] However, as Alp et al. pointed out, the type of fracture has a strong dependence on the microstructure; and often MVC appeared between the cleavage regions.[4]

2.5 Summary

From the above discussions, it is clear that for many years it was known that hydrogen interacted with steel. Hydrogen lowers the mechanical properties of steel, most noticeably the toughness as measured in the ductility. Yield and tensile strengths were largely unchanged by the ingress of hydrogen. The effects were related to the amount of ingress into the steel through the surface, through the bulk of the steel samples, to near the crack. The microstructural features in the steel such as number and placement of dislocations, inclusions etc, are also important to the diffusion and trapping of hydrogen. The microstructure and macrostructure will control the fracture mode. Hydrogen does not seem to change the fracture mode, but will accelerate whatever fracture mechanism is more prevalent.

3 Materials and experimental details

3.1 Materials

The three grades of pipeline steels used in this study were X65, X80 and an experimental X100 provided by TransCanada Pipelines Ltd. The chemical compositions of the steels are provided in Table 3-1. The microstructures of the three steels were examined with a scanning electron microscope. Figure 3-1 through Figure 3-3 show the various structures in three directions, transverse, radial and longitudinal. Tensile specimens were taken such that the tensile axis was in the transverse direction of the as-received pipes.

Table 3-1 Composition of steels

Grade	C	Mn	S	Si	Cu	Ni	Cr	Mo	Nb	Ti	Al	Sn	N
X65	0.03	1.49	0.008	0.25	0.27	0.12	0.08	0.203	0.065	0.015	0.015	0.014	0.0124
X80	0.03	1.79	0.008	0.27	0.29	0.12	0.07	0.251	0.087	0.021	0.028	0.016	0.0113
X100	0.06	1.91	-	0.36	-	0.24	0.04	0.294	0.043	0.014	0.018	0.003	0.0038

Balance Fe. P~0.01, V=0.003 only present in X80, B=0.0003 only in X80 and X100

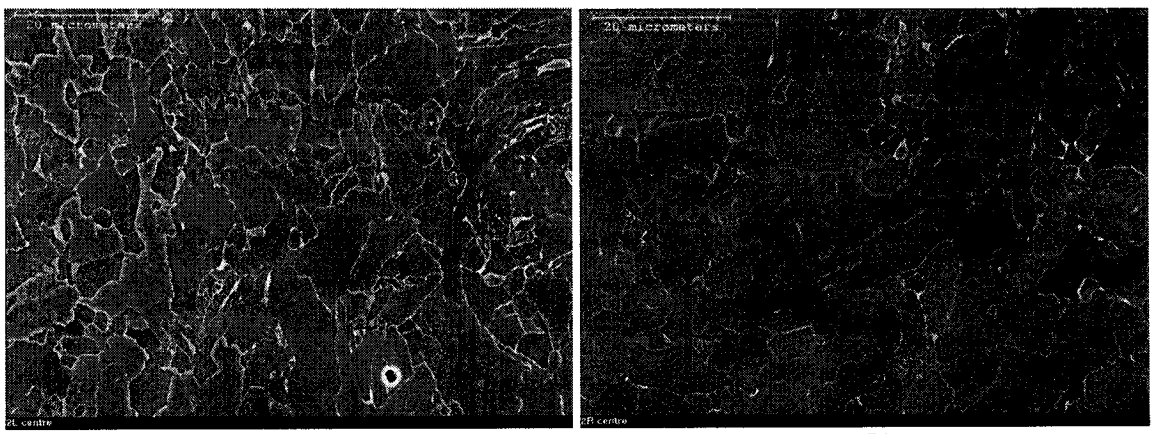

(a) **(b)**

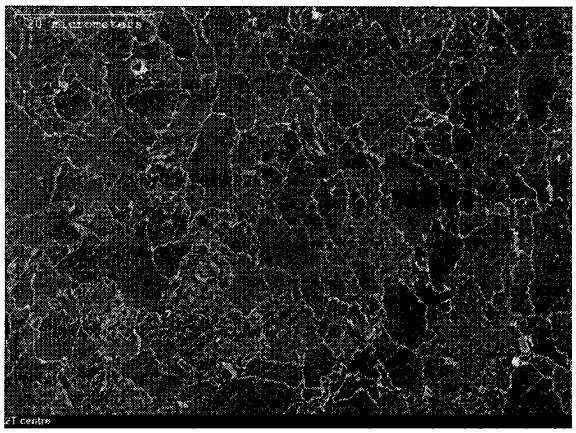

(c)

Figure 3-1 X65 microstructure (a) longitudinal, (b) radial, and (c) transverse

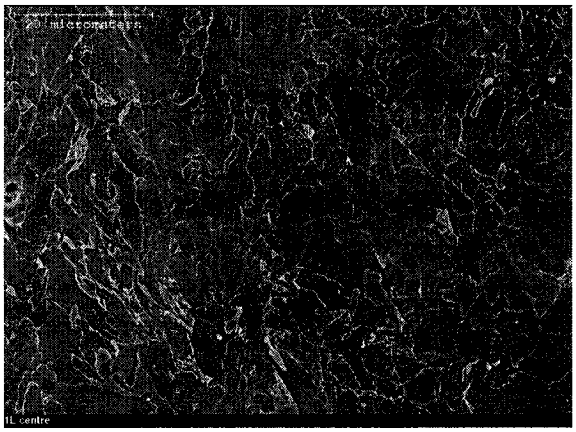

(a)

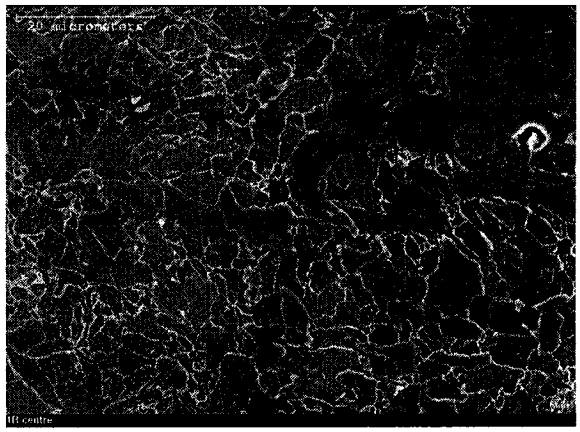

(b)

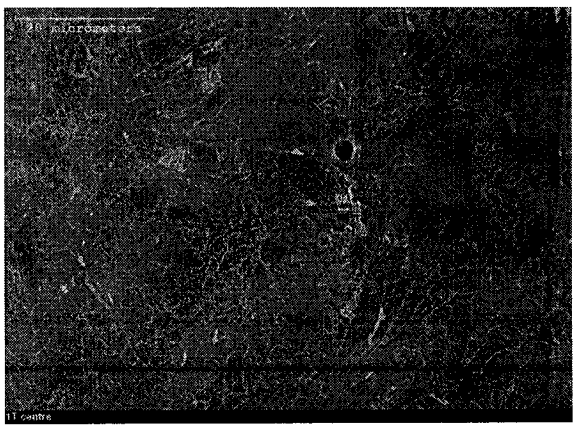

(c)

Figure 3-2 X80 microstructure (a) longitudinal, (b) radial, and (c) transverse

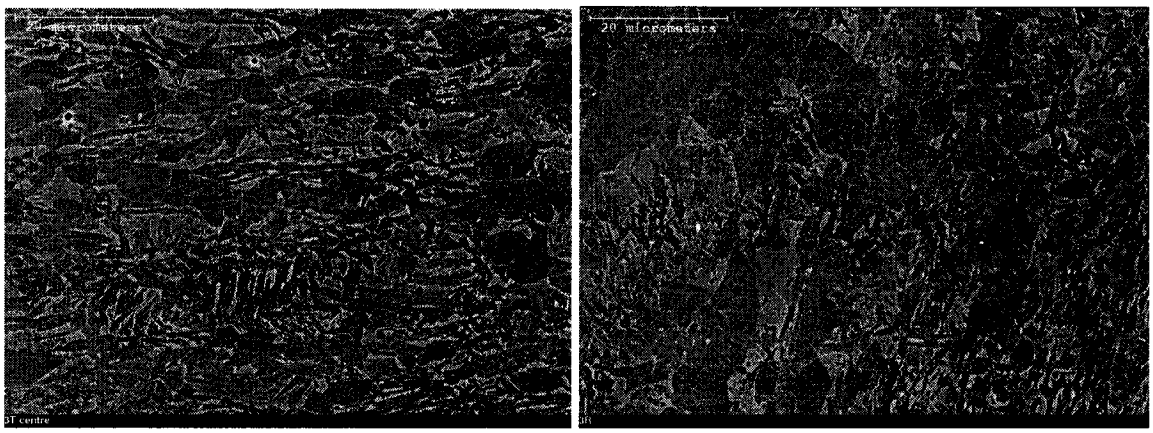

(a) (b)

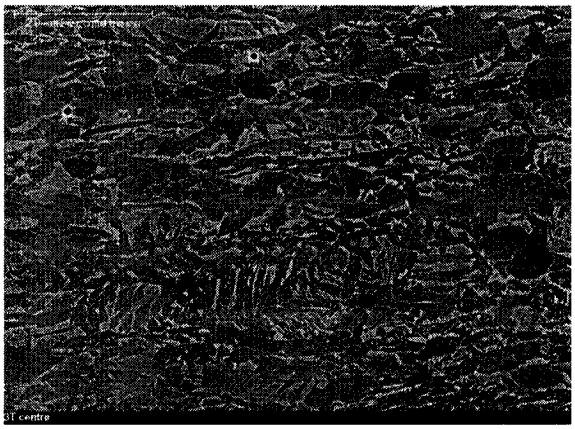

(c)

Figure 3-3 X100 microstructure (a) longitudinal, (b) radial, and (c) transverse

3.2 Solution

The solution used for hydrogen charging was 0.1N H_2SO_4 poisoned with 10 ppm As_2O_3 to prevent hydrogen recombination on the surface of the samples. The solution was purged with N_2 gas for 24 hours prior to being introduced to the test cell where the samples were charged, and for the duration of the charging. It was found by Farrel that 0.5 ppm As_2O_3 was needed in a sulfuric acid solution to cause poisoning.[67]

3.3 Samples

Identical samples were prepared from all three grades of steel used in this study. First, round bar samples were made to simulate the gauge section of a round tensile sample. These samples measured 6 mm in diameter and 45 mm in length; prior to charging, the samples were prepared such that only a 30 mm section would be exposed to the charging solution in order for only this section to be used for subsequent hydrogen analysis. These samples were left with a 600 grit surface finish.

Next, round tensile samples were prepared according to ASTM standard E38 with a diameter of 6 mm. Due to the small radius of the X65 pipe, the length of the reduced section was lowered from the recommended 36 mm to 30 mm, however, to prevent introducing an extra variable in this comparative study, the decreased length was used for all the steels. These samples were prepared with a ground finish as per ASTM requirements. These samples were used for the samples that were stressed prior to charging as well as for the concurrently stressed and charged samples. A schematic of the sample and the location in the pipe from which they obtained is shown in Figure 3-4.

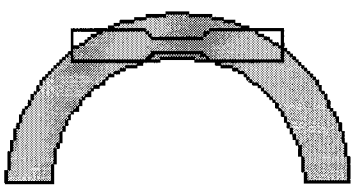

Figure 3-4 Schematic of location of specimens

The final test specimens prepared in this study were thin sheet specimens used for permeation testing. These samples had a thickness of 1.5 mm with the less crucial dimensions of width and length of 30 mm and 30 mm respectively. These samples were machined from the center thickness of the pipe.

3.4 Experimental

3.4.1 Materials characterization

Materials characterization was further carried out with Rockwell and Vickers hardness tests. Following this, stress-strain curves were generated using an Instron 8500 servo-hydraulic tensile testing machine. The stress-strain curves were generated both with and without the use of a clip-gauge extensometer.

3.4.2 Effect of time

The first hydrogen testing regimen used the round bar samples. This testing was done to establish a suitable charging time to saturate a 6 mm by 30 mm steel sample. Charging was carried out in the sulfuric acid solution described earlier at a current density of 0.05 mA/cm^2. Prior to charging, the samples were cut partially through the thickness such that they could be easily broken after charging. Charging was carried out for various times from 5 hours to 72 hours. A schematic of the hydrogen set up is shown in Figure 3-5; platinum wire was used as the counter-electrode, and charging was carried out at a constant current density of $0.5mA/cm^2$ unless otherwise stated.

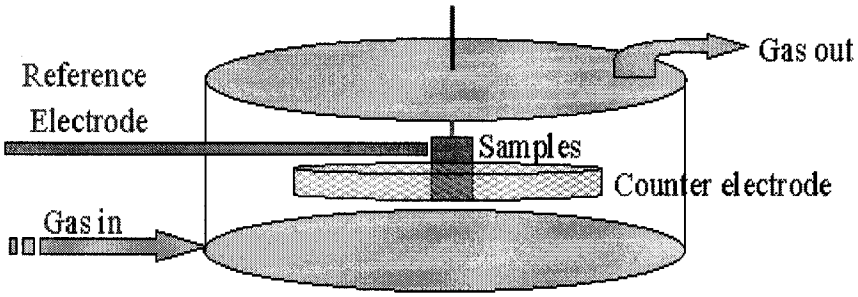

Figure 3-5 Schematic of hydrogen charging set-up [He, 2002]

After charging, the samples were quickly wiped dry and put in a bath of methanol at kept -60°C with dry ice. The samples were put in the bath in order to lock in diffusible hydrogen as per welding standard ANSI/AWS standard A4.3-93 and ISO 3690. The process of taking the samples out of the charging solution and placing them in the bath took less than 30 seconds for all samples. As per the diffusible hydrogen standards, the samples could be stored in the dry ice bath for an extended period of time at -60°C without any hydrogen escaping from the samples. Once removed from the dry ice, the samples were then rinsed with ethanol, then ether before being put in mercury eudiometer tubes under reduced pressure for a minimum of 72 hours as outlined in the welding standards. This method is suitable for removing the diffusible hydrogen from steel, without removing any of the trapped hydrogen.

Figure 3-6 Eudiometer tubes for diffusible hydrogen analysis

Once the diffusible hydrogen was obtained from the charged samples, the sample was sectioned, and the trapped hydrogen was obtained from two thirds of the sample with a LECO RH402 hydrogen determinator using the hot extraction method. Care was taken during sectioning of the sample to be sure that the temperature did not rise above 30°C. The smaller sections of the sample were then cleaned with soap and water, then rinsed in acetone and distilled water before being dried with lab compressed air. The samples to be used for hydrogen determination were weighed before being sealed in the induction furnace of the hydrogen determinator. The sample was then heated, and the liberated hydrogen carried to the analysis chamber by pure nitrogen gas that had been cleaned of traces impurities such as water, oxygen, CO and CO_2. The difference in the thermal

conductivity of the pure nitrogen gas and the nitrogen gas carrying the liberated hydrogen gas gave the hydrogen content of the sample. Figure 3-7 gives a flow chart of the process carried out by the hydrogen determinator.

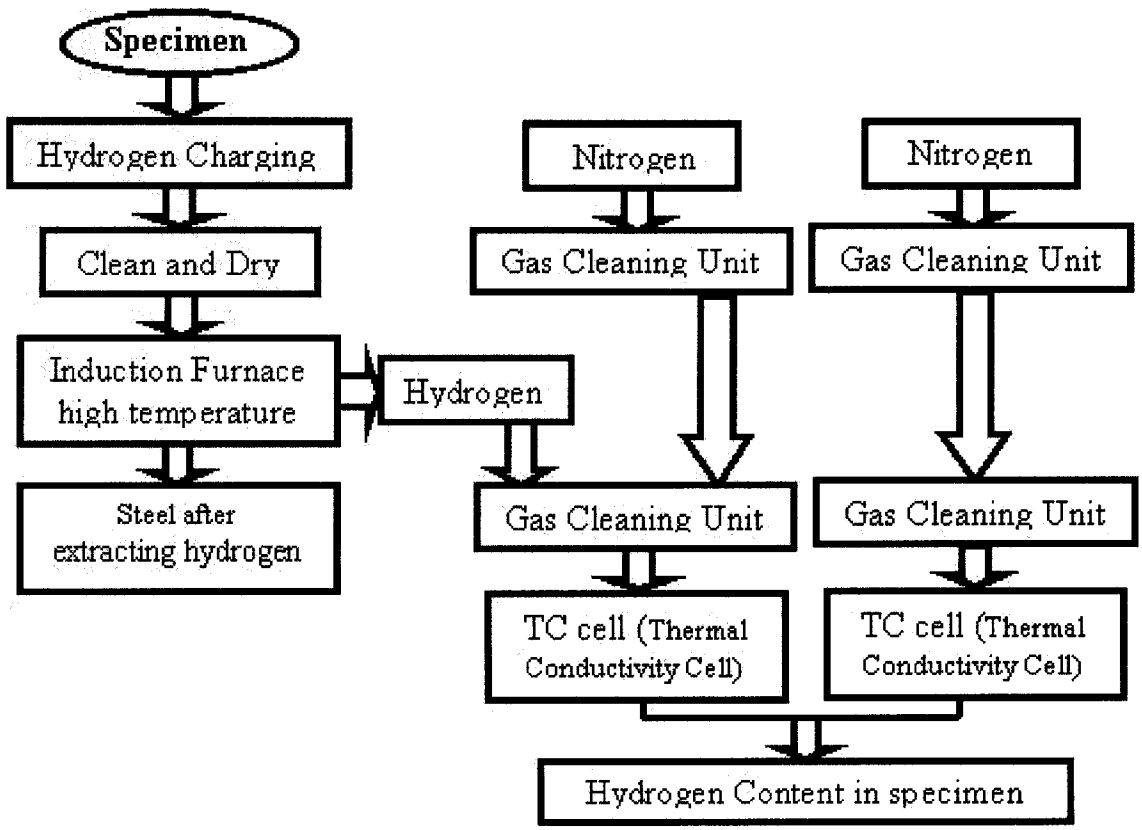

Figure 3-7 Flow chart of hydrogen determinator [He, 2002]

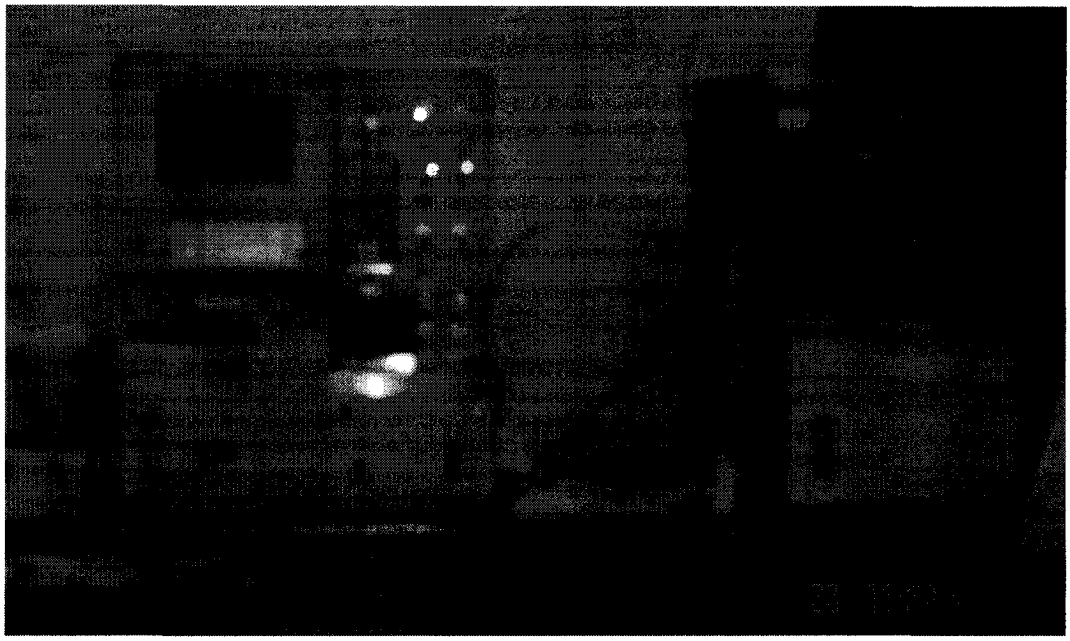

Figure 3-8 LECO RH-402 Hydrogen analyzer

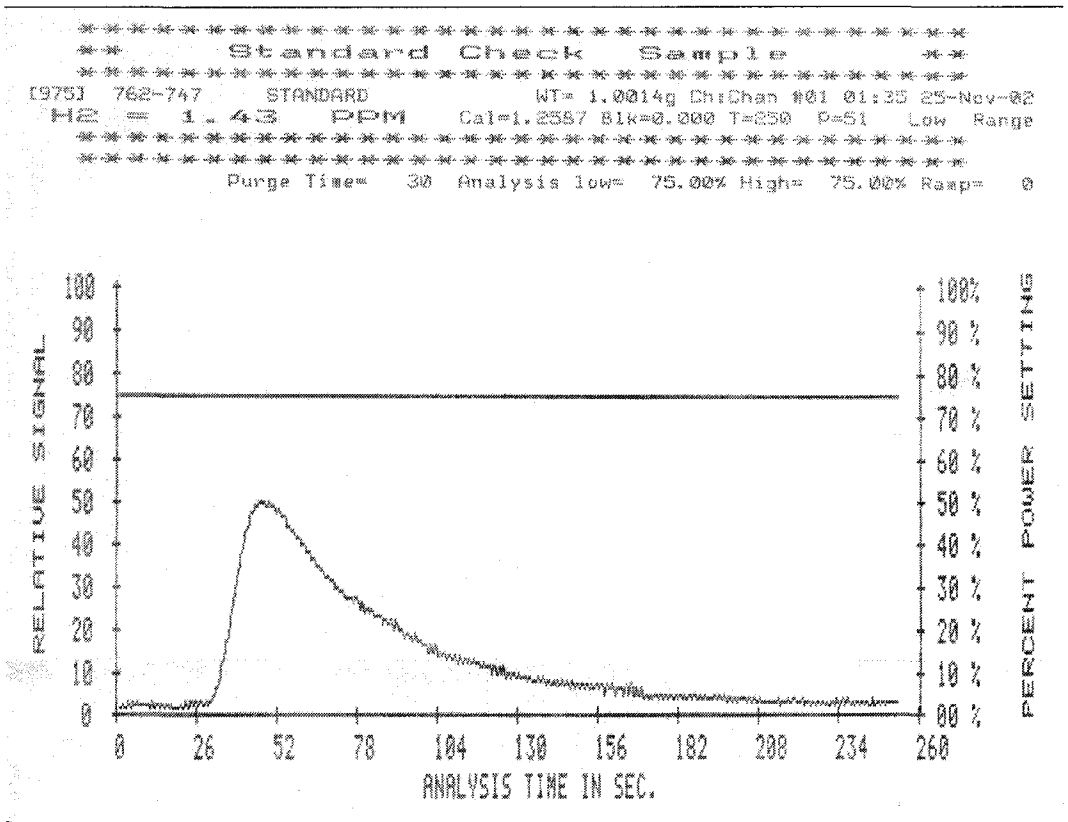

Figure 3-9 Standard hydrogen-time curve from LECO RH-402

The hydrogen analyzer was calibrated with at least 3 samples and several times throughout a testing day with steel pins containing 1.5 ± 0.4 ppm hydrogen. Figure 3-9 shows a typical hydrogen determination curve for a standard pin; the area under the curve represents the amount of hydrogen found in the sample. Figure 3-10 shows a typical curve for a sample in this study. The trapped hydrogen contents of the charged samples were then compared to the trapped content in the as-received condition.

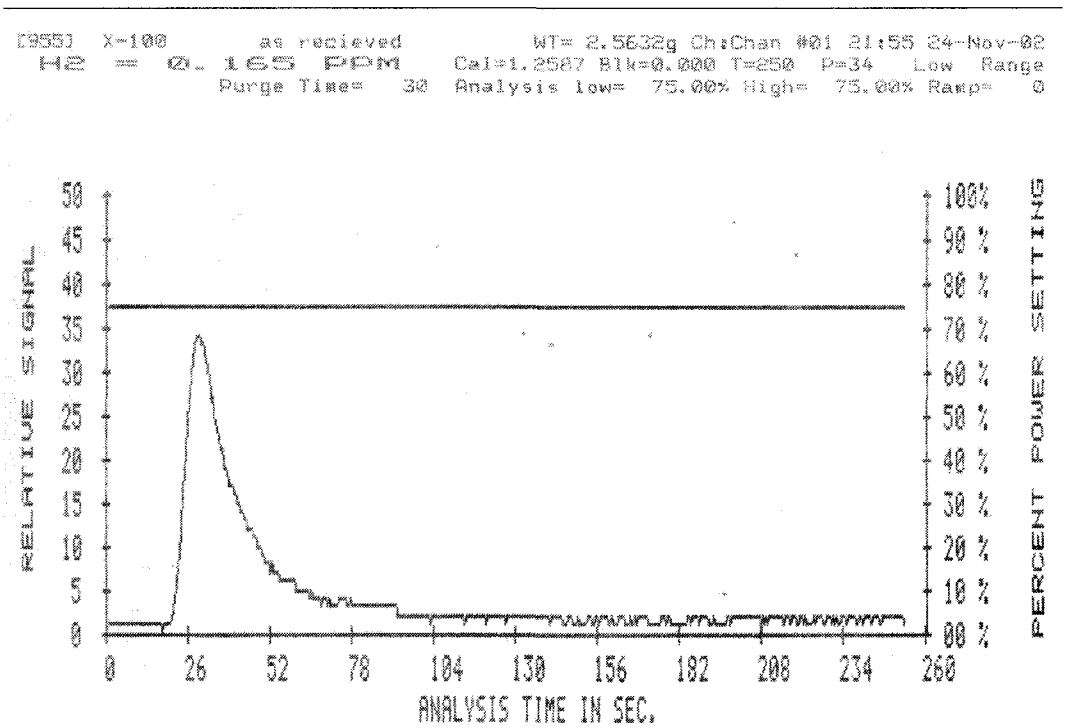

Figure 3-10 Typical hydrogen-time curve for steel sample in this study

3.4.3 Effect of prestressing

Once the charging time for saturation was established, tensile samples for each steel were stressed into the plastic region, then underwent an assortment of stressing conditions;

after the prestressing, these samples were charged for the "saturation time." The four stress conditions used for each grade of steel were as follows: 1) 2% strain and unload; 2) 2% strain and hold at load for 24 hours; 3) 2% strain then 100 cycles; and 4) 2% strain, 100 cycles then hold at load for 24 hours. The strain used here refers to the total strain the sample experienced as measured by the strain gauge. Stress conditions 3 and 4 were carried out with load control once the maximum load was obtained by straining the sample to 2% total strain as in load condition 1. Once the maximum load was obtained, the samples were quickly reloaded to the maximum load, corresponding to 2% strain, and then cycled at R-ratio=0.1 (R-ratio = minimum stress/maximum stress), and unloaded for load condition 3. For stress condition 4, after cycling, the sample was held at the maximum load for 24 hours before being unloaded. After going through the various stressing regiments, the samples were sectioned as with the bar samples such that only the reduced section of the tensile samples could be exposed to the charging solution. Then charging was carried out as with the round samples, and the hydrogen contents were also measured as mentioned before. Without stressing to 2% strain, stressing conditions 3 and 4 were repeated with the maximum stress being 90% of the yield strength for all three steels.

3.4.4 Effect of charging with stressing

The final type of testing on tensile samples was concurrent stressing and charging. For these samples, the concurrently stressed and charged specimen were prepared in the same fashion as the prestressed samples such that only the reduced section would be in contact with the solution. After coating the parts that were not to be charged with a non-

conducting paint, the specimens were enclosed in the charging cell, and dry nitrogen gas was passed through for a minimum of 4 hours before introduction of the charging solution. The samples were all charged for 24 hours before concurrent stressing and charging to ensure complete saturation of the gauge length. The charging current was fixed from the introduction of solution to the charging cell to the time the sample was removed from the sample. This was done to ensure that an adequate supply of hydrogen would always be present at the sample surface. After saturation, these samples were strained to 2% strain, as measured by a strain gauge outside the cells. It was possible to know the strain in the sample gauge length was 2% even though the strain was measured outside the hydrogen charging cell, as the strain was measured on a pair of "extension arms" which had been calibrated to the sample earlier.[†] In this set of tests, only the trapped hydrogen was measured as removing the samples from the set-up required a minimum of 5 minutes, by which time a substantial amount of diffusible hydrogen could escape from the sample. Figure 3-11 shows a concurrent charging and stressing sample being tested in the Instron servo-hydraulic tensile testing machine.

[†] Calibrations for 2% strain is included in Appendix I

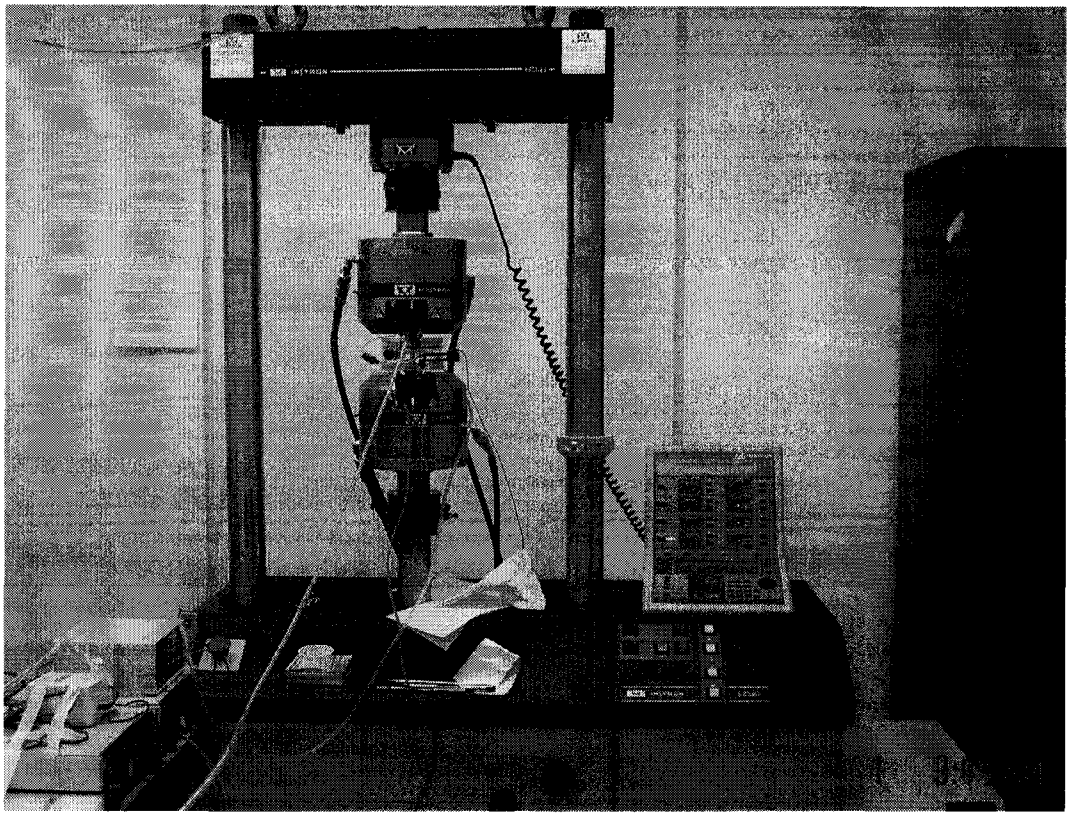

Figure 3-11 Concurrent charging and stressing test

3.4.5 Permeation testing

Permeation testing was the final set of testing experiments. This was done using two glass cells clamped together, with the specimen clamped between the two, in the same set-up as described by Devanathan and Stachursky.[89] In this set of testing, the charging current density was varied from 0.05 mA/cm^2 up to as high as 2 mA/cm^2 for the lower grades of steel. In one glass cell, the detection side, contained a Ni/NiO Barnacle electrode that had previously been charged in 10 N NaOH to a potential of 1.5 V. This side was next filled with 0.2 N NaOH that had been purged with nitrogen for 24 hours prior to use. The potential across a 2 kΩ resister which was connected between the

sample and the Barnacle electrode, the detection voltage, was tracked on a strip chart recorder. As the 0.2 NaOH was introduced to the detection side, the detection voltage shot up, then decayed with time. Once the detection voltage decayed to a stable value corresponding to below 1 μA, the charging solution was added to the charging side of the set-up. The constant current densities used in this testing were measured between the sample and a carbon counter-electrode; current densities between 0.05 and 0.5 mA/cm^2 were used. Figure 3-12 shows a schematic of this set-up.

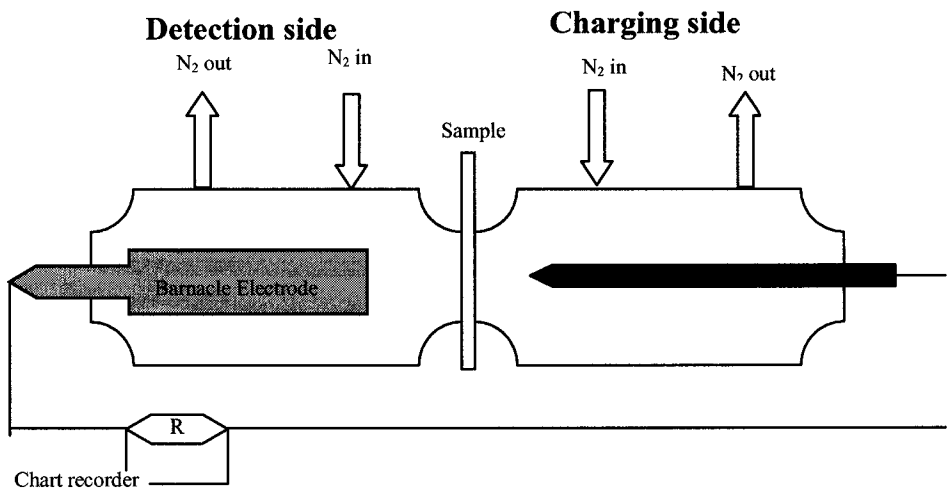

Figure 3-12 Schematic of permeation testing set-up

4 Results

4.1 Materials characterization

Before any hydrogen experiments were carried out on the steels, the materials were tested to verify the mechanical properties and chemical homogeneity. Firstly, hardness tests were performed on the three steels with special attention given to hardness differences of the banded structure of the X-100 steel. Rockwell hardnesses for the three steels are given in Table 4-1.

Table 4-1 Hardness values of three steels

	X65	X80	X100
HR_C	-	16	26
HR_B	78	90	100

The stress-strain curves generated for two samples of each grade are given in Figure 4-1. Table 4-2 gives the mechanical properties that were calculated from the stress strain curves. As can be seen, the yield strengths of the higher grades are somewhat higher than the specified minimum. Also, there is a noticeable drop in ductility when moving to the higher grades which is likely to be a result of strain hardening due to the controlled rolling process, and precipitation hardening in higher grades of steel.

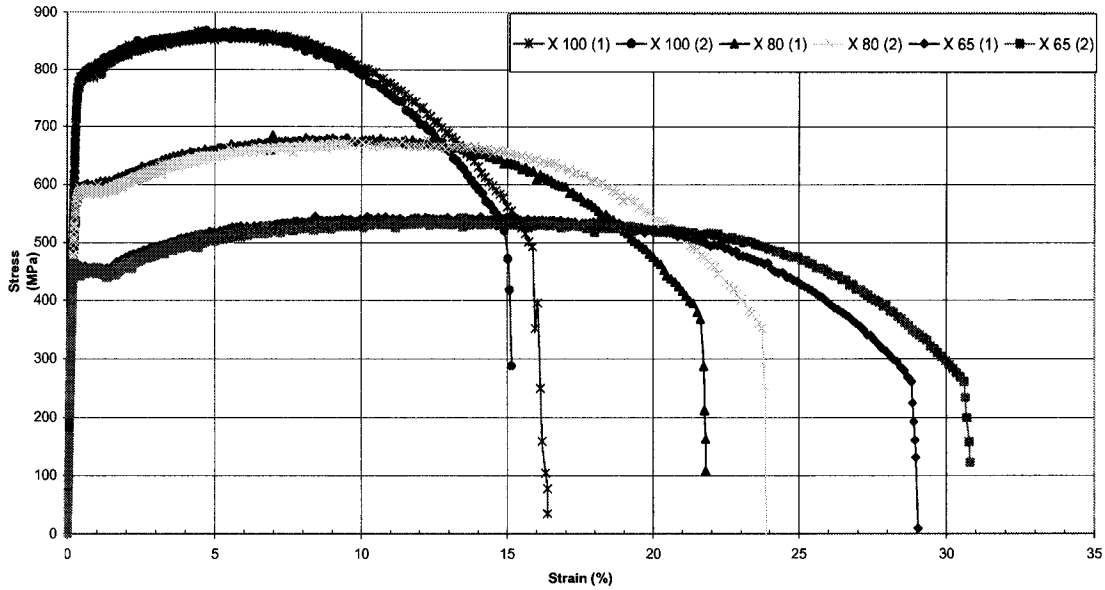

Figure 4-1 Two stress-strain curves for each grade of steel

Table 4-2 Mechanical properties of three steels

Grade	σ_{ys} MPa (ksi)	UTS MPa	$\varepsilon_{failure}$ %
X65	450 (65)	544	30
X80	585 (84)	682	23
X100	785 (113)	869	16

4.2 Effect of time

Round bar samples for each steel were charged at various times ranging from 5 hours to 72 hours. A minimum of two samples were charged at a time and both the diffusible and trapped hydrogen contents were measured for each sample. The diffusible hydrogen contents for the three steels are shown in Figure 4-2; the trapped hydrogen contents in Figure 4-3. Though the hydrogen content of the X100 was still somewhat erratic, the diffusible hydrogen contents for the X80 and X65 steels stabilized after roughly 24 hours of charging; thus 24 hours was taken as a convenient charging time for the prestressed samples. Farrell found that 12 hours was sufficient for complete saturation for round

samples 9mm in diameter.[67] The "stabilized" diffusible hydrogen contents for the steels are: 1 ppm for X65, 1.25 ppm for X80 and 2.25 ppm for X100.[‡] It should be noted that the trapped hydrogen contents did not appreciably increase with increased charging time. The trapped hydrogen values for the as-received steels are 0.20 ppm for X65, 0.17 ppm for X80 and 0.28 ppm for X100.

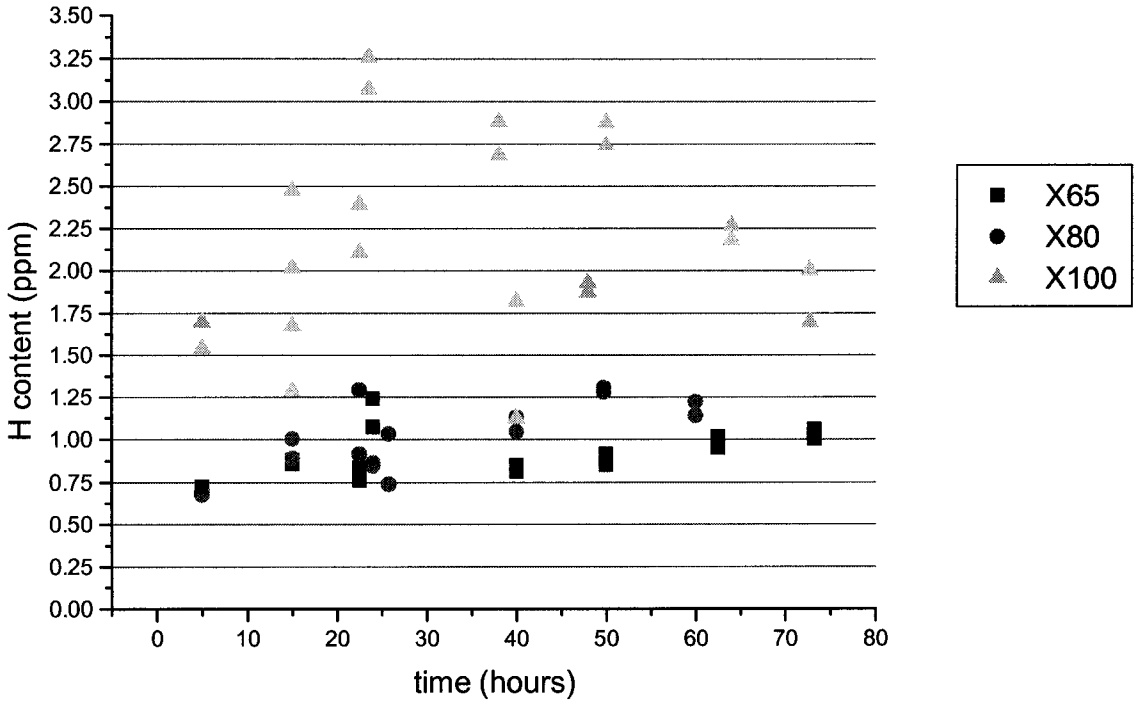

Figure 4-2 Diffusible hydrogen contents as a function of exposure time

[‡] Note: these values are the average at the specified times as taken from Figure 4-2 and were used for subsequent calculations. They do not represent a true stable value as there was too much scatter in the data. This procedure for averaging values was used throughout.

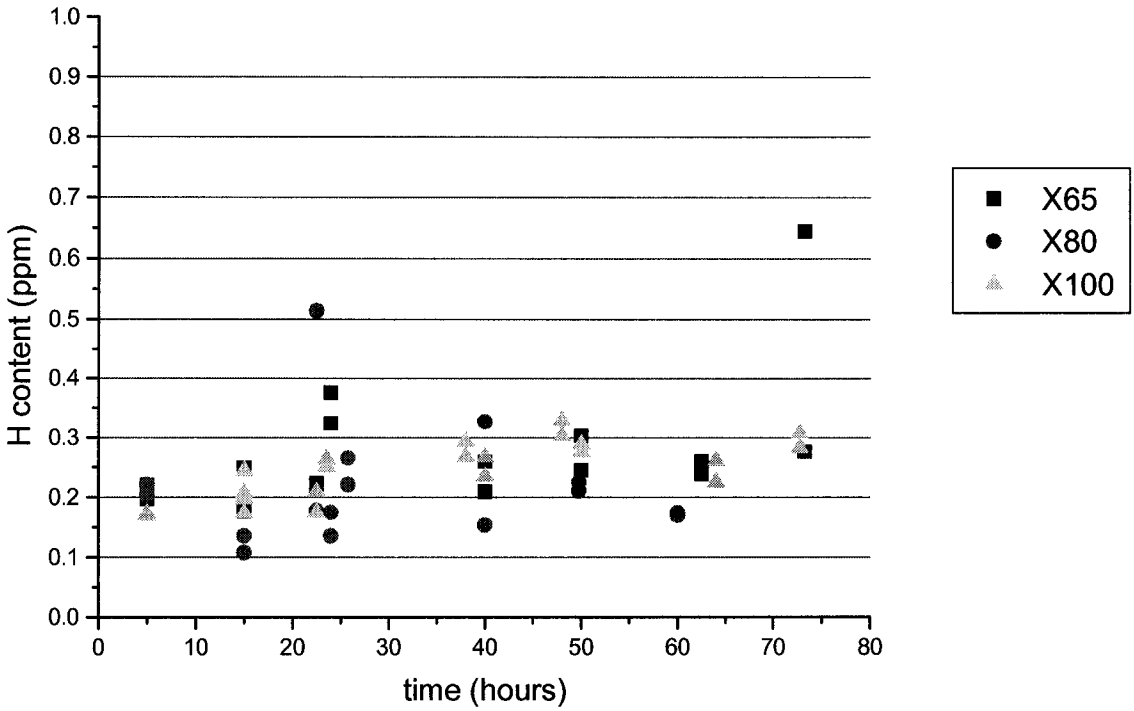

Figure 4-3 Trapped hydrogen contents as a function of exposure time

4.3 Effect of prestressing

The hydrogen contents for samples which had undergone the four stressing conditions at 2% strain then charged for 23.5 hours are given in Table 4-3. These are summarized in Figure 4-4 and Figure 4-5, where the x-axis represents each of the four stressing conditions, and the horizontal lines represent the "stabilized" hydrogen contents for the samples before prestressing. The diffusible hydrogen contents introduced in Table 4-3 were then normalized according to the stabilized diffusible hydrogen contents; and the trapped normalized according to the as received steel contents. These normalized results are shown in Figure 4-6 and Figure 4-7. It is clear from the figures that the X100

contained the greatest absolute amount of hydrogen, but it did not experience the largest increase.

Table 4-3 Hydrogen contents of prestressed samples[§]

Grade	2% strain		2% strain and hold 24 hours		2% strain, 100 cycles at R = 0.1		2% strain 100 cycles at R = 0.1 and hold at max load for 24 hours	
	diffusible	trapped	diffusible	trapped	diffusible	trapped	diffusible	trapped
X-65	2.32	0.34	1.70	0.28	1.43	0.36	1.73	0.22
	1.61	0.35	---	0.22	2.27	0.32	1.82	0.23
	1.29	0.21	1.71	0.31	1.88	0.36	1.54	0.25
	1.79	0.21	2.43	0.53	1.98	0.39	1.93	0.26
			1.75	0.22	1.90	0.23		
Avg	1.75	0.28	1.90	0.31	1.89	0.33	1.75	0.24
X-80	2.11	0.42	2.09	0.20	2.15	0.32	1.89	0.29
	1.95	0.40	2.43	0.37	2.13	0.32	2.13	0.34
	2.08	0.17	1.89	0.41	2.15	0.37	1.98	0.25
	2.28	0.25	1.81	0.24	2.13	0.28	2.03	0.25
			2.32	0.28			1.92	0.29
							2.07	0.29
Avg	2.10	0.31	2.11	0.30	2.14	0.32	2.00	0.28
X-100	1.26	0.37	3.82	0.59	3.09	0.44	3.34	0.43
	1.55	0.39	3.37	0.50	3.24	0.33	4.56	0.58
	2.65	0.36	3.39	0.56	2.13	0.35	3.16	0.55
	2.75	0.40	3.93	0.53	3.20	0.43	2.23	0.63
	3.03	0.25	4.37	0.55	3.53	0.50	2.67	0.58
							4.31	0.39
Avg	2.25	0.36	3.77	0.55	3.04	0.41	3.38	0.53

[§] As with previous hydrogen contents, these values were used for subsequent graphing. The average values were calculated as an average of the other results and used for graphs even through there was significant scatter in the individual data points is clear from the figures.

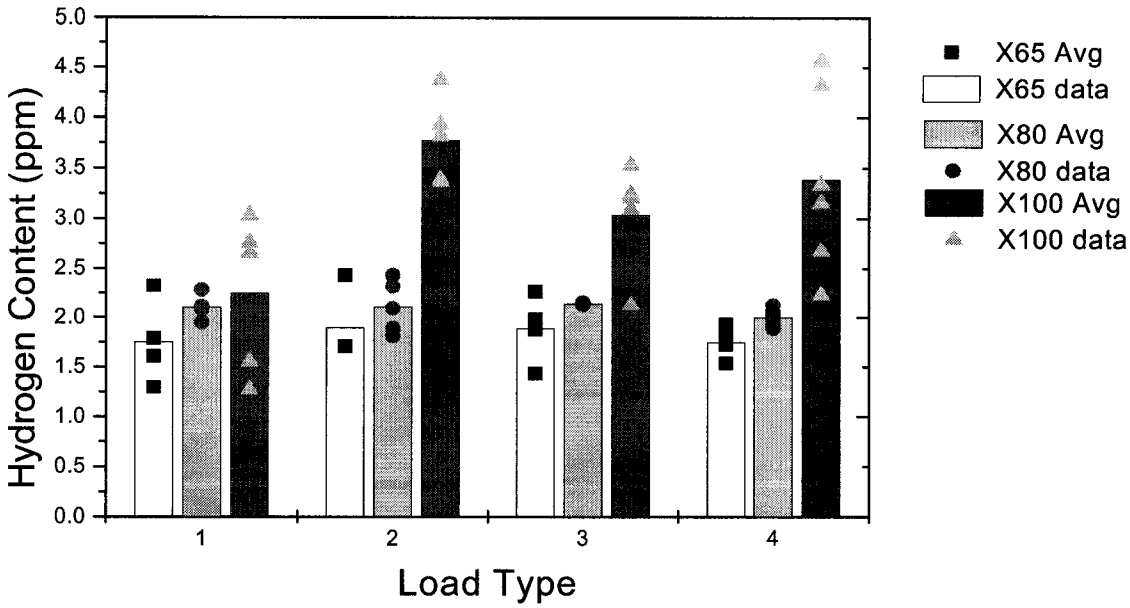

Figure 4-4 Diffusible hydrogen contents of prestressed samples

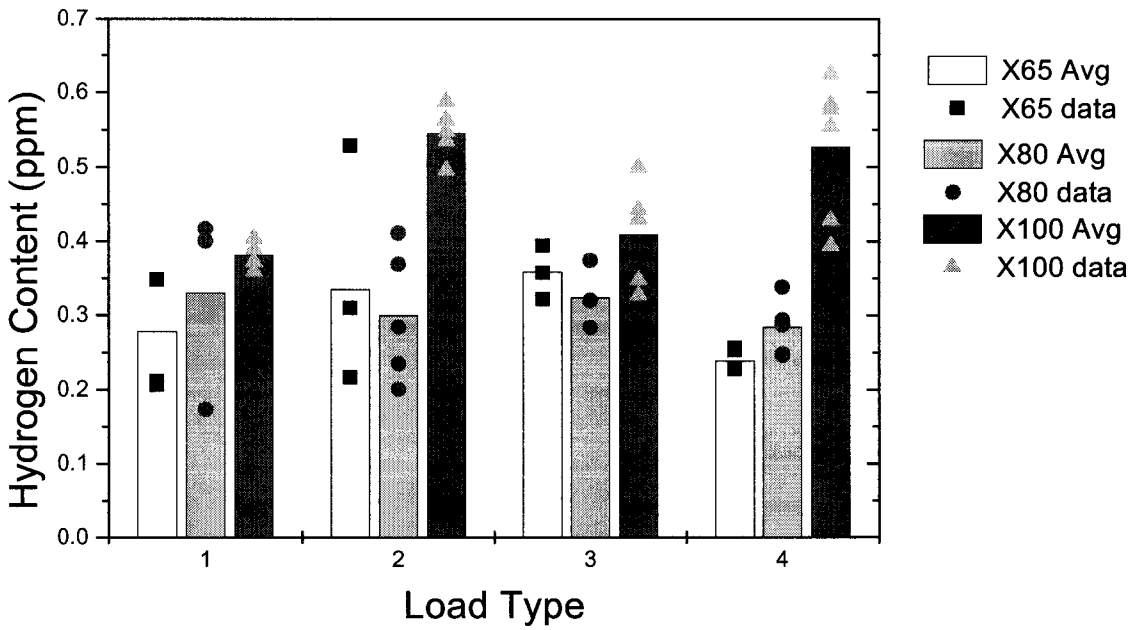

Figure 4-5 Trapped hydrogen contents of prestressed samples

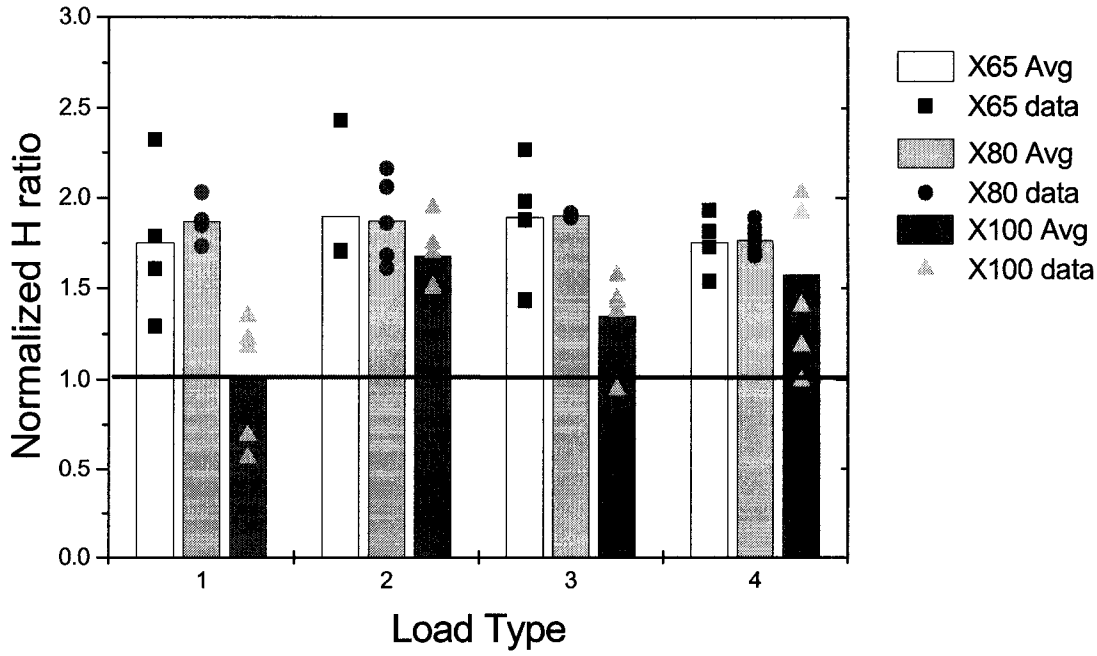

Figure 4-6 Normalized diffusible hydrogen ratios

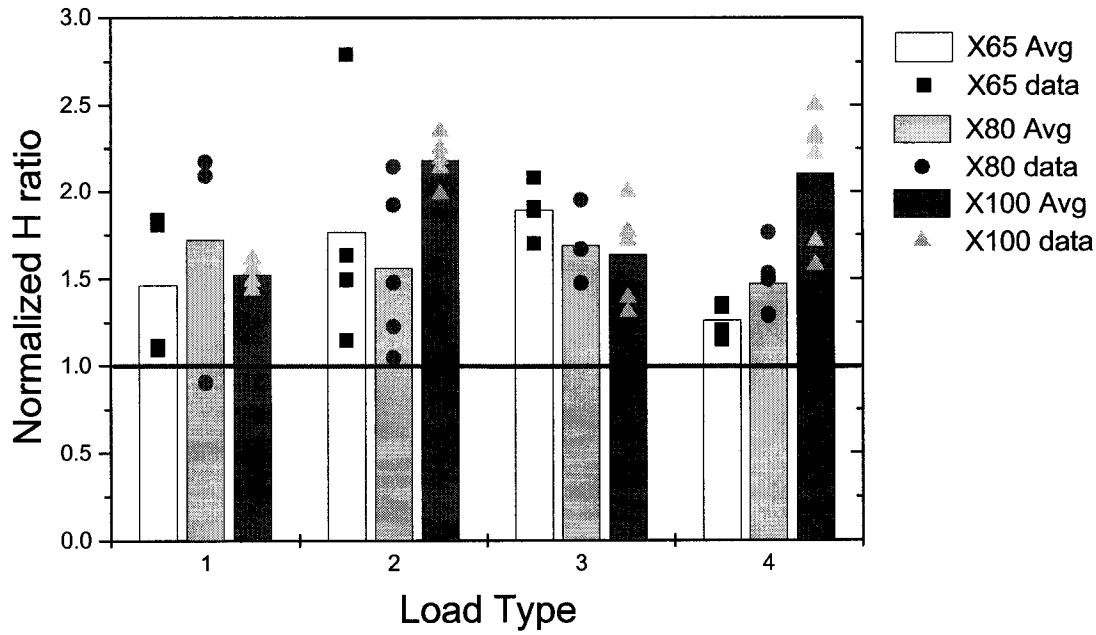

Figure 4-7 Normalized trapped hydrogen ratios

Stressing conditions 3 and 4, 100 cycles at R = 0.1 and 100 cycles at R = 0.1 then hold the maximum load for 24 hours, were performed on the steels at a maximum stress corresponding to 90% of the yield strength. Stressing condition 3 contained cyclic loading, to create dislocation cells, and condition 4 had the addition of static loading to possibly add some room temperature creep. The results of the hydrogen contents are given in Table 4-4. These are summarized in Figure 4-8 and Figure 4-9. The normalized values for the diffusible and trapped hydrogen are summarized in Figure 4-10 and Figure 4-11 respectively. From the normalized values in Figure 4-10 it appears that the X65 had a decrease in the diffusible hydrogen content. But from Figure 4-11 there is a clear increase in the trapped hydrogen contents of all three steels, with the greatest in the X100.

Table 4-4 Hydrogen contents of samples stressed to 90% YS

Grade	90% YS, 100 cycles at R = 0.1		90% YS 100 cycles at R = 0.1 and hold at max load for 24 hours	
	diffusible	trapped	diffusible	trapped
X-65	1.010	0.192	0.953	0.223
	0.857	0.310	0.919	0.270
	0.817	0.228	0.808	0.320
	1.060	0.195	1.025	0.223
Avg	0.936	0.231	0.926	0.259
X-80	1.207	0.227	1.396	0.261
	1.331	0.251	1.431	0.231
	1.362	0.245	1.587	0.250
	1.059	0.173	1.315	0.234
			1.466	0.280
Avg	1.240	0.224	1.439	0.251
X-100	3.090	0.420	2.817	0.448
	2.800	0.405	3.151	0.764
	2.746	0.444	3.192	0.500
	3.021	0.325	2.246	0.503
Avg	2.914	0.398	2.852	0.553

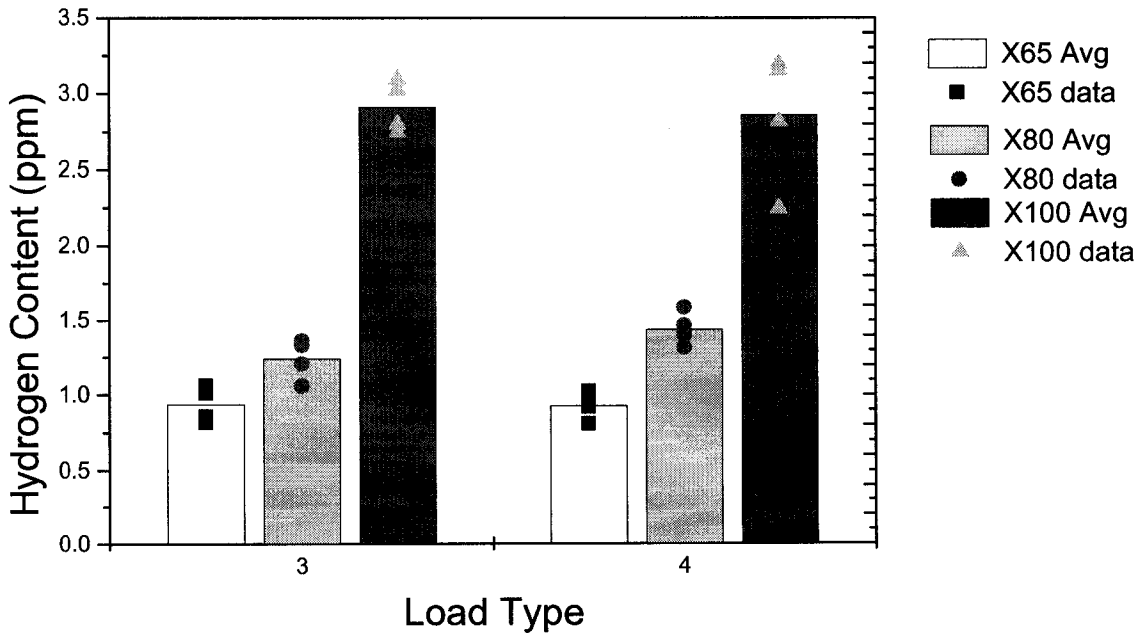

Figure 4-8 Diffusible hydrogen contents of samples stressed to 90% YS

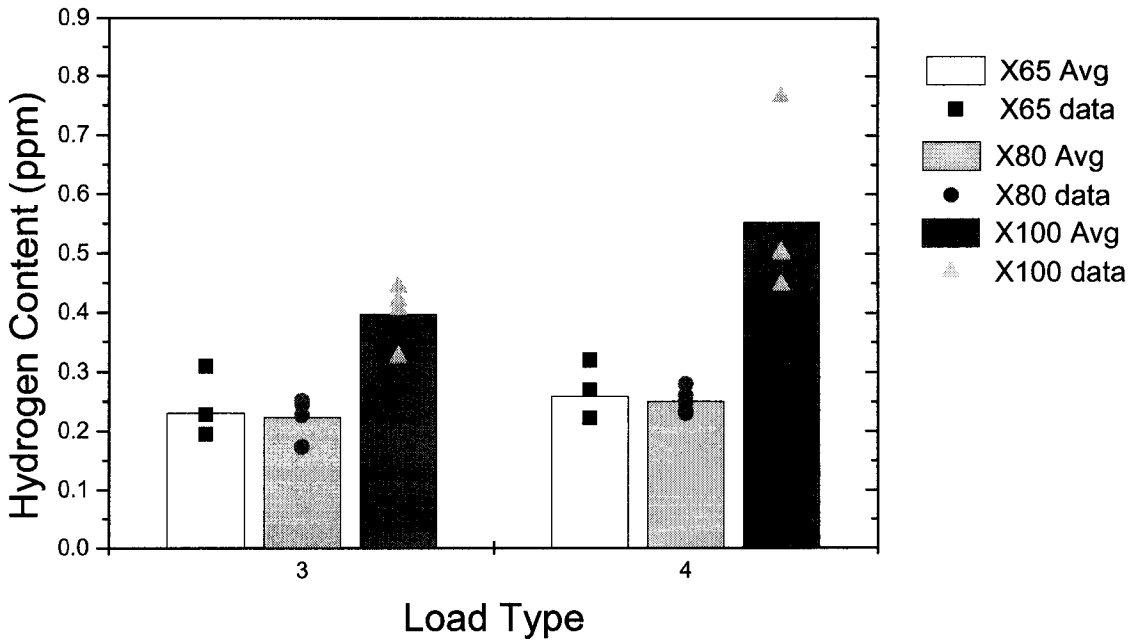

Figure 4-9 Trapped hydrogen contents of samples stressed to 90% YS

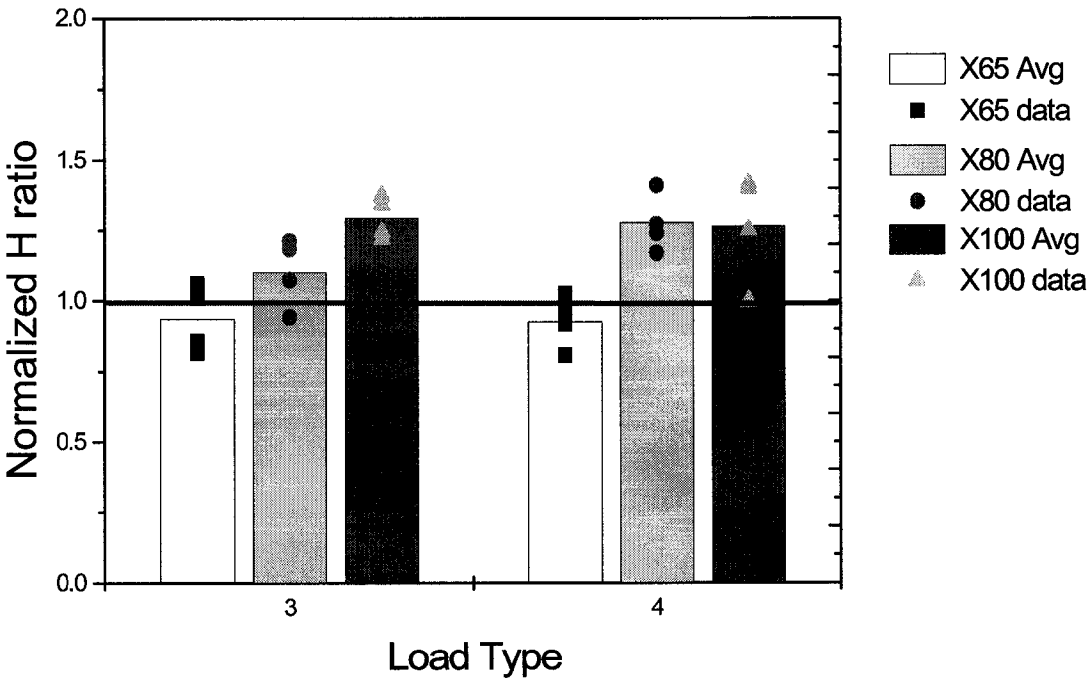

Figure 4-10 Normalized diffusible hydrogen ratios of samples stressed to 90% YS

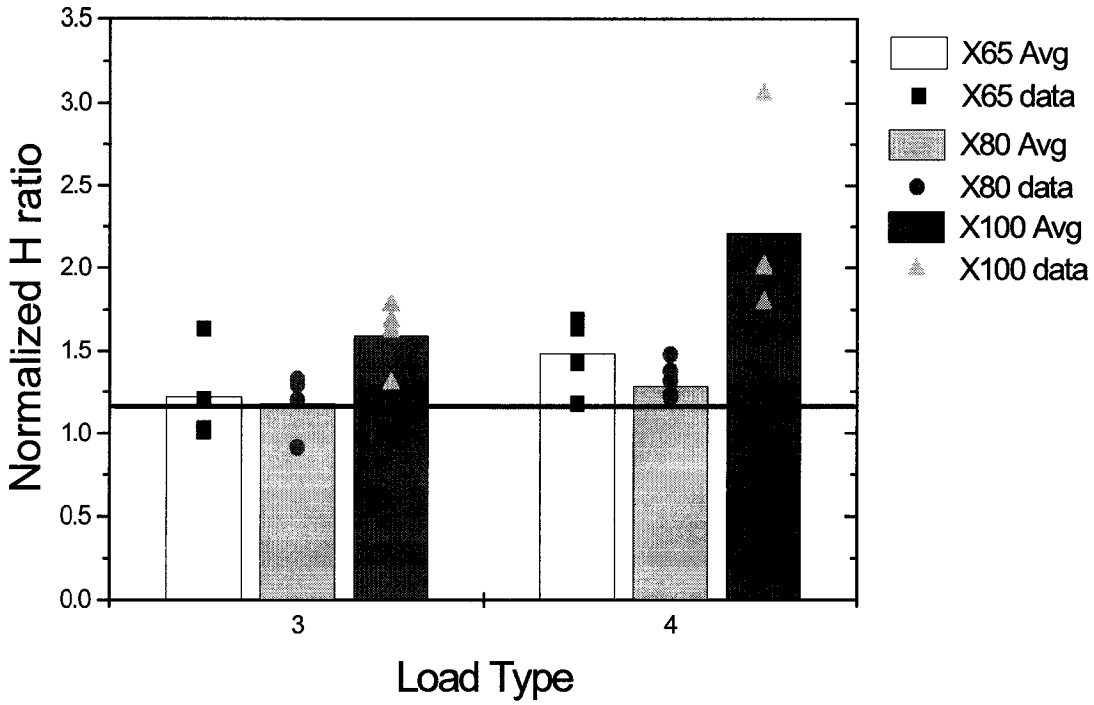

Figure 4-11 Normalized trapped hydrogen ratios of samples stressed to 90% YS

4.4 Effect of charging with stressing

As the fourth stressing condition (100 cycles at R=0.1 then hold maximum load for 24 hours) was the most severe, this stress condition was done first. In this stressing scheme, only the lower grades of steel were able to withstand the complete stressing regimen. The trapped hydrogen contents of the three steels with pre-charging then concurrent charging and stressing, as well as the trapped from the prestressed samples are given in Table 4-5, and summarized in Figure 4-12, as stress conditions 4 and 5 respectively. They are then normalized with respect to the as received steels, as before, with the normalized results given in Figure 4-13. It should be noted that most of the X100 samples on which this was attempted fractured before the testing could be competed.

Only the first of the seven samples tested did not fail before it had undergone the full stressing cycle. Table 4-6 gives the hydrogen content with failure details. As 2% strain prior to stressing was too severe a testing condition for the X100, the testing was carried out at 90% YS as with some of the earlier prestressed samples. These results are summarized in Table 4-7.

Table 4-5 Trapped hydrogen contents at 2% strain and with pre-charging

Grade	2% strain 100 cycles at R = 0.1 and hold at max load for 24 hours	90% YS 100 cycles at R = 0.1 and hold at max load for 24 hours	2% strain 100 cycles at R = 0.1 and hold at max load for 24 hours with precharging
X65	0.22	0.22	0.33
	0.23	0.27	0.43
	0.25	0.32	0.35
	0.26	0.22	0.33
Avg	0.24	0.26	0.36
X80	0.29	0.26	0.43
	0.34	0.23	0.47
	0.25	0.25	0.56
	0.25	0.23	0.51
	0.29	0.28	0.87
	0.29		
Avg	0.28	0.25	0.57

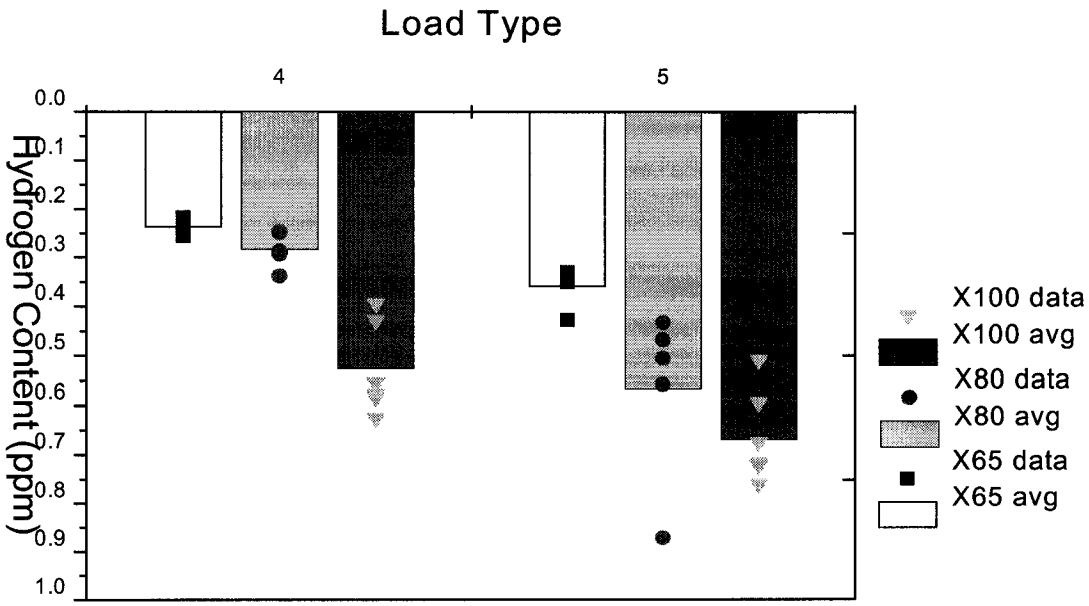

Figure 4-12 Trapped hydrogen contents at 2% strain and with pre-charging

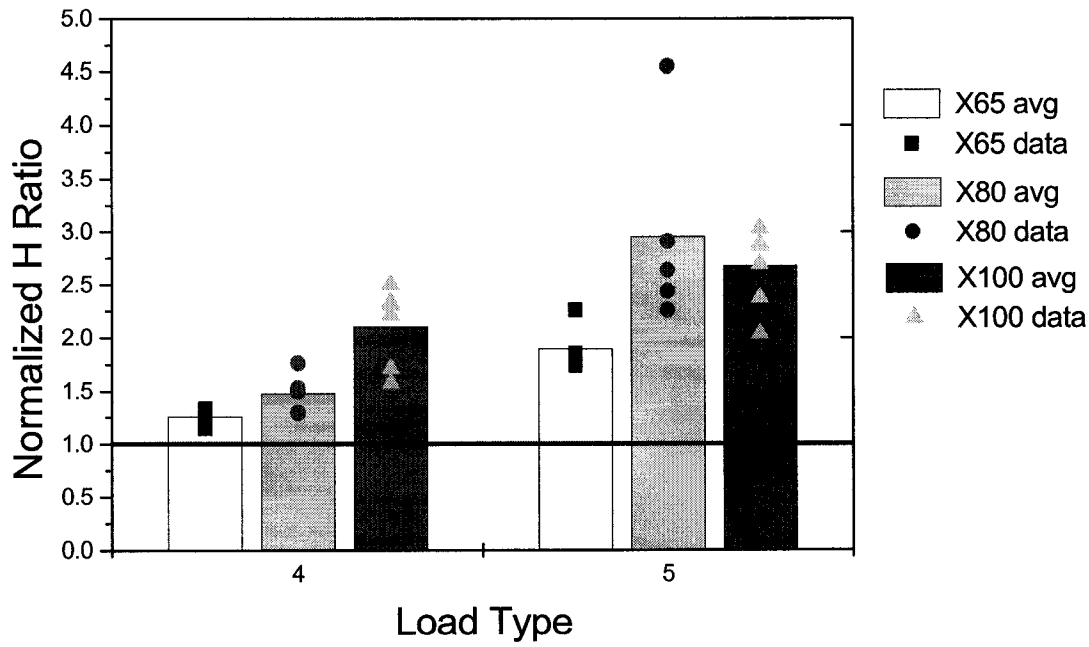

Figure 4-13 Normalized trapped hydrogen ratios at 2% strain and with pre-charging

Table 4-6 Hydrogen content and failure details of the X100 samples

	Time (min)	Event	max stress	[H] trapped
X100 time at fail	1474.264	None	846.5	0.72
	40.91962	6.75 minutes into static	856.0	0.59
	19.18542	56th cycle	867.2	0.51
	19.85565	58th cycle	860.7	0.72
	1.183817	3rd cycle	858.1	0.72
	101.7383	67.6 minutes into static	847.9	0.76
	74.37692	40.2 minutes into static	853.0	0.67

Table 4-7 Trapped hydrogen content of X100 samples

Grade	90% YS 100 cycles at R = 0.1 and hold at max load for 24 hours with precharging
100	0.27
	0.34
	0.29
	0.25
Average	0.29

Since the X100 samples were fracturing before the testing could be completed, it was determined that 2% strain in the gauge length could have been too extreme when compared to the failure strain in this condition. As such, samples of the X100 were precharged for 24 hours, then slow strain-rate tensile tests were performed. The results of these tests are summarized in Figure 4-14 and in Table 4-8 below. As with the as received materials, the tabulated values were calculated from the figure.

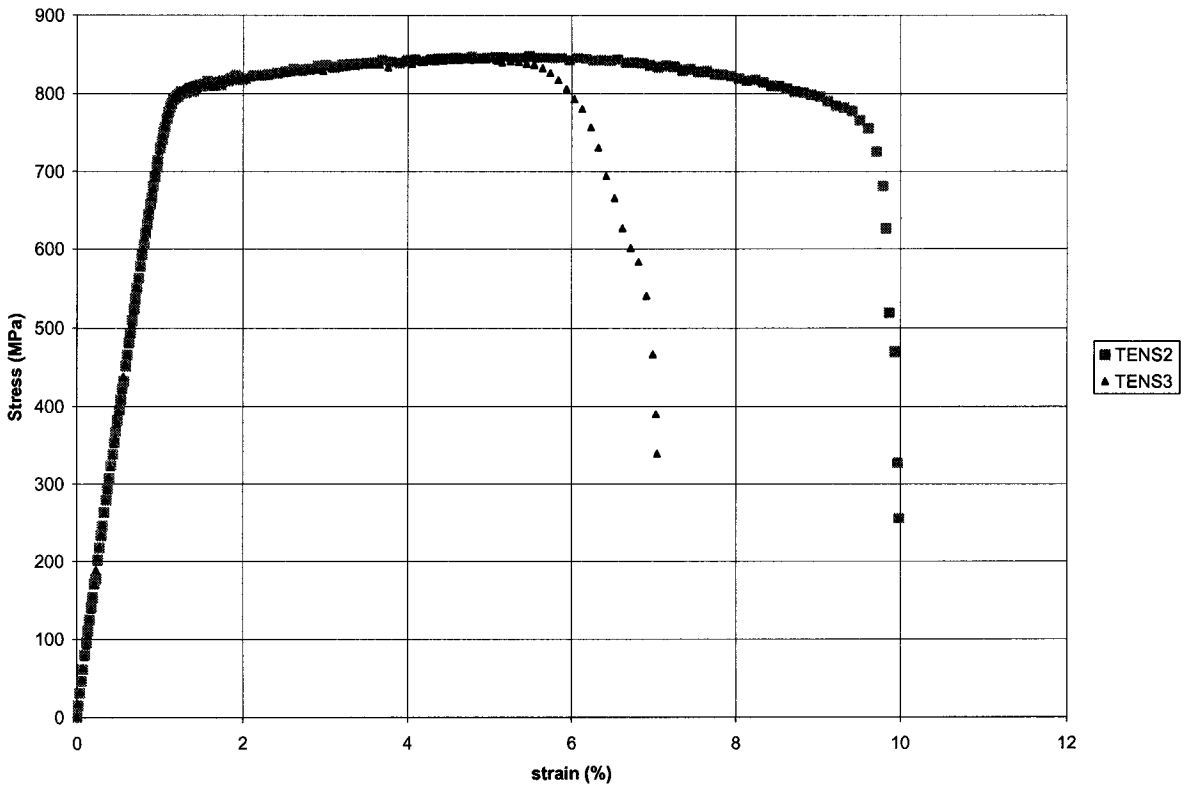

Figure 4-14 Stress-strain curved for X100 precharged

Table 4-8 Mechanical properties of X100 as received and precharged

Grade	σ_{ys} MPa (ksi)	UTS MPa	$\varepsilon_{failure}$ %
Uncharged	785 (113)	853	19.1
Charged	800 (116)	862	8.57

The above two tests were performed without an extensometer on the samples, and as such the strain rate was slightly different than with previous tensile tests. Tensile tests were performed in air also without strain gauges for comparison of the Young's Modulus. As can be seen from Figure 4-15, the slope of the stress-strain curve is the same for the precharged samples, as well as the samples tested in air without strain gauges. From Figure 4-16 it is obvious that the elastic slope of the curve for precharged specimens was the same as the uncharged samples, and there was only a little increase in the yield strength. Figure 4-17 and Figure 4-18 show that removing the strain gauges from the

tensile tests, all the steels behaved similarly with the reduced slope in the elastic region of the stress-strain curves; in addition, there was little change in the yield strength.

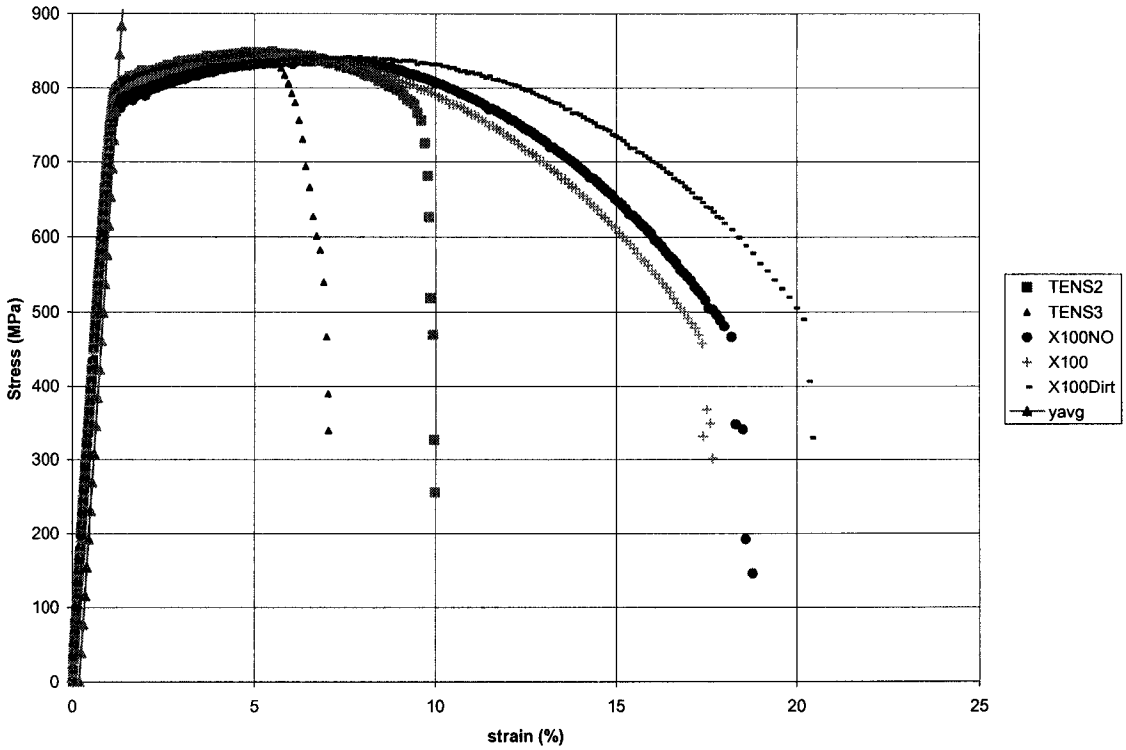

Figure 4-15 Stress-strain curves for X100 without strain gauges as received and precharged

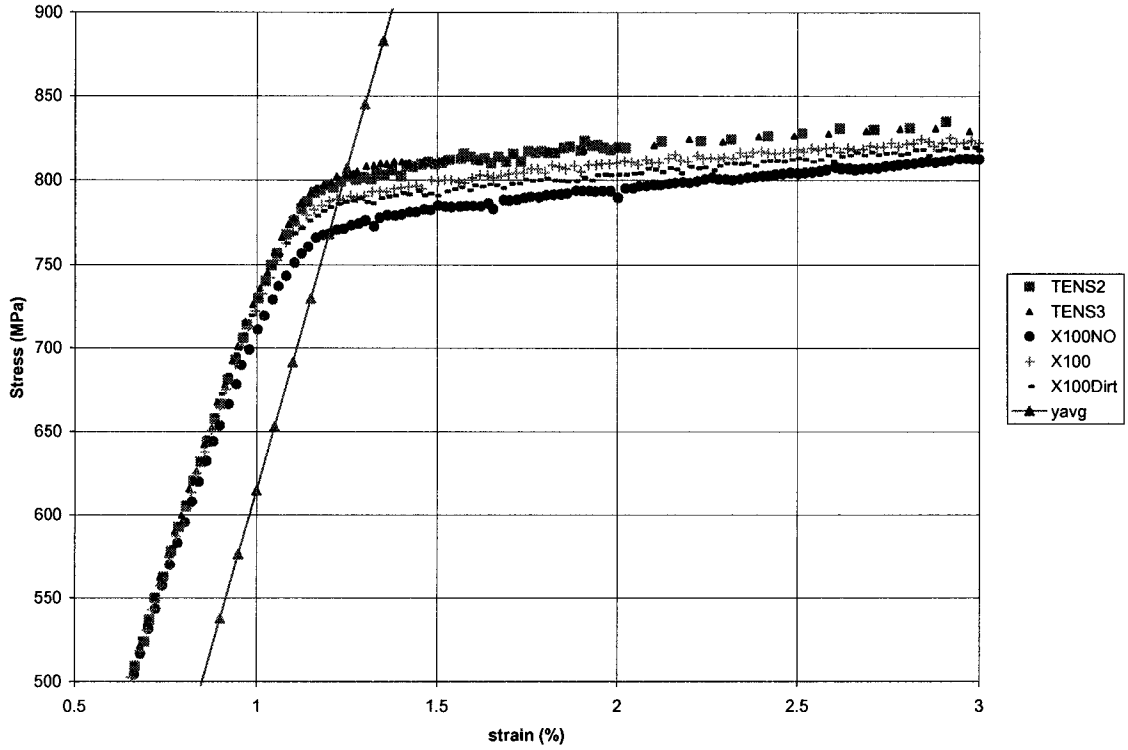

Figure 4-16 Expanded view of stress-strain curves for X100 without strain gauges

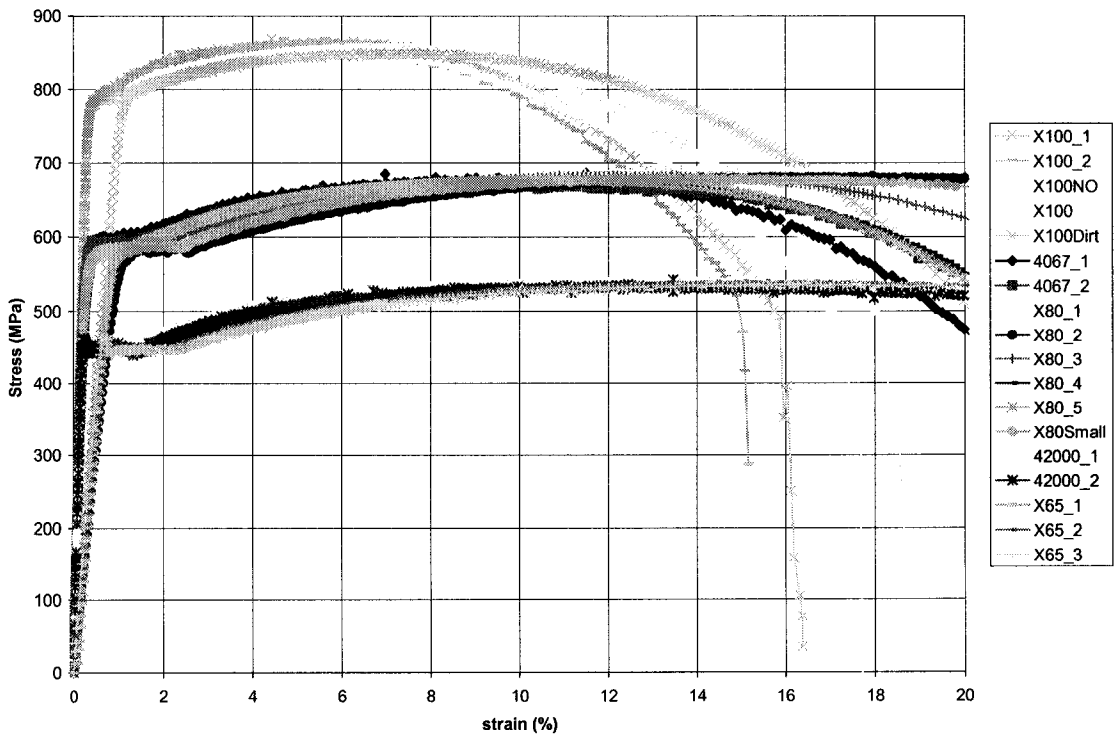

Figure 4-17 Stress-strain curves with and without strain gauges for all steels tested in air

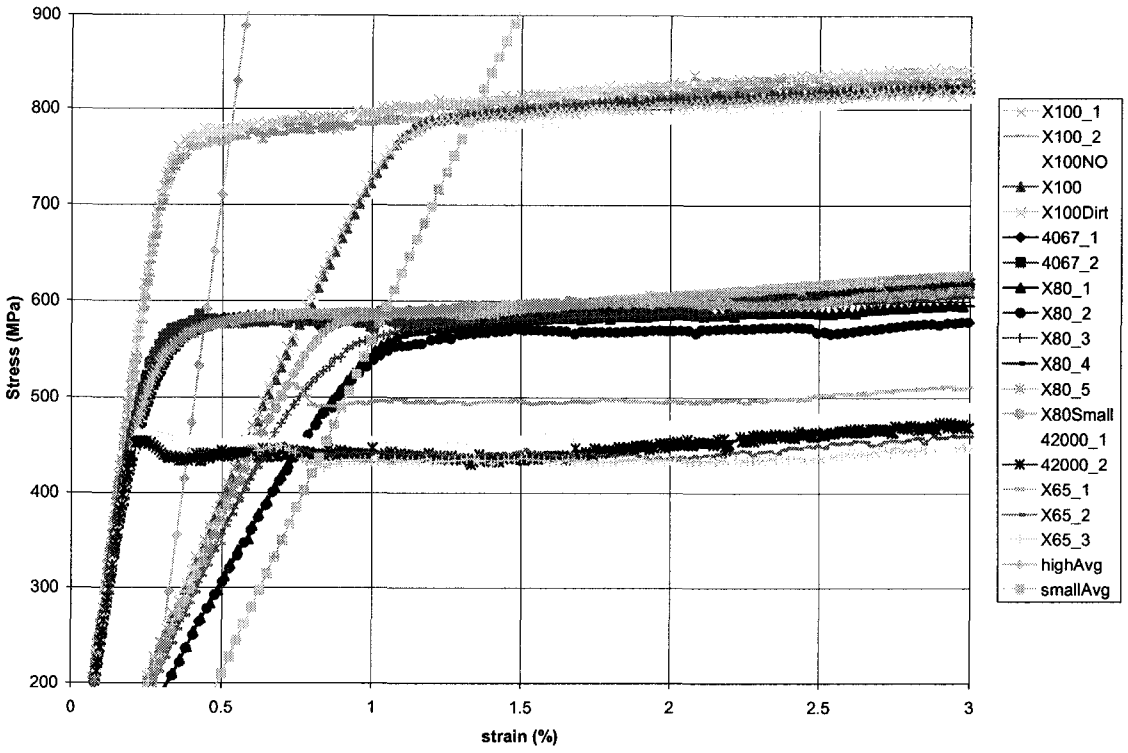

Figure 4-18 Expanded view of stress-strain curves with and without strain gauges for all steels in air

It should be noted that much of the fracture surfaces of the samples which were undergoing the testing regimen looked remarkably similar to the fracture surfaces of the tensile samples; this is shown in Figure 4-19 through Figure 4-22. The ground surface a little away from the fracture surfaces also looked similar to the tensile samples, as shown in Figure 4-25 through Figure 4-26. Similar results of cracking occurring away from the fracture surface was found in Figure 4-27 type 304L stainless steel by Louthan et al. when tested in 10,000 psi H_2.

Figure 4-19 Fracture surface of X100 concurrent sample #6 (low mag)

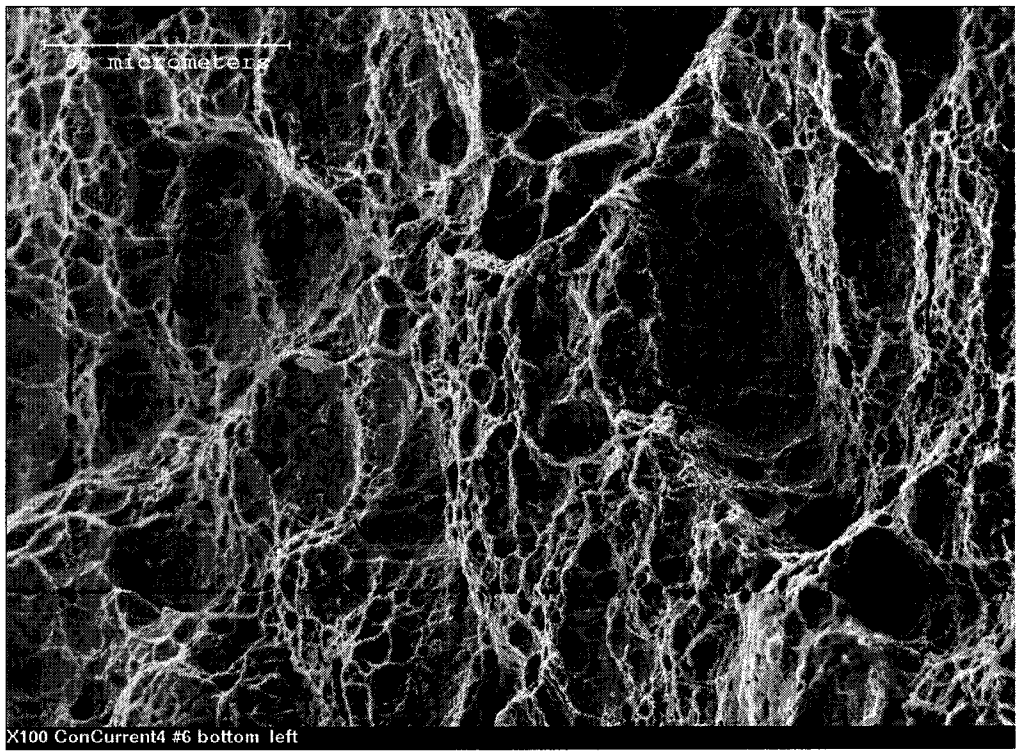

Figure 4-20 Fracture surface of X100 concurrent sample #6 (high mag)

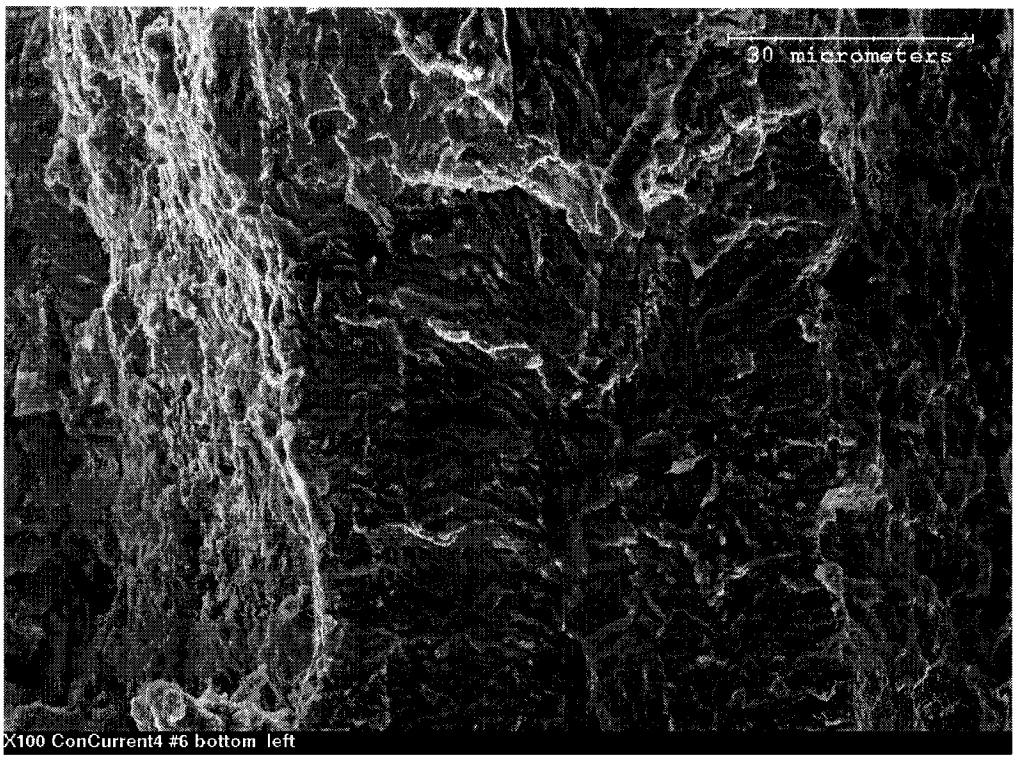

Figure 4-21 Fracture surface of X100 concurrent sample #6 (high mag)

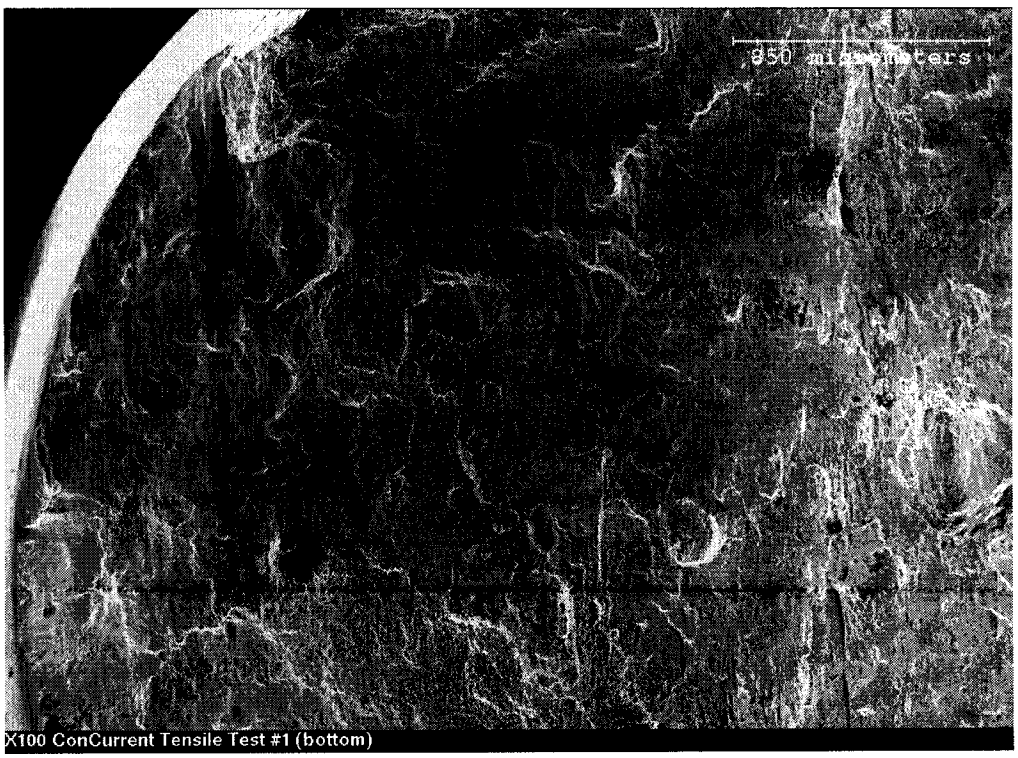

Figure 4-22 Fracture surface of X100 concurrent slow-strain rate tensile test (low mag)

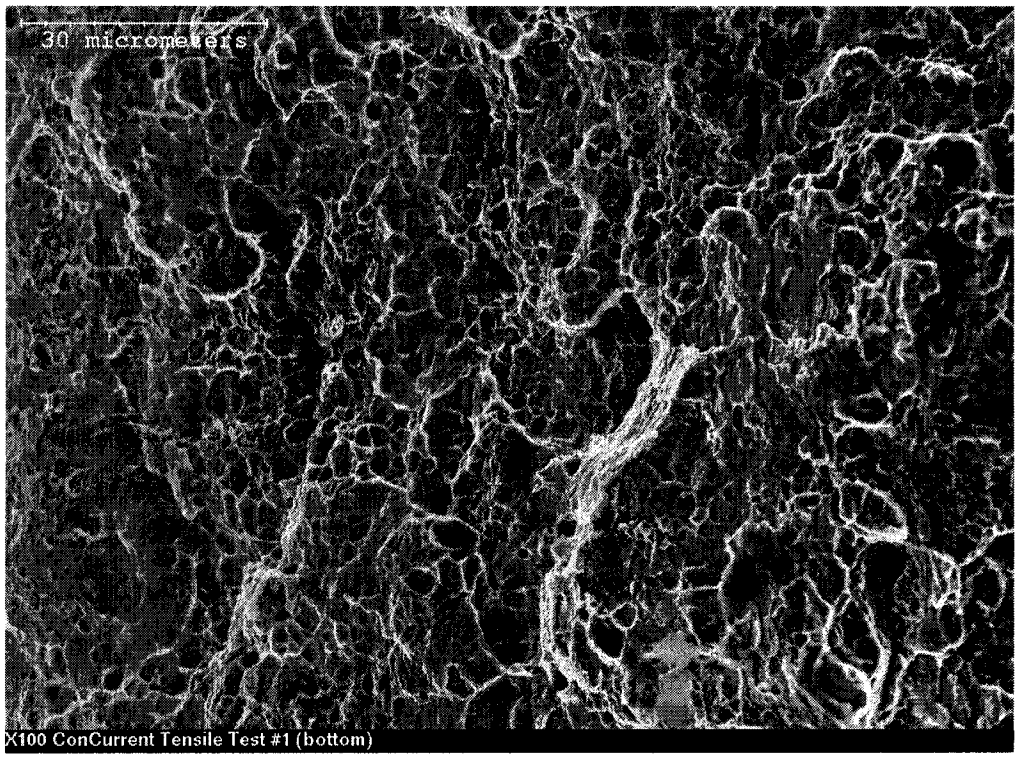

Figure 4-23 Fracture surface of X100 concurrent slow-strain rate tensile test (high mag)

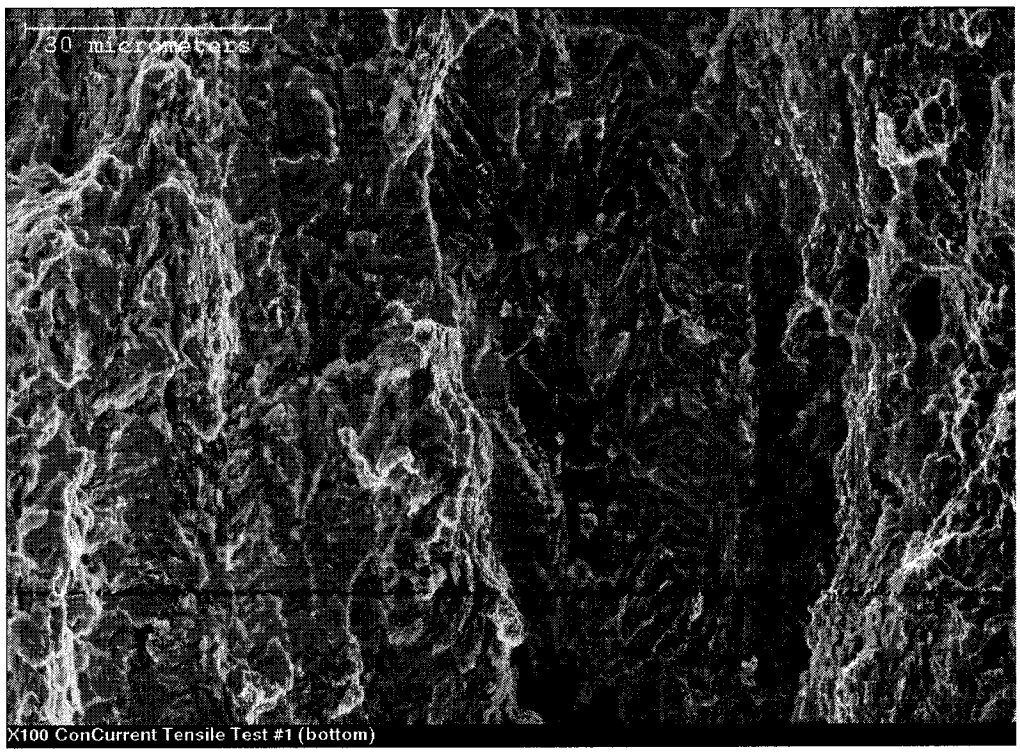

Figure 4-24 Fracture surface of X100 concurrent slow-strain rate tensile test (high mag)

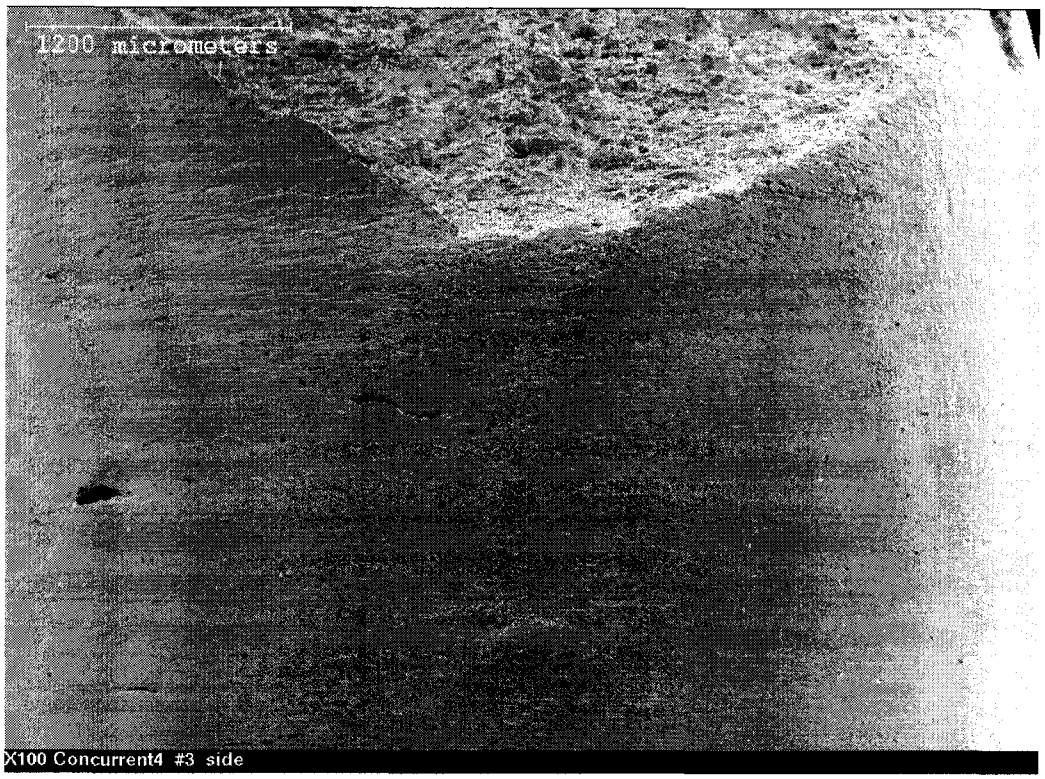

Figure 4-25 X100 concurrent sample #3 surface away from fracture

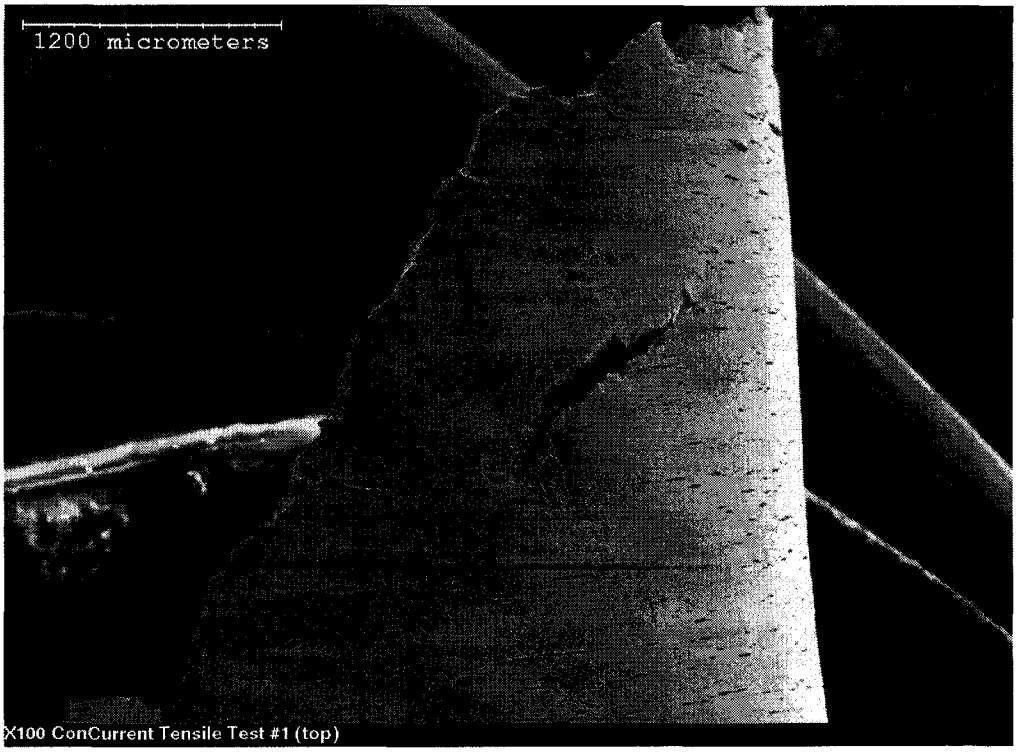

Figure 4-26 X100 concurrent tensile sample surface away from fracture

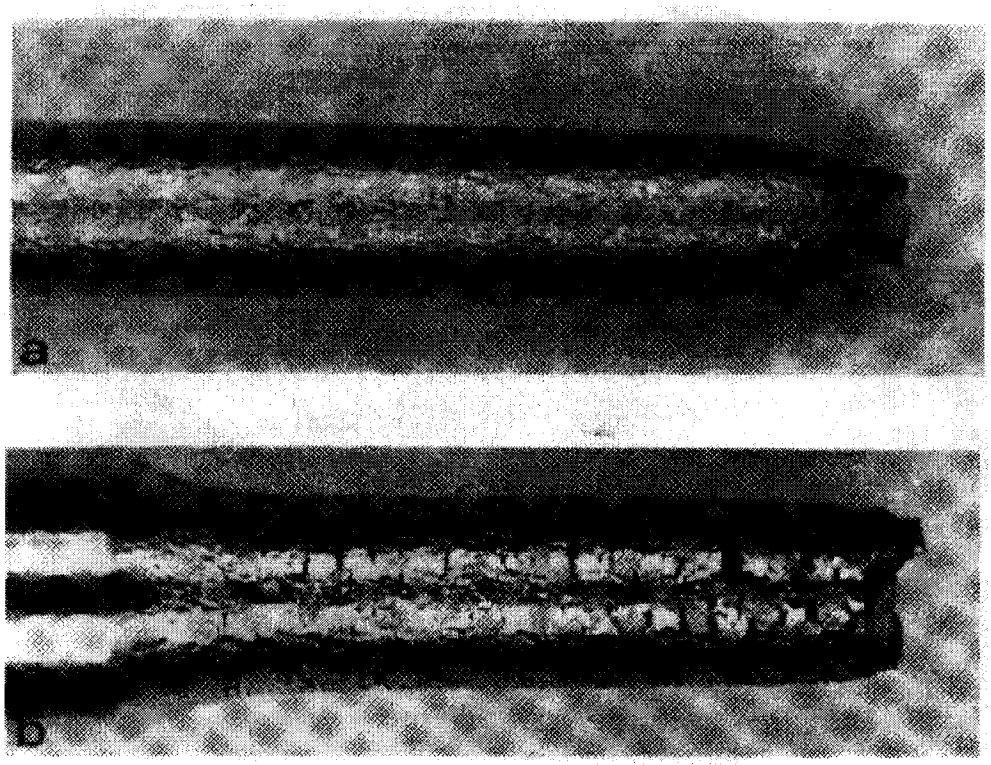

Figure 4-27 Type 304L stainless steel (a) tested in air; (b) tested in 10,000 psi H_2 [Louthan et al., 1972]

4.5 Permeation testing

Calculations on the hydrogen permeability were based on the permeation curves obtained as previously described. A permeation curve of each of the steels tested at a current density of 0.075 mA/cm^2 are included in Figure 4-28. Similar curves were obtained for other charging currents. As is clear, after a short delay, there is a rapid increase in the amount of hydrogen detected. This reaches a peak after some time, then the amount of hydrogen detected drops to a steady value. It should be noted that time to reach the peak amount of diffusible hydrogen is always longer in the X100, indicating longer diffusion

paths, though more likely, as indicated from previous sections, more hydrogen being trapped internally.

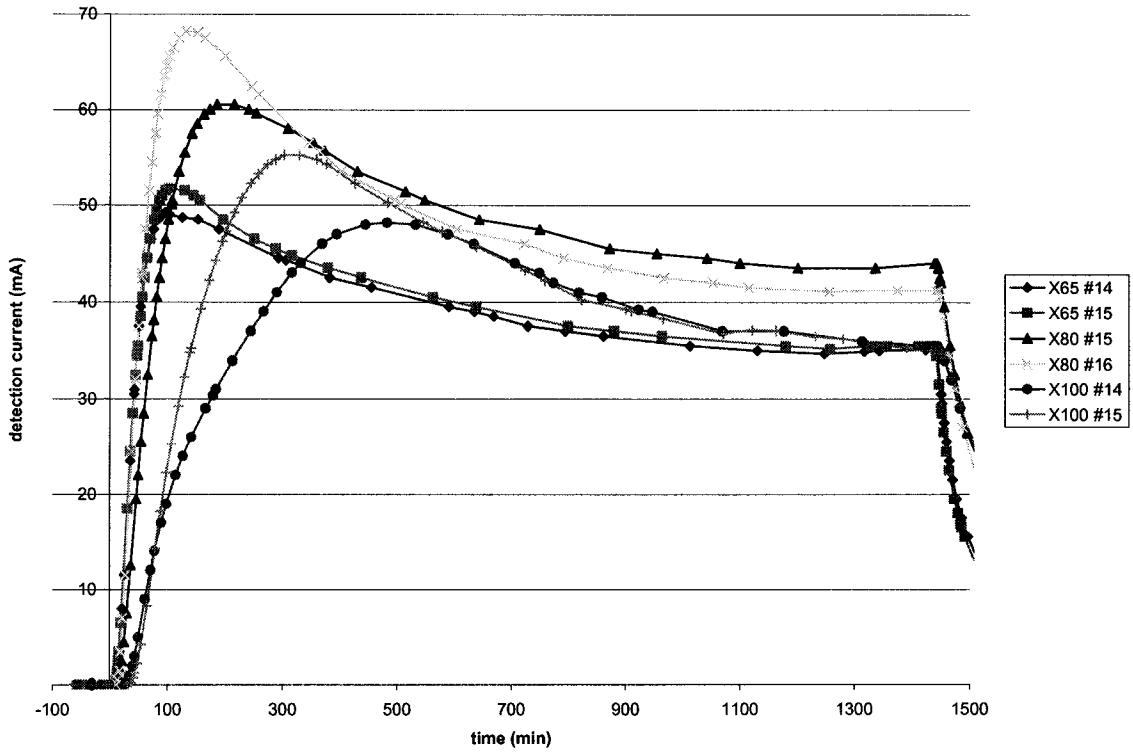

Figure 4-28 Sample permeation curves at charging current density 0.075 mA/cm^2

Diffusion coefficients were measured from the breakthrough time as well as the lag times as defined by Devanathan. These times are shown plotted with the current density in Figure 4-29 and Figure 4-30. The diffusion coefficients were also calculated using both methods. It was expected that the diffusion coefficients would increase with increasing current density; this is seen in both cases as shown in Figure 4-31 and Figure 4-32.

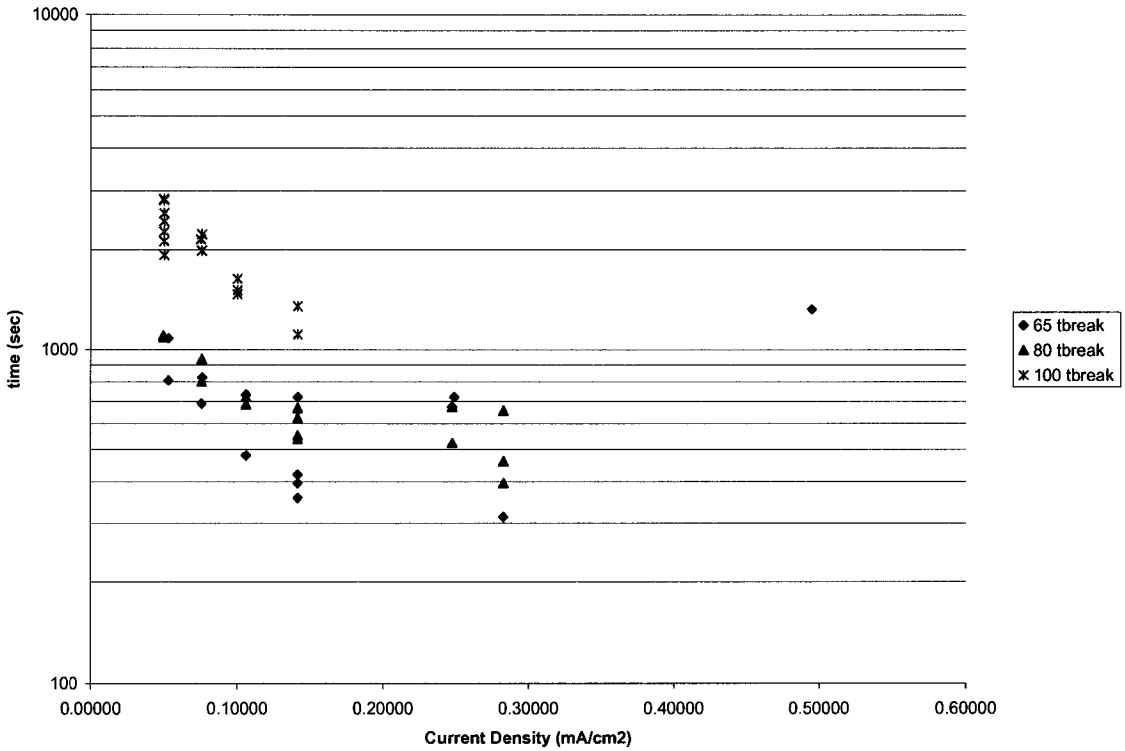

Figure 4-29 Breakthrough times versus charging current density

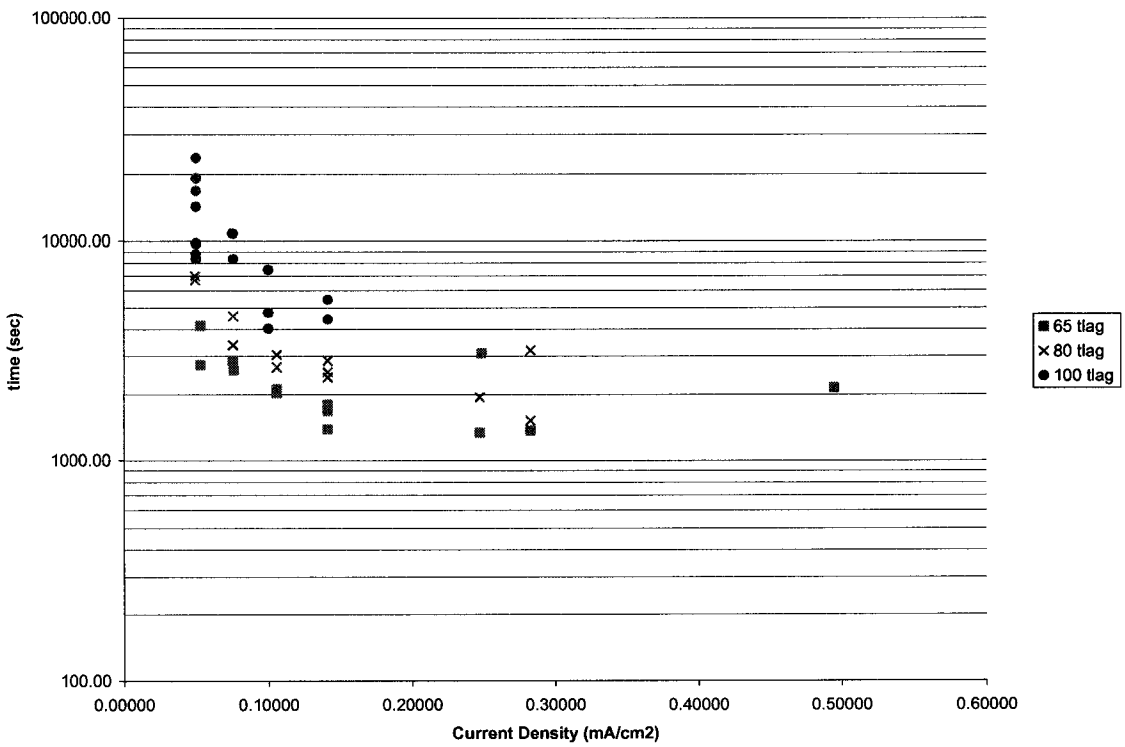

Figure 4-30 Lag time versus charging current density

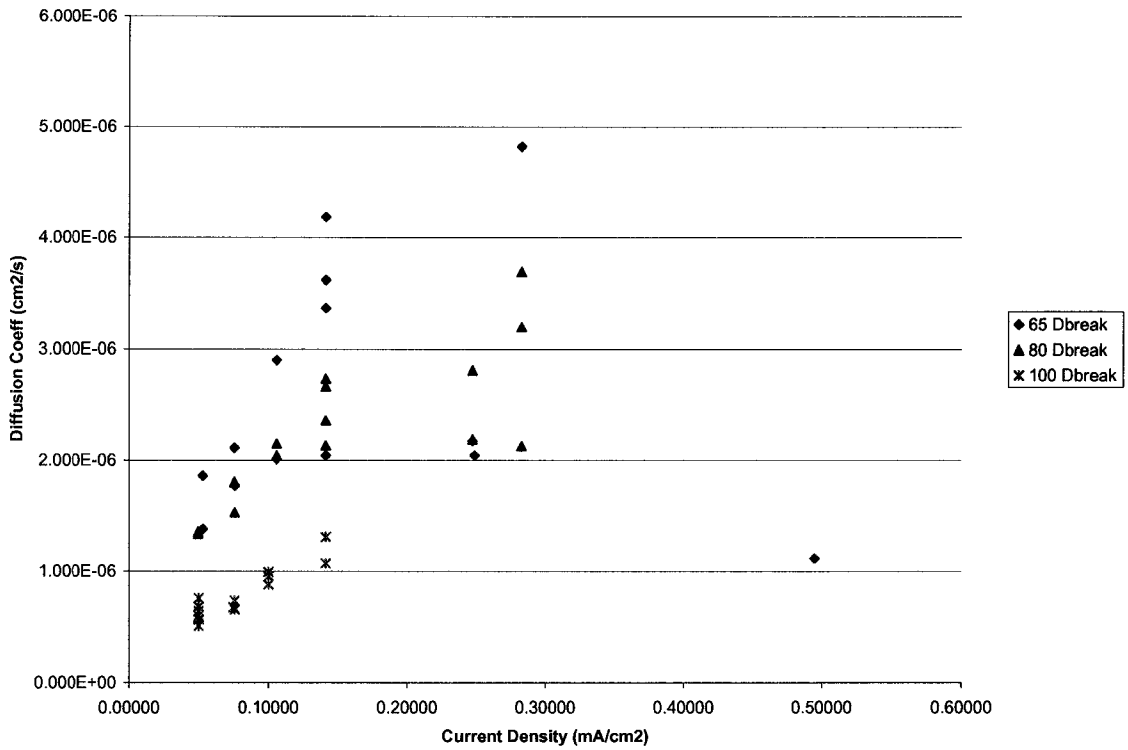

Figure 4-31 Diffusion coefficients calculated from breakthrough time versus charging current density

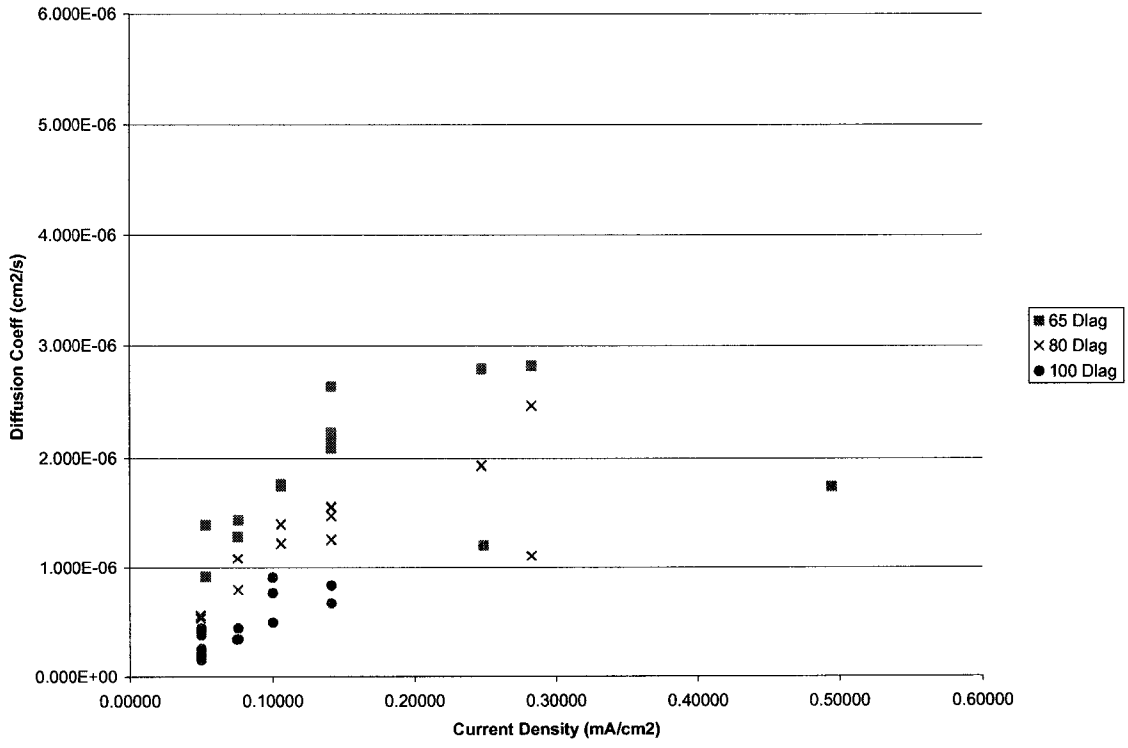

Figure 4-32 Diffusion coefficients calculated from lag time versus charging current density

From the diffusion coefficients, the diffusible concentration of hydrogen adsorbed on the surface was calculated. All results calculated from charging the permeation specimens are given in Table 4-9. The C_o concentrations were calculated using the diffusion coefficients calculated both using the breakthrough time and the lag time for hydrogen permeation.

Table 4-9 Permeation data with calculated diffusion coefficients and hydrogen concentrations[**]

grade	Run#	curdensity	thick (mm)	t break (min)	t lag (min)	peak current	D break (cm2/s)	D lag (cm2/s)	Co break	Co lag
X65	2	0.49505	1.5	22	35.7689	76	1.114E-06	1.747E-06	106.06	67.61
	3	0.24894	1.5	12	51.4739	75.5	2.042E-06	1.214E-06	57.47	96.65
	4	0.24752	1.495	11.2	22.2369	84.6	2.173E-06	2.792E-06	60.31	46.94
	5	0.14144	1.5	12	29.9185	78.4	2.042E-06	2.089E-06	59.68	58.34
	6	0.14144	1.47	7	27.9524	74.6	3.362E-06	2.147E-06	33.80	52.92
	7	0.14144	1.48	6.6	23.0987	70.9	3.614E-06	2.634E-06	30.08	41.28
	8	0.10608	1.5	12.2	35.2849	61.8	2.009E-06	1.771E-06	47.83	54.23
	9	0.10608	1.46	8	33.7507	57.8	2.902E-06	1.754E-06	30.14	49.85
	10	0.05304	1.515	13.44	45.5626	34.9	1.860E-06	1.399E-06	29.46	39.16
	11	0.05304	1.51	18	69.0272	37.3	1.380E-06	9.176E-07	42.31	63.61
	12	0.14144	1.51	5.94	28.4279	52.8	4.181E-06	2.228E-06	19.76	37.08
	13	0.28289	1.52	5.22	22.7614	81.4	4.820E-06	2.820E-06	26.60	45.47
	14	0.07610	1.495	13.74	43.0169	49.2	1.772E-06	1.443E-06	43.02	52.81
	15	0.07567	1.49	11.46	47.6609	51.7	2.110E-06	1.294E-06	37.84	61.69
X80	1	0.14144	1.5	10.4	42.2014	75	2.356E-06	1.481E-06	49.48	78.72
	2	0.14144	1.475	11.12	47.6954	81.4	2.131E-06	1.267E-06	58.39	98.19
	3	0.10608	1.5	12	50.6818	84.6	2.042E-06	1.233E-06	64.40	106.64
	4	0.10608	1.5	11.4	44.4462	73.2	2.150E-06	1.406E-06	52.93	80.92
	5	0.04950	1.5	18.36	111.0109	38.1	1.335E-06	5.630E-07	44.37	105.19
	6	0.04950	1.5	18.12	116.3536	44.55	1.352E-06	5.372E-07	51.21	128.92
	7	0.28289	1.46	10.92	53.1597	72.6	2.126E-06	1.114E-06	51.67	98.61
	8	0.28289	1.495	6.6	25.2382	99	3.688E-06	2.460E-06	41.59	62.35
	9	0.14144	1.5	8.96	39.8651	74.5	2.735E-06	1.568E-06	42.34	73.86
	11	0.24752	1.5	8.72	32.3000	98.2	2.810E-06	1.935E-06	54.32	78.89
	15	0.07581	1.48	15.6	76.2942	60.5	1.529E-06	7.975E-07	60.68	116.35
	16	0.07567	1.485	13.32	56.2054	68.2	1.803E-06	1.090E-06	58.21	96.30
X100	1	0.14144	1.485	22.48	90.8985	71.75	1.068E-06	6.739E-07	103.35	163.84
	2	0.14144	1.49	18.48	73.7577	68	1.308E-06	8.361E-07	80.25	125.58
	3	0.10014	1.48	25.08	79.1582	54.2	9.512E-07	7.686E-07	87.39	108.15
	4	0.10014	1.49	24.42	124.2820	51.1	9.901E-07	4.962E-07	79.69	159.01
	5	0.05007	1.49	40.38	138.9047	9.1	5.988E-07	4.440E-07	23.47	31.65
	6	0.05008	1.49	42.72	318.5933	29.55	5.660E-07	1.936E-07	80.61	235.71
	7	0.05003	1.485	35.22	238.3124	43.25	6.819E-07	2.570E-07	97.60	258.93
	8	0.05008	1.49	32.04	162.3430	39.25	7.546E-07	3.799E-07	80.31	159.54
	10	0.07511	1.485	35.7	179.5613	50.5	6.727E-07	3.411E-07	115.52	227.80
	12	0.05004	1.48	46.8	393.8364	27.875	5.097E-07	1.545E-07	83.87	276.72
	13	0.05000	1.485	37.62	145.6207	39.8	6.384E-07	4.207E-07	95.94	145.60
	14	0.07581	1.49	33	179.2177	48.2	7.327E-07	3.441E-07	101.57	216.28
	15	0.07581	1.49	36.9	138.7689	55.25	6.553E-07	4.444E-07	130.19	191.96
	16	0.04996	1.48	47.16	279.6236	38.1	5.058E-07	2.176E-07	115.52	268.54
	17	0.10014	1.48	27.18	66.9325	43.4	8.777E-07	9.090E-07	75.84	73.22

[**] Note: some runs had to be aborted for various reasons therefore there are missing run numbers.

Normally in permeation testing, the current density is plotted with the blister density. The blisters were not counted in this set of testing as they varied in size as well as number. The size varied to such a degree that in some cases, the blisters overlapped to such a degree that they were indistinguishable from one another. There was no accurate method available to calculate the surface area covered by blisters on all the samples. Therefore, the samples were examined only for the presence of a blister. It was determined from qualitative observations that no blisters would form on the surface of any of the steel at 0.05 mA/cm^2 but at a slightly higher current density (0.075 mA/cm^2) blisters were seen on the surface of the X100 steel.

After the diffusion coefficients were determined, a quick back calculation was performed using the diffusion equation $L^2 = 15.3tD$ determined that in 24 hours charging time at a current density of 0.05 mA/cm^2, a hydrogen atom could indeed travel past the 3 mm required for saturation of the steel cylinders (round bars and gauge sections). It was therefore determined from this testing that 0.05 mA/cm^2 was an adequate current density to saturate the samples without causing any blistering of the steel. If blisters were possible at this current density at this charging time, then during testing of the tensile samples saturated with hydrogen, fracture would have been observed in all three steels.

From the permeation testing, the time for the hydrogen detection current to start to decay was also determined. This was done by turning off the cathodic charging current, the hydrogen source, but leaving the detection side intact. It was observed, in all cases, that

the detection current remained at a constant value for a few minutes after the charging current was removed. This showed that for a short time after the charging current is removed, there is still sufficient hydrogen on the surface of the metal such that, even though the hydrogen is being "pulled" through the steel to the detection side, there is a high enough concentration of hydrogen that the detection current does not drop. However, eventually the detection current could drop to the steady-state value prior to the introduction of the charging current. Figure 4-33 shows the time for the first indication of drop in detection current as a function of charging current density. As is clear, the minimum time that is required for the detection current to drop greater than one minute. Therefore, the 30 seconds necessary for cleaning between charging and placing in the dry ice bath, no appreciable hydrogen was lost.

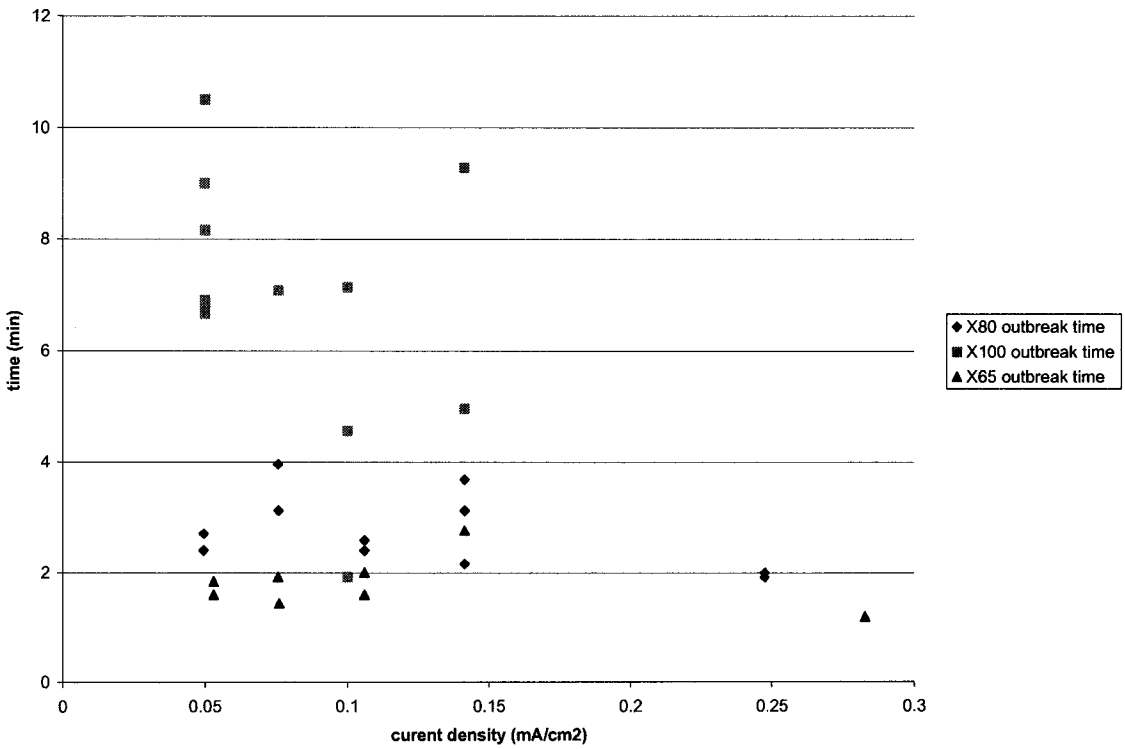

Figure 4-33 Time for detection current drop versus charging current density

5 Discussion

5.1 Materials characterization

As was seen in Table 3-1, there were chemical differences across the steels. The X100 steel had a higher carbon equivalent[††] than the other steels, as seen by the greater amount of C, Mn, Mo, Si, and Ni, making it more hardenable. The X80 also had more alloying than the X65 as was seen by the greater amount of Ti, Al, Nb, Mn and Mo. In Chapter 2 it was mentioned that titanium significantly reduces the permeability of hydrogen. As well, the X100 and X80 were the only grades where boron was detectable, thus making them harder than the X65. The effect of increasing the alloy content on reducing hydrogen uptake was mentioned in Chapter 2 and will be more evident throughout this chapter.

The strain-to-failure showed a marked decrease with increasing strength. As well it was seen that the yield-point phenomenon was reduced going from the X65 to the X80 and all but disappeared completely in the X100. In steels, the yield point phenomenon is known to disappear in the high-strength low-alloy steels on reloading, when the material has been previously strained past the yield point.[86] It is well known that with increasing cold work, the stress-strain behavior of steel is changed. The ductility is reduced, the yield and ultimate strengths, and the discontinuous yielding behavior disappears as the cold work is increased.

[††] The Carbon Equivalent formula for the weldability of steels shows the effect of composition on hardenability. $CE = \%C + \frac{\%Mn}{6} + \frac{\%Cr + \%Mo + \%V}{5} + \frac{\%Si + \%Ni + \%Cu}{15}$

5.2 Effect of time

The relative amounts and the binding energies of the various types of traps that can be present in different steels determine the amount of hydrogen that can enter into and will stay in a charged steel sample. As was seen, prior to stressing the steels do not have many deep traps for hydrogen so that even when charged for 72 hours, there was no increase in trapped hydrogen. However, across grades, the X100 steel had the most diffusible hydrogen, whereas the X80 and X65 steels had lower, relatively equal amounts. This was most likely due to the similar microstructures in the two lower grades of steel having similar types and densities of low energy traps. This was shown with the trapped hydrogen of the samples prior to stressing.

The large difference in the diffusible hydrogen contents appears to be more closely related to the microstructure due to the previous thermo-mechanical processing. As was shown in the previous chapter, the hydrogen contents of the X65 and X80 were very similar, as were the microstructures, but the X100 was much higher and there was much more scatter in the diffusible hydrogen results.

As can be seen in Figure 5-1 and Figure 5-2 X100 samples that were heat-treated, when the microstructure collapsed, and completely recrsytallized at 650°C, the hydrogen numbers were much lower, and there was much less scatter. With the samples that were heated to the lower temperature, the hydrogen content was again lower, indicating that the locations to which diffusible hydrogen could migrate, such as dislocations, discussed

in Chapter 2, were also lost. While the content was lower, it could also be seen that the hydrogen contents were much more uniform in the two heat-treated subsets of testing. Keeping the steel at 450°C prior to machining seemed to remove and rearrange much of the dislocation structures where hydrogen could migrate, without significantly altering the predominant microstructure. This is evidenced by the relatively constant hardness values in Figure 5-3 as the heating temperature increased, and the similar microstructures in the samples heated to 400°C and 500°C.[‡‡] Scanning electron microscopy could not detect any significant change in the microstructures for any of these samples. They looked identical to the 'as-received' X100. It was also shown the diffusible hydrogen content was much lower for the samples heated to 650°C. As can be seen from the micrographs in Appendix II, the significant microstructure change did not occur until 650°C, at which point there was much recrystallization as well as formation of small precipitates. The light phase, which was a lamellar structure, disappeared in at this temperature. With less interfacial area, which is a location for diffusible hydrogen, as was shown in the 650°C samples.

[‡‡] See Appendix II for procedure of X100 heat-treated samples

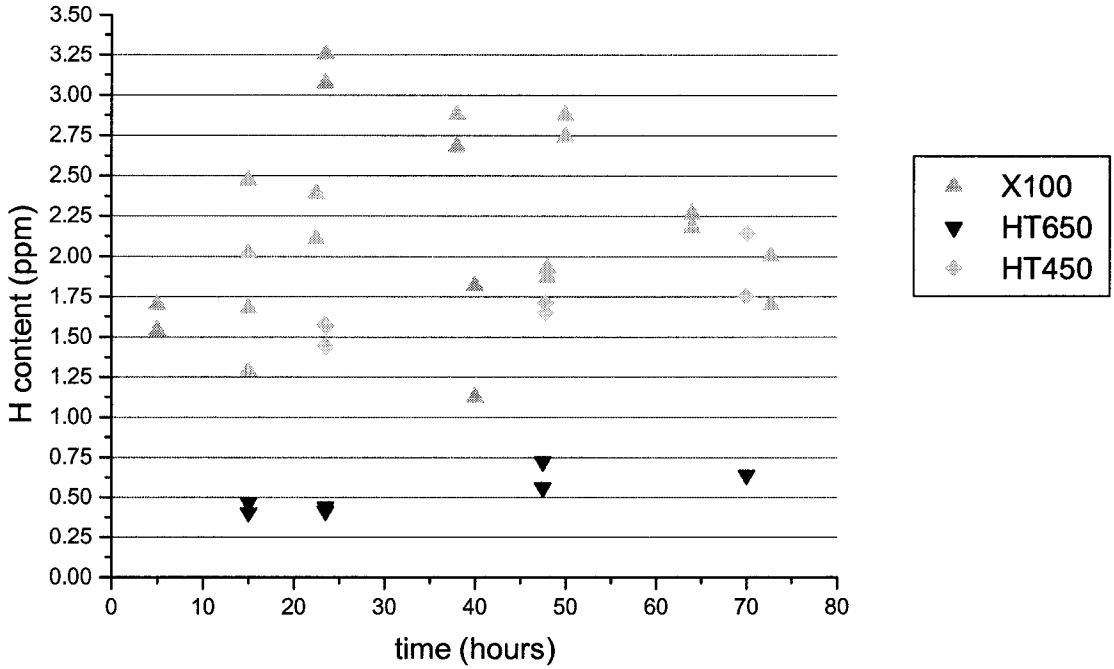

Figure 5-1 Diffusible hydrogen contents of X100 steels without stressing

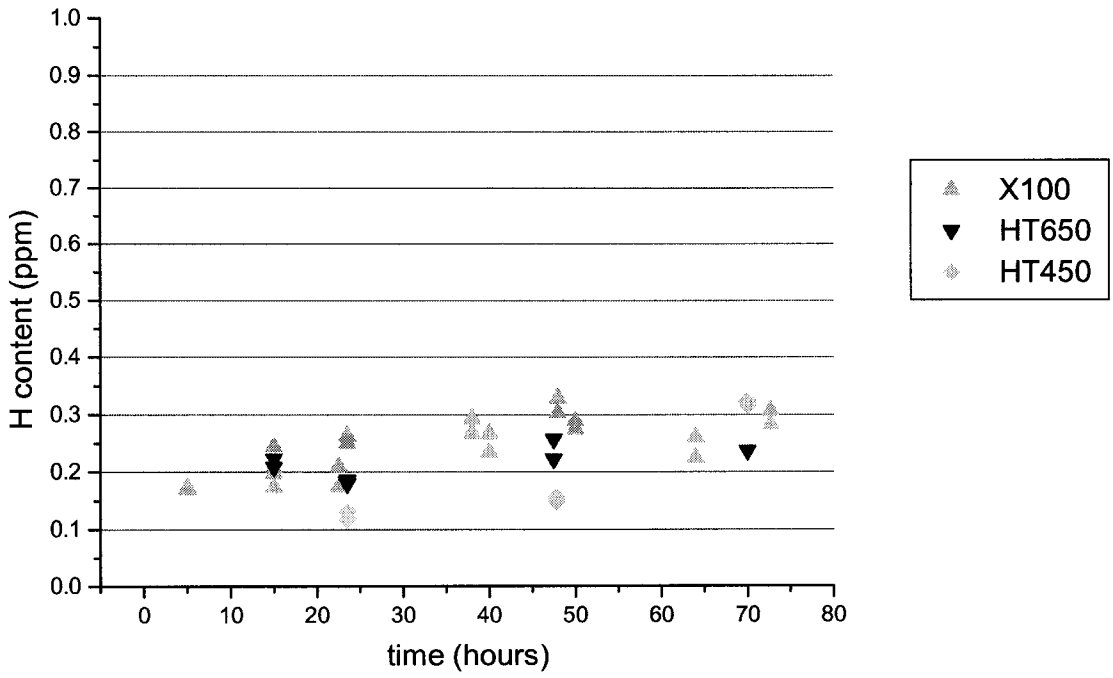

Figure 5-2 Trapped hydrogen contents of X100 steels without stressing

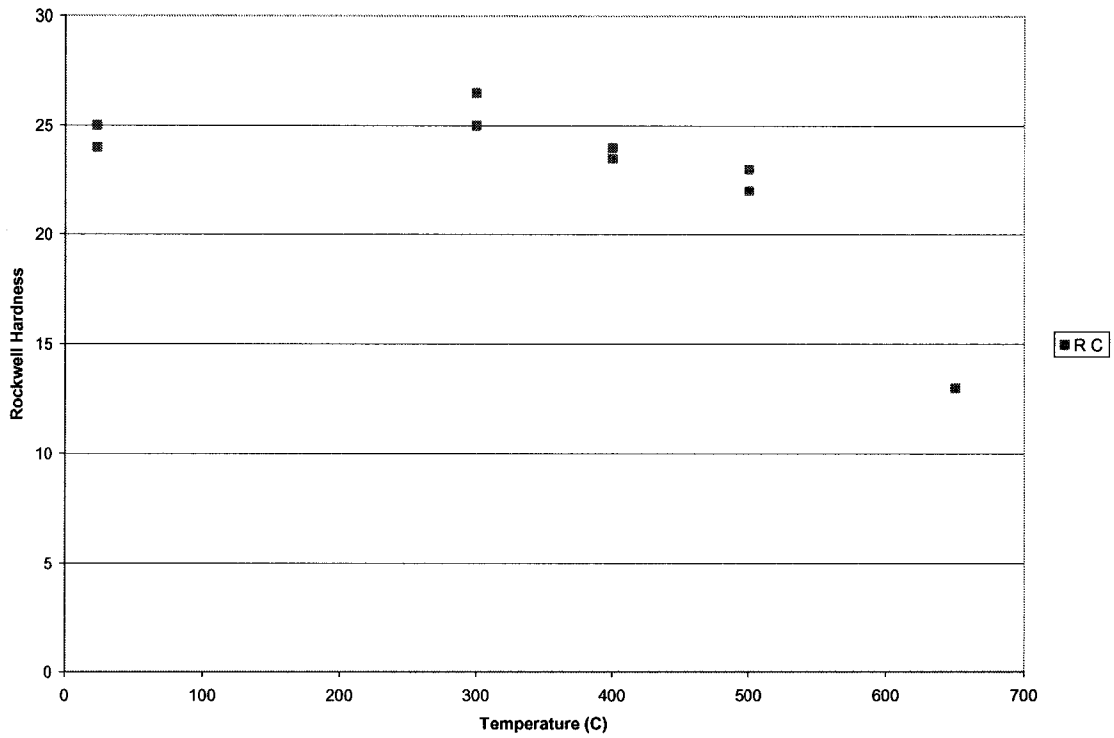

Figure 5-3 Hardness of X100 after heat-treated at various temperatures

When Figure 4-2 and Figure 4-3 are compared to Figure 5-1 and Figure 5-2 it is clear that the hydrogen behavior of the X100 steel when heated to 650°C is closer to the lower grades of steel. When the X100 heated to 450°C is similarly compared, and taking the hardness results from Figure 5-3, it is understandable that this heating retains much of the strength while removing the some of the substructure, and the dislocations that lead to the large scatter that was present in most of the X100 hydrogen results. Thus, it can be said that heating the steel to temperatures up to 500°C for up to 24 hours influences the dislocation concentration, but not the main microstructure. Then the influence of heating the steels on the hydrogen content was greater for the higher heat treating temperatures as the microstructure was changed more at the higher temperatures.

As can be seen from Figure 5-4 the samples that were heated to 450°C still had more diffusible hydrogen than the lower grades, but the samples heated to 650°C had consistently less than the rest of the samples. As was clear from the micrographs in Appendix II and Appendix III[§§], the major changes in X100 microstructure came when the steel was heated to 650°C, and so it followed that this set of samples had the lowest amount of hydrogen. By heating to 650°C, the dislocation substructure was completely destroyed as the samples recrystallized. These new grains in the 650°C samples were now with fewer dislocations, and hence had less hydrogen than the lower grades of steel. The X65 and X80 steels still had more dislocations than the HT650 samples, but the HT450 samples had even more dislocations.

[§§] Appendix III contains micrographs of fracture surfaces as well heat treated samples

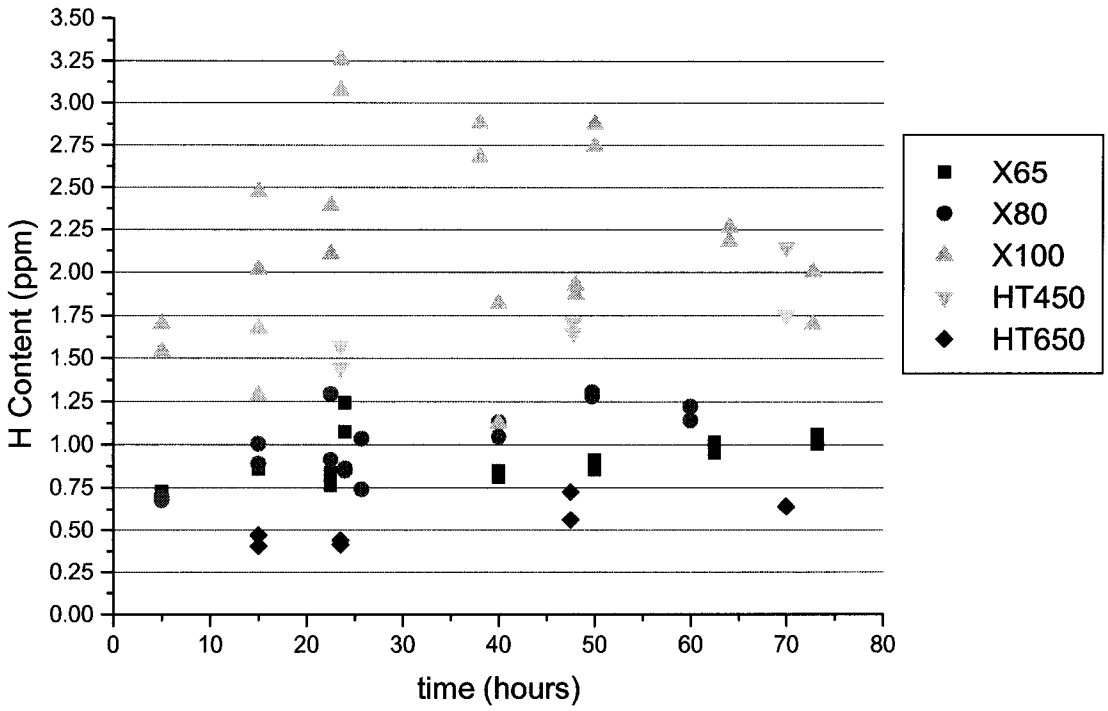

Figure 5-4 Diffusible hydrogen contents of steels without stressing

Further discussion on the steels without heat-treating or prestressing is presented in the permeation testing.

5.3 Effect of plastic deformation

Plastic strain increased the number of both weak and strong hydrogen traps in all steels tested, is shown by the increases in both diffusible and trapped hydrogen. The increase was by differing amounts, depending on the grade of steel. In service, this could lead to very different behaviors with respect to hydrogen when pipes of the various grades are operated to near their various yield strengths. In other words, the response to hydrogen

would be very different even when operated at the same stress level, relative to yield strength.

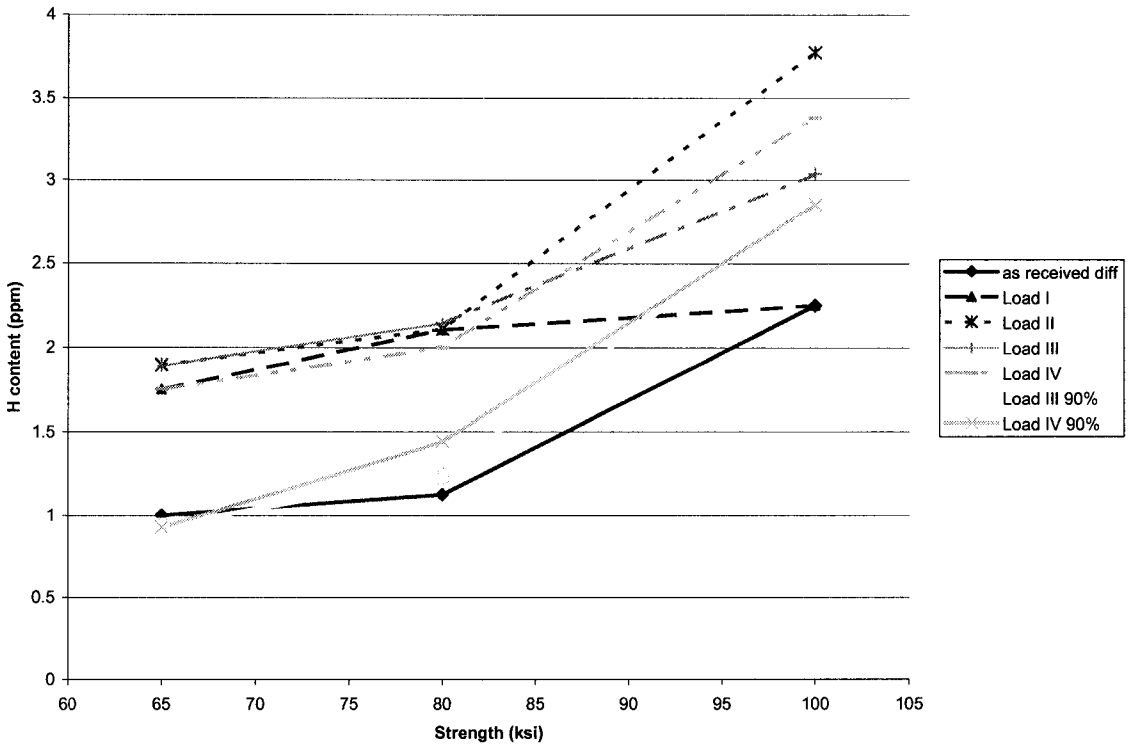

Figure 5-5 Diffusible hydrogen content as a function of grade

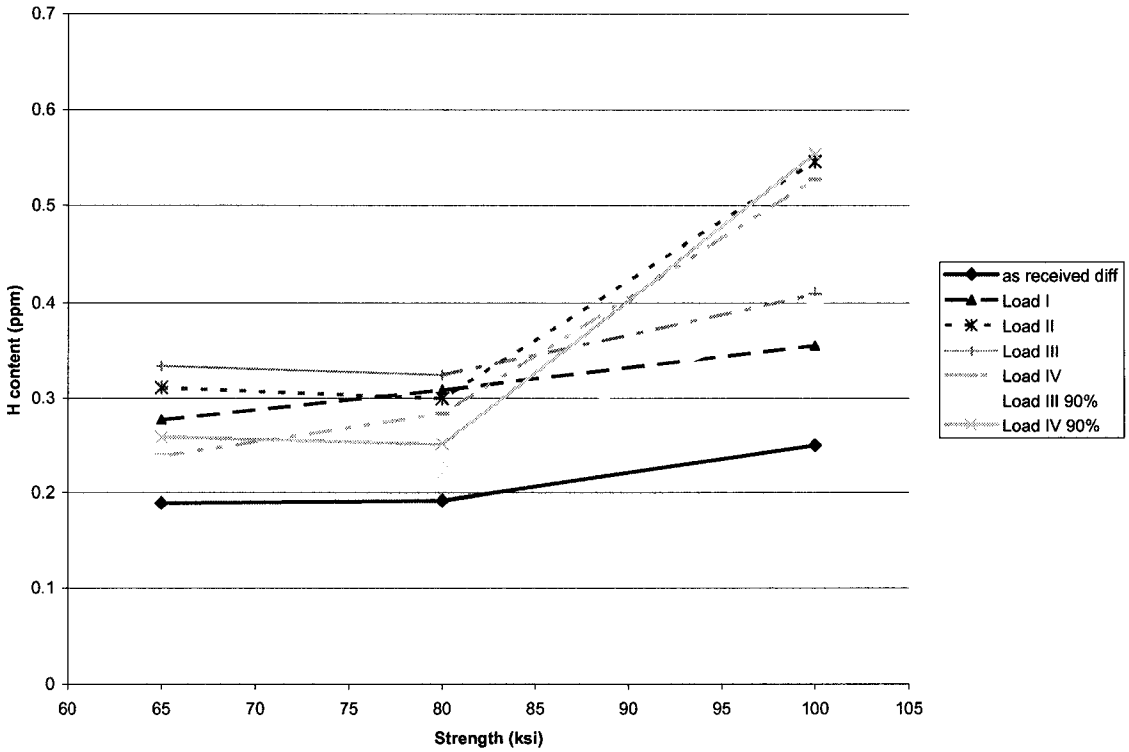

Figure 5-6 Trapped hydrogen content as a function of grade

As was shown previously, dislocations, and/or microvoids, generated due to straining of the samples, in all the stressing conditions, did increase the amount of diffusible hydrogen. The highest absolute hydrogen content was always in the X100 steel. However, when the hydrogen content was normalized with respect to the 'as-received' condition, the largest increase was not in this steel. The plastic strain has more of an effect on the lower grades as a greater percentage of the dislocations contained in the material before charging were introduced from the stressing regimen. As was seen in the microstructures, the X100 had a more discontinuous microstructure, and hence more interfacial area, than the other grades, and as each discontinuity is a potential location for hydrogen, the X100 would therefore have greater absolute hydrogen content. This is

made clear with the average hydrogen content versus grade for the same stressing conditions in Figure 5-5 and Figure 5-6.

Lowering the applied prestress to 90% of the measured yield strength, there was still an increase in diffusible as well as trapped hydrogen. Though, as expected, the increase was not as large as for the samples that were strained with 2% strain. This is because there was little measurable deformation to the samples with the lower stress level. Remarkably, in the higher grades, there was still some activation of possible sites for diffusible and trapped hydrogen as is shown by the hydrogen ratio being greater than 1 in Figure 5-7 and Figure 5-8. In the testing regime at 90% of the yield strength, there was little macroscopic deformation as the testing was below the measured yield strength of the steels. However, there was a measurable increase in the amount of hydrogen accumulated in the samples. This was a result of microscopic strain in the sample that were small enough for hydrogen to accumulate, but too small to be macroscopically measured by the strain gauges. Also microscopically, dislocations could have been generated in the samples at grain boundaries, etc. as was mentioned in Chapter 2.

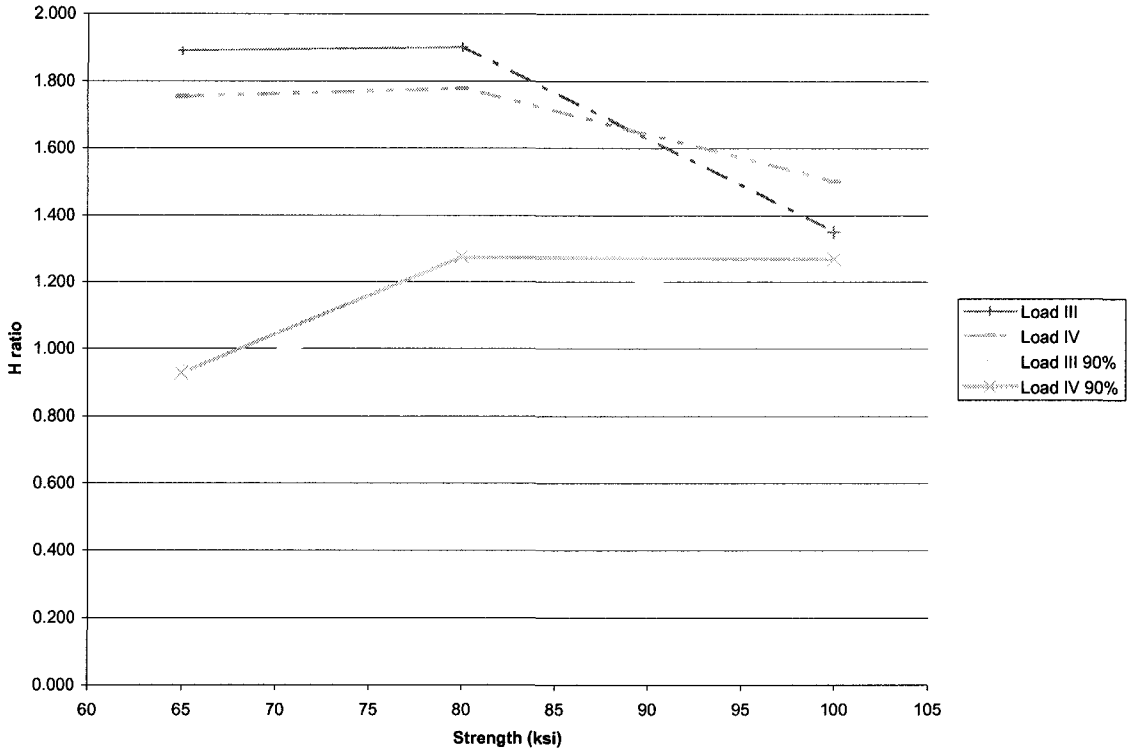

Figure 5-7 Diffusible hydrogen ratio versus strength for selected stress conditions

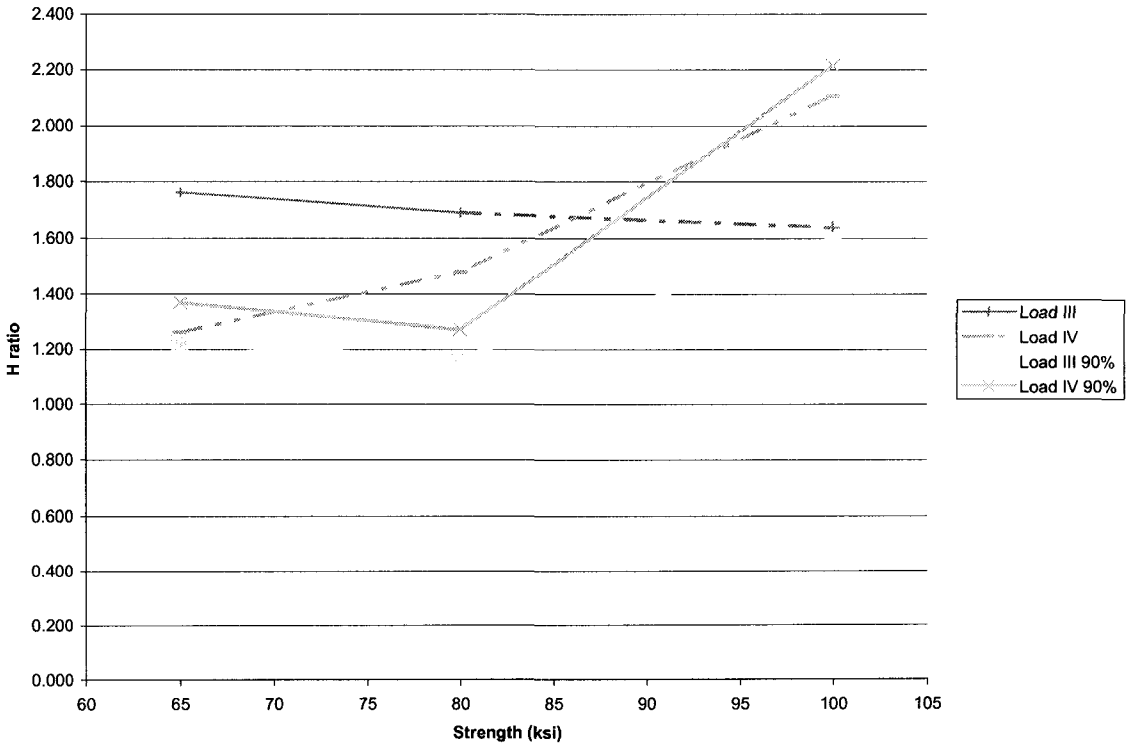

Figure 5-8 Trapped hydrogen ratio versus strength for selected stress conditions

In contrast to the timed only testing, the trapped hydrogen contents also increased in this testing regimen. This was likely due to the activation of strong traps with stressing in all the steels. As was shown in Chapter 4, there was much more interfacial area such as grain boundaries in the X100 than in the lower grades of steel. Each of these interfacial areas are locations to which the hydrogen could accumulate due to residual stresses from the prior stressing. Prestraining introduced plastic deformation at the interfaces between the phases, allowing for easier hydrogen accumulation.

5.4 Effect of charging with stressing

Charging the samples for 24 hours before stressing effectively filled all the possible sites for diffusible hydrogen. This was shown previously with the timed tests. Once the stress was introduced, the sites with stronger binding energy for hydrogen were activated, allowing increase in trapped hydrogen. Again this was shown previously with the prestressed samples, where plastic strain left in the material provided sufficient energy for activation of trap sites. However, keeping the source of hydrogen on the previously hydrogen saturated sample as stresses were introduced to the samples increased the trapped hydrogen content, as is clear from Figure 5-9. The greatest hydrogen content was again in the X100, however, this steel did not have the greatest increase in hydrogen content, shown in Figure 5-10, as there are already many trap sites in the as received material as was previously discussed.

In Fig. 5-8, there is an opposite trend for X-100 stressed to 2% strain and 90% YS. For the stressing to 2% strain, the trapped hydrogen in the pre-charged case is higher than that in the non-precharged one. However, the behavior is reversed for the stressing at 90% YS. As the testing regime at 90% YS is load controlled, not strain controlled, there was little strain in those samples. As well, in the 90%YS tests there was discoloration, likely rust, on the surfaces of the samples that immediately formed as they were removed from the testing apparatus. This thin layer was removed prior to measuring the hydrogen content. On the samples tested at 2% strain, it was impossible to fully remove locations that were rusted as the samples had fractured. In addition, as was seen in the previous chapter, there were openings on the surface away from the actual fracture surface. If there was any rust inside these holes, it was impossible to see or remove. There is a small possibility that hydrogen, either from testing, or washing, could have been trapped in the rust in these areas, leading to higher "trapped" hydrogen contents.

After the gauge length of the samples were saturated with hydrogen, and the samples were stressed, without removing the hydrogen source, but instead keeping a steady supply of hydrogen at the charging surface, it was possible for even more hydrogen to enter the samples. In the previous sections, it was seen that diffusible hydrogen always increased with increased charging time, and since the hydrogen source was not removed, it can be assumed that there is an increase in diffusible hydrogen together with the measured increase in trapped hydrogen. Hydrogen introduced prior to stressing was mostly weakly trapped, diffusible hydrogen, which fills interstitial sites in the lattice of

the steel. As the hydrogen atom is larger than the spacing between the iron atoms in the lattice, there is some strain introduced into the lattice by hydrogen.

If the bonds of the iron matrix require a finite amount of energy to break bonds (see Chapter 2), then the introduction of hydrogen straining the bonds reduces the amount of energy required by other process to break the bonds. Hence, with the X100 steel, when 2% strain was mechanically added to the sample after it was already saturated with hydrogen, only one of the samples did not fail before the mechanical testing was complete. The fracture surfaces for the X100 samples that were charged prior to stressing was identical to the tensile specimens that were charged prior and during testing as well. Referring back to the concept of interatomic bonds in a crystal as springs,[30 31 43] it can be said that to break a spring, or the interatomic bond, sufficient energy would need to be provided to stretch the spring first, then fracture it. With the X100 steel, it could be assumed that hydrogen charged into the sample provided sufficient energy to stretch the spring most of the way, thus when the external stress was introduced, only a small amount of energy was required to stretch the spring the rest of the distance, and fracture it. In other words, the mechanism for fracture of the X100 samples, both the charged tensile tests, and the charged samples that underwent other testing programs, were identical. The fracture was caused by a buildup of hydrogen, as well as the continued migration of hydrogen to the regions where there was high triaxial stress.

Since hydrogen is migrating to these regions of high triaxial stress, it can cause both further lattice distortion, as well as accelerate microcracks. The pressures due to

hydrogen gas buildup are demonstrated in permeation testing by the formation of blisters on the surfaces of the samples. This gas pressure at already strained regions, can increase the chances of microcrack formation even ahead of the crack, as was shown by Troiano.[3] [30] Once a crack is already formed, as more hydrogen from the outside source enters the steel, it recombines ahead of the crack tip, causing further increase in the gas pressure.[86] Since the samples were regular tensile samples, there was not necessarily one particular region of high triaxial stress in the beginning stages of testing. Thus, there could have been many locations along the gauge length of the samples where hydrogen was recombining into hydrogen gas. The hydrogen gas would form in "pockets" giving the fracture surfaces a dimpled appearance, as well as increasing the trapped hydrogen content. This added pressure from the recombination, along with the external stress will increase the crack propagation rates. As can be seen, breaking of the atomic bonds, which lead to microcrack formation and propagation, and finally catastrophic failure, was due to the synergistic action of hydrogen and the external stress.

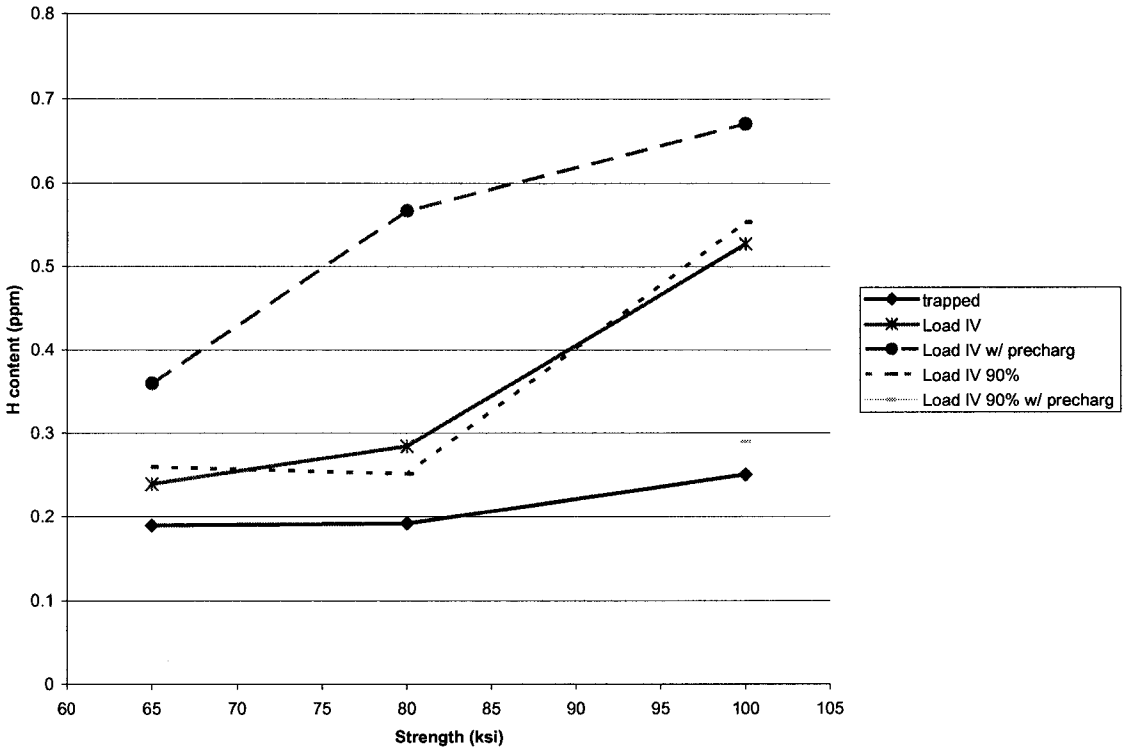

Figure 5-9 Trapped hydrogen content versus grade for selected prestressed and precharged samples

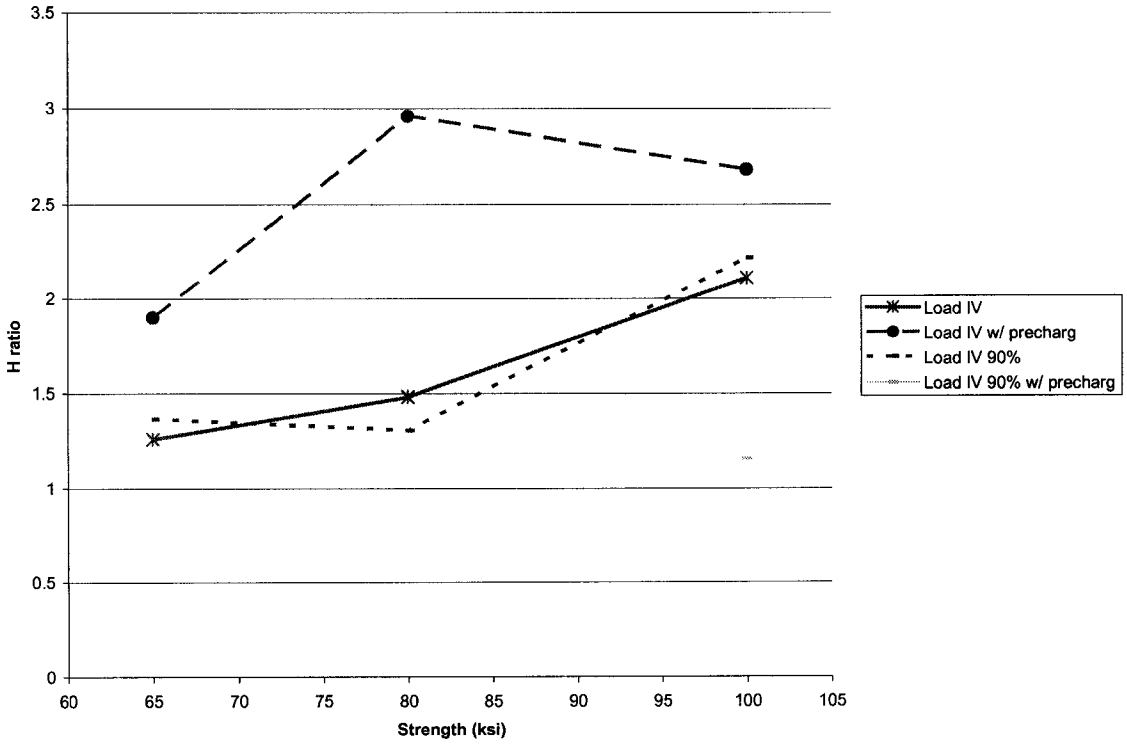

Figure 5-10 Trapped hydrogen ratio versus grade for selected prestressed and precharged samples

The fracture surfaces of the X100 concurrently charged and stressed samples were all at 45° to the applied load. Microscopically, the fracture surface appeared mostly ductile, except for one small region which was brittle. Most of the fracture surfaces exhibited the dimples characteristic of ductile fracture. The small brittle region showed typical cleavage fracture of a brittle material. This was shown in Figures 4-19 through Figure 4-26, and further in Appendix III. However, macroscopically, it was qualitatively observed that there was much less reduction in area normal to the tensile stress than in the uncharged steel. Ideally, it would have been measured, however, many of the fracture surfaces were too long, making it impossible without damaging the fracture surface. As was mentioned in Chapter 2, changes in reduction of area is but one way of measuring changes in mechanical properties after hydrogen charging.

The elongation to failure, as well as other mechanical properties, were measured and tabulated in the previous chapter. As was seen in the X100, there was a slight increase in the yield and ultimate strengths when tested with hydrogen. The changes in strength were minimal, as was found by other researchers; however, the drop in elongation was more noticeable. There was no noticeable change in the Young's Modulus when compared to similarly tested samples in air. The changes in yield and ultimate strengths were small, and close to being within the experimental scatter of the tests.

From the surfaces away from the fracture surface, it was evident that the interatomic bonds were weakened to the degree that without the constraint of adjacent material, the

surface of the steel were failing. Microscopic observation inside these surface cracks did not show a brittle surfaces, but showed many dimpled surfaces. Previous research with stainless steel samples in hydrogen gas had almost identical results as was shown in the previous chapter.

5.5 Permeation testing

Permeation testing with hydrogen is usually done as a method of finding the diffusion coefficient as well as the current density required for the onset of blistering. In this study, it was done as a means to observe the behavior of hydrogen with time. It was shown that the amount of hydrogen diffusing through the steel always increased with charging time, reached a peak, then lowered to a stable value. Blisters were observed in all but the lowest charging current density, which implied that this was sufficiently low to avoid blister formation. Hence, in the previous testing regime, precharging with stressing, there was likely very little hydrogen recombination without the introduction of deformation.

Across all grades tested, the charging conditions were the same, therefore it can be assumed that the number of hydrogen atoms generated due to the various charging conditions were the same. But as has been seen, the hydrogen content was different in all the grades. Additionally, as was seen from Table 4-9, the calculated hydrogen concentration on the charging side (C_o) was different, even when the charging conditions were equivalent. This is shown Figure 5-11 for some of the charging conditions. As is clear, for the same number of hydrogen atoms generated, there is greater diffusible hydrogen in the steel system as the grade is increased.

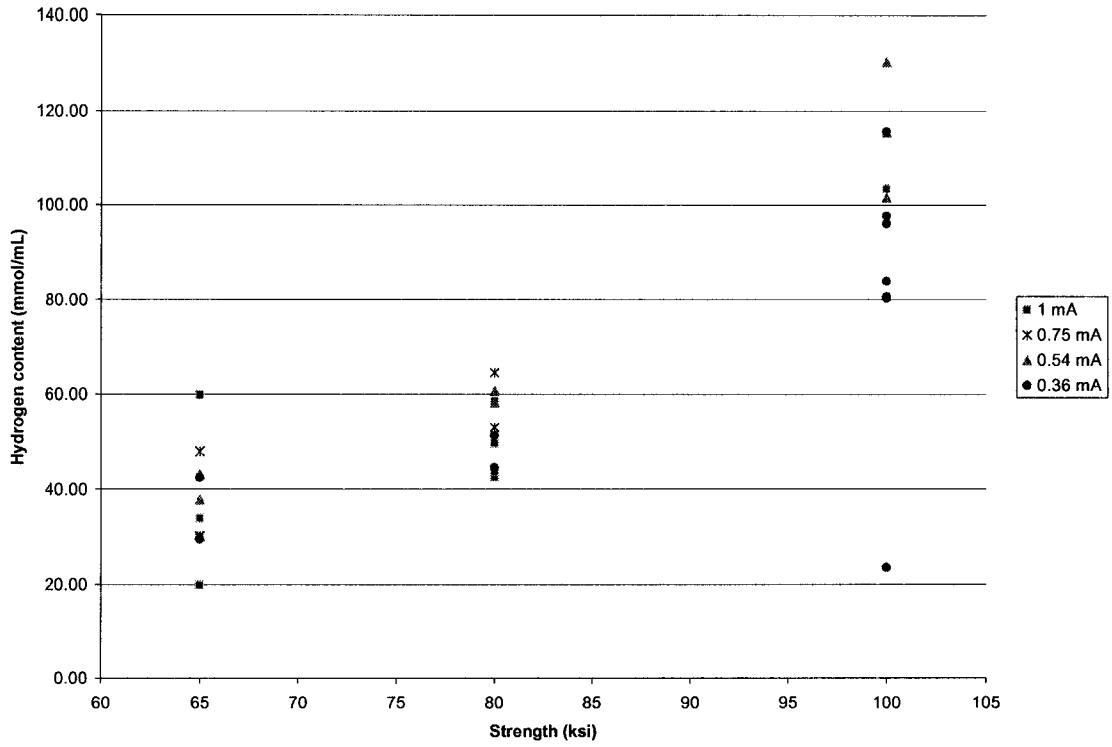

Figure 5-11 Hydrogen concentration on charging side calculated using breakthrough times

Figure 3-1(b), Figure 3-2(b) and Figure 3-3(b) show the microstructures of the three grades of steel in the direction of permeation testing. The varying microstructure played a large part in hydrogen trapping. As well, the dislocations generated due to the controlled rolling played an additional role adding trapping sites for hydrogen as was discussed in Chapter 2. This is evident in Figure 5-12 which shows that the X100 with the non-uniform microstructure had a longer breakthrough time. As well, the X80 had a slightly higher breakthrough time than the X65 steel. It is evident from the figure above that there was more diffusible hydrogen in the system of the X100 steel for the same charging conditions, however, the longer breakthrough times can only be attributed to the

additional trapping sites that are present. The additional trapping sites in the X100 were also evident in the tensile samples that were tested as was shown in Figure 4-5 and Figure 4-9.

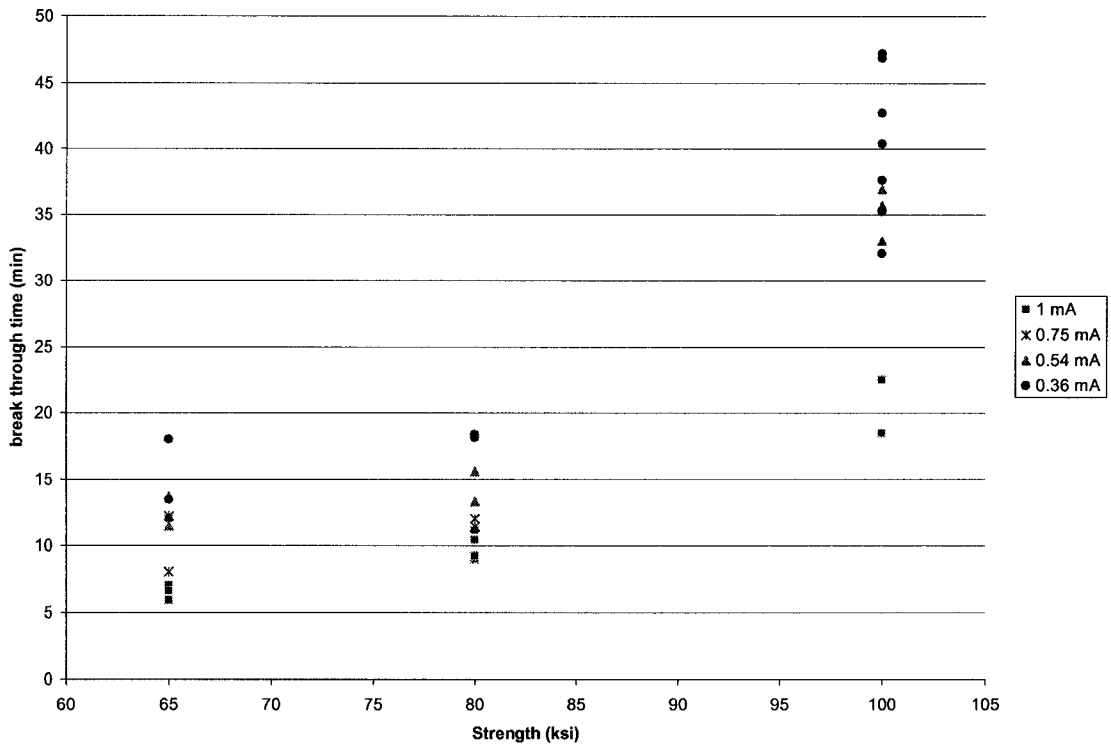

Figure 5-12 Breakthrough times for selected permeation tests versus grade

In addition to the higher breakthrough times, the X100 steel also had the lowest peak detection current as is shown in Figure 5-13. From this it is even more evident that more hydrogen was trapped in the X100, hence the higher breakthrough times that were shown in Figure 5-12. As was mentioned in the earlier discussion, this is most likely due to the non-uniform microstructure, as the lower grades had more uniform microstructures, and also less trapped hydrogen. From the above discussions, it is clear that the X100 steel always has the most hydrogen present in it.

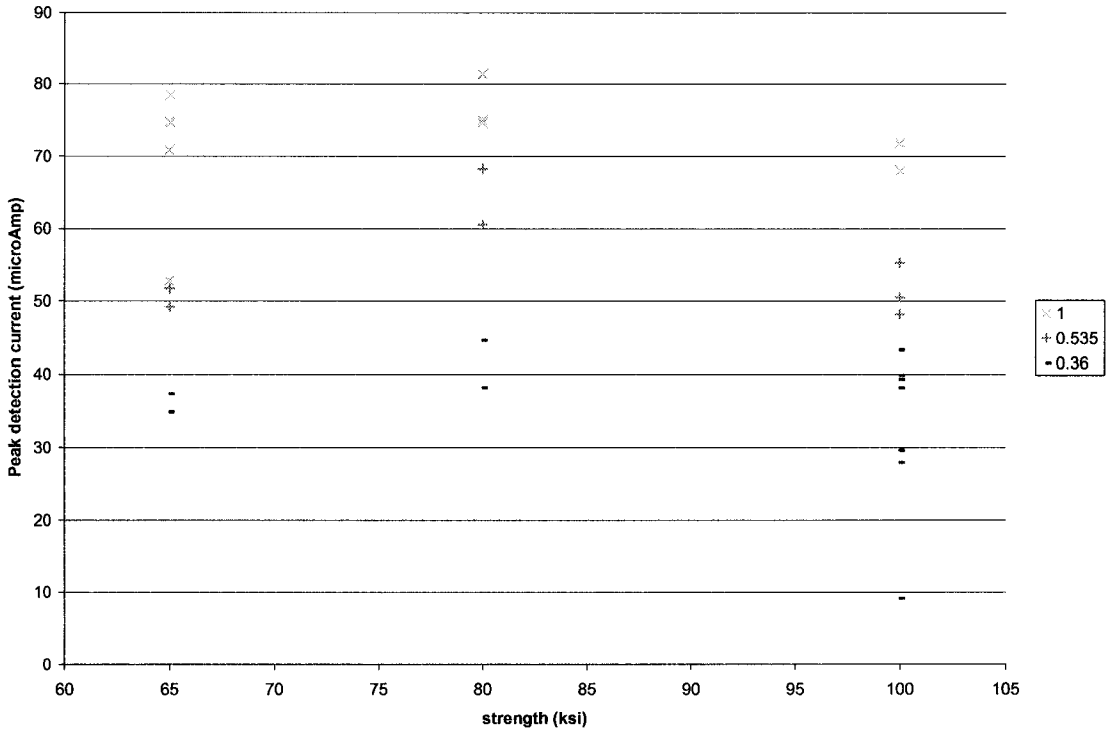

Figure 5-13 Peak detection current for selected permeation tests versus grade

6 Conclusions and suggestions

6.1 Conclusions

This work has focused on the interactions between hydrogen and three grades of pipeline steels, with attention focused on the mechanical properties. Firstly, the effect of charging time on hydrogen contents was investigated in the absence of external stressing to find the grade effect. Once a suitable charging time was established, the effect of previous stressing on the hydrogen contents was investigated with the mechanical stresses corresponding to the strength of each grade. The hydrogen content with concurrent stressing and charging of previously hydrogen saturated samples was next investigated. The final testing was permeation testing to observe hydrogen transport in the as received steels as a function of charging current density. The following is a list of the conclusions of this work.

1. In the three grades of steel investigated, there was no increase in the trapped hydrogen content with time. Diffusible hydrogen did increase with charging time across all three grades. The diffusible hydrogen contents were similar for the X65 and X80 steel, with the highest amount of hydrogen in the X100.
2. Charging with hydrogen after any stressing into the plastic regime (2% total strain) results in an increase in diffusible hydrogen content. Again, the highest amounts of hydrogen were in the X100 steel. The ratio of the hydrogen after stressing to the hydrogen contents prior to stressing showed that the greatest relative increase was in the lower grades of steel. Again, the

X65 and X80 steels showed very similar behavior with respect to diffusible hydrogen.

3. The trapped hydrogen content of all three steels increases with mechanical stressing into the plastic regime. Again, the most hydrogen was in the X100, with the X65 and X80 showing similar results. When normalized to the samples without prestressing, the greatest increase varied depending on the stressing regime. With long periods of static stressing, both with prior cyclic stressing and without any previous stressing, the greatest increase was in the X100.

4. Precharging with hydrogen results in increased trapped hydrogen in all three steels. The testing was too extreme for the X100, as most of the samples failed prior to completion of testing.

5. The failure of the X100 was typical hydrogen embrittlement, similar to what was experienced with a stainless steel in a pure hydrogen gas environment. Whether simple a simple tensile test, or testing in with cyclic and static stressing, the fracture surface was macroscopically and microscopically the same.

6. There is a marked decrease in ductility of the fractured X100 when precharged with hydrogen, but little effect on either yield or ultimate strength. This concurs with previous research.

7. In permeation testing, the results of the X65 and X80 steels were again very similar. The X100 had the longest time for hydrogen to be detected. The peak currents were again similar for the X65 and X80 steels.

8. Blistering was observed on all the steels at higher charging current densities, but at the lowest tested current, which was used in previous testing, did not produce blisters in any of the steels. The X100 steel was the most susceptible to blistering as it had the most and largest blisters at all charging current densities.

9. The microstructure of the steels played a more important role than the stressing with respect to hydrogen content. The X65 and X80 steels had a more uniform microstructure, and thus always had a lower hydrogen content. The X100, on the other hand, had a harder microstructure, as well as more interfaces between phases, and was therefore most susceptible to hydrogen assisted cracking.

6.2 Suggestions for future work

Mechanical stressing. Testing should be carried out with a mechanical stressing regime that approximates actual operating conditions would be better to show which steel would be best suited for industrial use. For example, if testing were carried out in the elastic regime, the results may have shown that the X100 was not the most susceptible to hydrogen assisted cracking.

Solutions. Solutions which closely resemble the environment that the steel would be in contact with in application should be investigated. Some of the solutions may promote SCC, which could again alter the ranking of these steels.

Microstructural effects. By testing three steels with similar strength, but different microstructures would allow the development of an alloy where the strength is maintained, but the detrimental effects of reaching the strength may be lowered. From this study, it was obvious that decreasing the interfacial area between phases would greatly decrease the susceptibility to hydrogen assisted cracking.

Steel chemistry. Related to the microstructural effects, the chemistry may be altered to achieve the desired strength. By altering the chemistry while maintaining the strength levels, it may be possible to develop a steel which has inclusions and precipitates that are not detrimental to hydrogen behavior, but achieve the desired strength level.

Coatings. Hydrogen assisted cracking in pipelines often happens when coatings disband from the surface of the steel. Hydrogen buildup on a surface of the steel, under the coating, can also lead to disbonding. Research could be conducted to develop a coating which delays SCC, but is permeable to hydrogen gas such that blisters under the coating may be avoided.

Specimen type. Using prenotched samples could give an idea of the hydrogen behavior at a crack front. The different microstructures of the steels may behave differently with notched samples. The X100 steel with its banded structure could behave much differently than the X65 and the X80 whose microstructures were relatively homogeneous.

7 References

[1] C A Zappfe,C E Sims; "Hydrogen embrittlement, internal stress and defects in steel;" Transactions of AIME; Vol 145, 1941

[2] W H Johnson; "On some remarkable changes produced in iron and steel by the action of hydrogen and acids;" Proceedings of the Royal Society of London; Vol 23, 1875

[3] F de Kazinczy; "A theory of hydrogen embrittlement;" Journal of The Iron and Steel Institute; vol 177, May 1954

[4] T Alp, B Dogan, T J Davies; "The effect of microstructure in the hydrogen embrittlement of gas pipeline steel;" Journal of Materials Science;" 22 pp 2105-2112, 1987

[5] D J Christenson, I M Bernstein, A W Thompson, E J Danielson, M Elices, F Gutierrez-Solana; "Hydrogen Compatibility of a Line Pipe" pp 997

[6] J E Costa, A W Thompson; "Hydrogen cracking in nominally pearlitic 1045 steel;" Metall Trans; 13A pp 1315, 1982

[7] B R W Hinton, R P M Procter; "The Effects of Cathodic Protection and Over Protection on the Tensile ductility and Corrosion Fatigue Behaviour of X-65 Pipeline Steel;" Hydrogen Effects in Metals; Moran, Wyo., 26-31 TMS/AIME, pp. 1005-1015, 1981

[8] J T Brown,W M Baldwin Jr; "Hydrogen embrittlement of steels;" Transactions of AIME; vol 200, 1954

[9] M. Szczepanski; "Hydrogen in Metals;" John Wiley and Sons, NY, 1963

[10] B Ule, F Vodopivec, L Vehovar, J Zvokelj, L Kosec; "Evaluation of threshold stress intensity in high strength hydrogen charged steel in low strain rate tension tests;" Materials Science and Technology; Vol 9 Nov 1993 pp 1009

[11] P Bastien, P Azou; "Effect of hydrogen on the deformation and fracture of iron and steel in simple tension;" Proceedings of the First Metallurgical Congress, ASM, 1951

[12] W Beck, J O'M Bockris, J McBreen, L Nanis; "Hydrogen permeation in metals as a function of stress;" Proceedings of the Royal Societyof London; Series A, vol 290, 1965

[13]Hanninen, Hakkarainen; Fractographic Characterization of a Hydrogen-Charged AISI 319 Type Austenitic Stainless Steel;" Met trans A 1979

[14] C D Beacham; "A new model for hydrogen-assisted cracking (hydrogen embrittlement);" Metallurgical Transactions, Vol 3, Feb 1972

[15] H Lukito, Z Szklarska-Smialowska; "Susceptibility if Medium-Strength Steels to Hydrogen-Induced Cracking;" Corrosion Science, vol 39 no 12 pp 2151, 1997

[16] B Sasmal, S K Singh, "Apparent Anomalous Behavior of a Cathodically Charged Low Alloy Steel Under Tension" Scripta Materialia, vol 40 no 4, 1999

[17] Callister

[18] J E Shelby; "Handbook of Gas Diffusion in Solids and Metals;" ASM Int'l, pp 103, 1996

[19] Z F Wang, C L Briant, K S Kumar, X J Wei, J Li, W Ke; "Effect of anodic dissolution and hydrogen absorption on plastic zone at fatigue crack tip in structural steel;" Materials Transactions, JIM; vol 39 no 3, pp 365-369, 1998

[20] M RLouthan Jr, G R Caskey Jr, J A Donovan, D E Rawl Jr; "Hydrogen embrittlement of metals;" Materials Science and Engineering; vol 10, 1972

[21] D HE MSc Thesis

[22] B G Pound; "The effect of aging on hydrogen trapping in precipitation-hardened alloys;" from The Journal on Environmental Degradation of Materials and its Control (ed G T Burnstein); Vol 22 No 11, pp 1941, 2000

[23] H Tamehiro, K Nishioka, M Murata, Y Kawada, A Takahashi: "High-toughness Age-Hardenable Copper-bearing Steel for Large-Diameter Line Pipe" 9th ASME, Offshore Mechanical & Arctic Engineering Conference Proceedings, vol 5 p 13, Houston, 18-23 Feb 1990

[24] M F Galis, D Petelot, J L Dauptain, A Sulmont; "Action of Copper on Hydrogen Induced Cracking Resistance of Steels Study of Mechanisms by Hydrogen Permeation Measurements," Corrosion '87, Paper no 57, San Francisco, March 9-13, 1987

[25] R N Parkins, "Strain Rate Effects in Stress Corrosion Cracking," Corrosion Vol 46 no 3, pp 178, 1990

[26] K G Schmitt-Thomas, P M Wollrab, B Hoffmeister; "The influence of mechanical surface treatment to hydrogen embrittlement of a high-strength steel;" 2nd International Congress on Hydrogen in Metals; paper 4A6, Paris, France, 6-10 June, 1977

[27] J Toribio; "Numerical modelling of hydrogen embrittlement of cylindrical bars with residual stress fields;" Journal of Strain Analysis; vol 35 no 3, pp 189-203, 2000

[28] Z Szklarska-Smialowska, Z Xia; "Hydrogen trapping by cold-worked X-52 steel;" Corrosion Science; vol 39 no 12 pp 2171-2190, 1997

[29] A S Tetelman, W D Robertson; "The mechanism of hydrogen embrittlement observed in iron-silicon single crystals;" Transactions of The Metallurgical Society of AIME; vol 224, Aug 1962

[30] A R Troiano; "The role of hydrogen and other interstitials in the mechanical behavior of metals;" (1959 Edward De Mille Campbell Memorial Lecture) Transactions of the ASM; vol 52, 1960

[31] R A Oriani; "A mechanistic theory of hydrogen embrittlement of steels;" Berichte der Bunsen-Gesellschaft für Physikalische Chemie; vol 76, 1972

[32] Estela Rodriguez de Schiapparelli; "Effect of hard inclusions on susceptibility to hydrogen damage;" Materials Performance; 27 no 2 pp 21, 1988

[33] M Uhlemann, B G Pound; "Diffusivity, Solubility and Trapping Behavior of Hydrogen in Alloys 600, 690tt and 800;" Corrosion science, Vol 40 no 4/5, pp 645-662, 1998

[34] T J Marrow, M Aindow, P Prangnell, M Strangwood, J F Knott; "Hydrogen-Assisted Stable Crack Growth in Iron-3 wt% Silicon Steel;" Acta Metal; vol 44 # 8 pp 3125; 1996

[35] L C M Li, R A Oriani, L S Darken; Zh Fiz Khim; 49 pp 271; 1966

[36] Y Sakamoto, U Hanada; "Diffusion of hydrogen in heat treated martensitic Type 403 stainless steel;" 2nd International Congress on Hydrogen in Metals; paper 1A7, Paris France, 6-10 June, 1977

[37] G J Thomas; "Hydrogen Trapping in FCC Metals;" Hydrogen Effects in Metals, Moran, Wyo., 26-31 TMS/AIME, pp. 77-85, 1981

[38] Estela Rodriguez de Schiapparelli; "On the effect of non-metallic inclusions on hydrogen damage in aluminum killed steels;" Journal of Materials Science 23, pp 3338, 1988

[39] I Nakagawa, T Obinata, J Kudo, F Kawabata, M Kimura, K Amano; "Production of Line Pipe Steel with high resistance to hydrogen induced cracking;" Metallurgy of Vacuum-Degassed Steel Products (eds R Pradhan); pp 437, TMS, 1990

[40] B Gu, J Luo, X Mao; "Hydrogen-Facilitated Anodic Dissolution-Type Stress Corrosion Cracking of Pipeline Steels in Near-Neutral pH Solution;" Corrosion vol 55 no 1 pp 96, Jan 1999

[41] Y Nakatani, T Higashi, K Yamada; "Effect of tempering treatment on hydrogen-induced cracking in high-strength steel;" Fatigue Fract Engng Mater Struct; 22 pp 393-398, 1999

[42] Liao, Nan, Hu, Kang; "In Situ Investigation of the Effect of Hydrogen on the Plastic Deformation Ahead of the Crack tip and the Crack Propagation for 0.15C-1.5Mn-0.17V-0.012N Steel;" J of Mat Eng & Performance, vol 7 no 1, 1998

[43] J Marrow, M Aindow, P Prangnell, M Strangwood, J F Knott; "Hydrogen-Assisted Stable Crack Growth in Iron-3 wt% Silicon Steel;" Acta Metal; vol 44 # 8 pp 3125; 1996

[44] J Toribio, A M Lancha, M Elices; "Characteristics of the new tearing topography surface;" Scripta Metallurgica et Materialia; vol 25 pp 2239-2244, 1991

[45] M I Luppo, J Ovejero-Garcia; "The influence of Microstructure on the Trapping and Diffusion of Hydrogen in a Low Carbon Steel;" Corrosion Science; vol 32 no 10 pp 1125-1136, 1991

[46] S L I Chan, H L Lee, J R Yang; "Effect of retained austenite on the hydrogen content and effective diffusivity of martensitic structure;" Metallurgical Transactions A; vol 22A pp 2579-2586, 1991

[47] G M Pressouyre, I M Bernstein; "A quantitative analysis of hydrogen trapping;" Metallurgical Transactions A; vol 9A pp 1571-1580, 1978

[48] T J Davies, F H Hayes, E Strecker, D A Ryder; "The influence of structure on the diffusion and trapping of hydrogen in a plain carbon eutectoid steel;" 2nd International Congress on Hydrogen in Metals; paper 2B7, 1977

[49] D A Jones; "Principles and prevention of corrosion, 2nd edition;" Prentice Hall Inc, NJ, 1996

[50] F Ellyin; "Fatigue damage, crack growth, and life prediction;" Chapman and Hall, London, 1997

[51] A J Kumnick, H H Johnson; "Hydrogen transport through annealed and deformed Armco iron;" Metallurgical Transactions; vol 5 pp 1199-1206, 1974

[52] H J Maier, A Schettleer, H Kaesche; "A hydrogen permeation study of cyclically deformed low alloy steel;" Werkstoffe und Korrosion; 42 no 5 pp 212-218, 1991

[53] S P Lynch, N E Ryan; "Mechanisms of Hydrogen Embrittlement – Crack Growth in a Low Alloy Ultra-High-Strength Steel Under Cyclic and Sustained Stresses in Gaseous Hydrogen;" Proceedings of the 2nd International Congress in Hydrogen in Metals; 1977

[54] H Matsui, H Kimura, S Moriya; "The effect of hydrogen on the mechanical properties of high purity iron: I. Softening and hardening of high purity iron by hydrogen charging during tensile deformation;" Materials Science and Engineering; 10 pp 207-216, 1979

[55] H Matsui, H Kimura, A Kimura; "The effect of hydrogen on the mechanical properties of high purity iron: III. The dependence of softening on specimen size and charging current density;" Materials Science and Engineering; 40 pp 227-234, 1979

[56] G E Dieter Jr; "Mechanical Metallurgy;" McGraw-Hill Book Co Inc, 1961

[57] B S Chaudhari, T P Radhakrishnan; "A reexamination of the trapping of hydrogen in iron and steel;" Materials Trans, JIM; vol 34 no 5, pp 443-449, 1993

[58] B G Pound; "Effect of heat treatment on hydrogen trapping in alloy K-500;" Corrosion; vol 54 no 12, pp 988-995, 1998

[59] J L Lee, J T Waber, Y K Park; "The effect of mechanical polishing on hydrogen permeation in iron single crystal;" Scripta Metallurgica; vol 20 pp 823-828, 1986

[60] M F Galis, G Guntz; "Stepwise cracking and blistering resistance of line pipes up to X 80 grade" Int'l conf on the Interaction of Steels with Hydrogen in Petroleum Industry Pressure Vessel Service, Paris, 28-30 March 1989

[61] P H Pumphrey; "The Effect of Sulphide Inclusions on the Diffusion of Hydrogen in Steels;" Sulphides and Hydrogen Diffusion in Steels; pp 105-112 (not sure of date)

[62] B M Patchett, A C Bicknell, W Chen; Response of Differing steels to H Flux in Devanathan Cell

[63] J J Renault, F Braouezec, J L Cornuey, G Guntz; "Susceptibility of seamless line pipe to hydrogen induced cracking;" Corrosion/85; March 25-29, paper no 238, 1985

[64] M G Hay, D W Rider; "Integrity Management of a HIC-Damaged Pipeline and Refinery Pressure Vessel Through Hydrogen Permeation Measurements;" Corrosion/ 98; Paper no 395, NACE, 1998

[65] F Terasaki, A Ikeda, M Takeyama, S Okamoto; "The hydrogen induced cracking susceptibilities of various kinds of commercial rolled steels under wet hydrogen sulphide environment;" The Sumitomo Search; no 19 pp 103-117, 1978

[66] R W K Honeycombe; "Steels: Microstructure and Properties;" Edward Arnold, London, 1981

[67] K Farrel; "Cathodic Hydrogen Absorption and Sever Embrittlement in a High Stength Steel;" Corrosion; vol 26, pp 105-110, 1970

[68] J R Rice; "Hydrogen and Interfacial Cohesion;" Effect of Hydrogen on Behavior of Materials, 1976

[69] Y Murakami, T Nomoto, T Ueda, Y Murakami; "On the mechanism of fatigue failure in the superlong life regime ($N>10^7$ cycles). Part I: influence of hydrogen trapped by inclusions;" from Fatigue & Fracture of Engineering Materials & Structures; Vol 23 No 11, pp 893-902, 2000

[70] K Takai, Y Honma, K Izutsu, M Nagumo; "Identification of trapping sites in high-strength steels by secondary ion mass spectrometry for thermally desorbed hydrogen," J Japan Inst Metals, vol 60 no 12, pp 1155-1162, 1996

[71] K Takai, J Seki, G Yamauchi, Y Honma; "Observation of trapping sites of hydrogen and deuterium in high-strength steels by secondary ion mass spectrometry," J Japan Inst Metals, vol 58 no 12, pp 1380-1385, 1996

[72] M Nagumo, M Nakamura, K Takai; "Hydrogen thermal desorption relevant to delayed-fracture susceptibility of high-strength steels;" Met and Mat Trans; 32A pp 339-347, 2001

[73] B Pathiraj, R Vasudevan; "X-ray measurement of lattice residual strains produced by hydrogen diffusion in a 0.09% carbon steel;" 2nd International Congress on Hydrogen in Metals; paper 2C9, 1977

[74] Metals Handbook, Desk Edition 2nd Edition, J.R. Davis, ASM, 1998

[75] H X Li, R H Jones, J P Hirth, D S Gelles; "Fracture Toughness of the F-82H steel-effect of loading modes, hydrogen and temperature;" Journal of Nuclear Materials pp 258, 1996

[76] J M Densley, J P Hirth; "Mixed Mode Fracture of an HSLA-100 Steel;" Scripta Materialia, vol 39 no 7, pp 881, 1998

[77] K Tsuboi, H Yatabe, K Yamada; "Hydrogen induced cracking in high strength steel;" Mater Sci Tech; Vol 12 pp 400-404, 1996

[78] R Garber, I M Bernstein, A W Thompson; "Effect of Hydrogen on Ductile Fracture of Spheroidized Steel;" Scripta Metallurgica, Vol 10, 1976

[79]M Nagumo, M Nakamura, K Takai; "Hydrogen thermal desorption relevant to delayed-fracture susceptibility of high-strength steels;" Metallurgical and Materials Transactions A; vol 32A p 339-347, 2001

[80] H K Uhlig; "New Perspectives in the Stress Corrosion Problem;" Physical Metallurgy of Stress Corrosion Factors; TMS of AIME, 1959

[81] K Kannan, J P Hirth; "Mixed mode fracture toughness and low cycle fatigue behaviour of an HSLA-80 steel;" Scripta Materialia; vol 39 no 6 pp 743-748, 1998

[82] K Banerjee, U K Chatterjee; "Hydrogen permeation and hydrogen content under cathodic charging in HSLA 80 and HSLA 100 steels;" Scripta Materialia; 44 pp 213-216, 2001

[83] W Beck, J O'M Bockris, M A Genshaw, P K Subramanyan; "Diffusivity and Solubility of Hydrogen as Function of Composition in Fe-Ni Alloys;" Metal Trans, 2 pp 883, March 1971

[84] Y Sakamoto, K Takao; 2nd Int Cong on Hydrogen in Metals; Paris, paper 1A8, 1977

[85] G Sandoz; "A Unified Theory for Some Effects of Hydrogen Source, Alloying Elements, and Potential on Crack Growth in Martensitic AISI 4340 Steel;" Metallurgical Transactions, Vol 3, May 1972

[86] R W Hertzberg, "Deformation and fracture mechanics of Engineering Materials, 4th ed," John Wiley and Sons, Inc. NY, 1996

[87] R N Parkins, Z A Foroulis: "The SCC of mild Steel in MonoEthanlAmine (C_2H_7NO) Solutions;" from CORROSION/87, paper no 188, San Francisco, 9-13 March 1987

[88] R N Parkins, W K Blanchard, B S Delanty "Transgranular Stress Corrosion Cracking of High-Pressure Pipelines in Contact with Near Neutral pH," Corrosion vol 50 no 5 pp 394, 1994

[89] M A V Devanathan, Z Stachurski "The Adsorption and Diffusion Electrolytic Hydrogen Palladium," Proceeding of the Royal Society of London. Series A, Mathematical and Physical Sciences, vol 270 issue 1340 pp 90-102, 1962

APPENDIX I

Determining load at 2% strain

The preloaded samples used in these tests were first strained to 2% total strain in order to determine the maximum load at which this strain occurred. For consistency between these previous samples and later tests, there needed to be a method to know the load when the same strain was achieved at the later test sample gauge length. These later tests were to be performed with the electrolytic charging solution still providing hydrogen to the samples as they were being tested.

One method would be to attach a clip-type strain gauge to the sample gauge length as they were being strained in air, and use the same one when the samples were being charged in the electrolytic solution. Two potential problems would have to be solved in order to continue along this path. First, it would be necessary for the strain gauge used to be able to withstand the environmental attack caused by the sulfuric acid solution used in the testing. As well, the strain gauge should not interfere with the hydrogen charging solution. The second potential problem would be with the knife edges on the clip-gauge. Where the knife edges come into contact with the samples, they could create the potential for crevice corrosion. Just the first concern would require much research into the acquisition of a proper strain gauge that would be compatible with the Instron tensile testing equipment.

Instead of directly measuring the strain at the samples, an indirect method was used for measuring strain when they were immersed in the hydrogen charging solution. In the method used, two "extension arms" were attached to a sample. The "extension arms" and contact points were outside charging solution. The strain of the sample was then measured on these extension arms and the maximum load taken from the measurement. These extension arms needed to be manufactured then calibrated. Simple machining was all that was required to manufacture the extension arms. Calibration between the sample gauge length and "extension arms" was easily accomplished with equipment that was readily available.

Calibration was accomplished by attaching the "extension arms" to the samples at the exact distance they would be from the gauge length, then attaching two strain gauges as the tests were being performed. One strain gauge attached to the sample on the reduced section as per usual testing, and the second on the extension arms. Then would simply be a matter of conducting the tests in air as usual, while collecting data from the two strain gauges. The final step would then be determining the differences, if any, in the readings of total strain as measured by the two strain gauges. For my testing, the differences would be especially important around 2% total strain as measured by the strain gauge directly on the sample. If necessary, this process could easily be repeated for all three grades of steel tested, or for any material.

In the following pictures, Strain 1 refers to the strain directly being measured on the sample. Strain 2 refers to the strain being measured by the extension arms attached to the

sample. All the strains are measured in percent strain. Data from all three grades of steel was used to generate these curves. The data is from samples that were loaded to 2% strain at the sample, then unloaded. Data from the loading to 2% strain was taken from samples that were loaded to 2% strain and held at that maximum load for 24 hours.

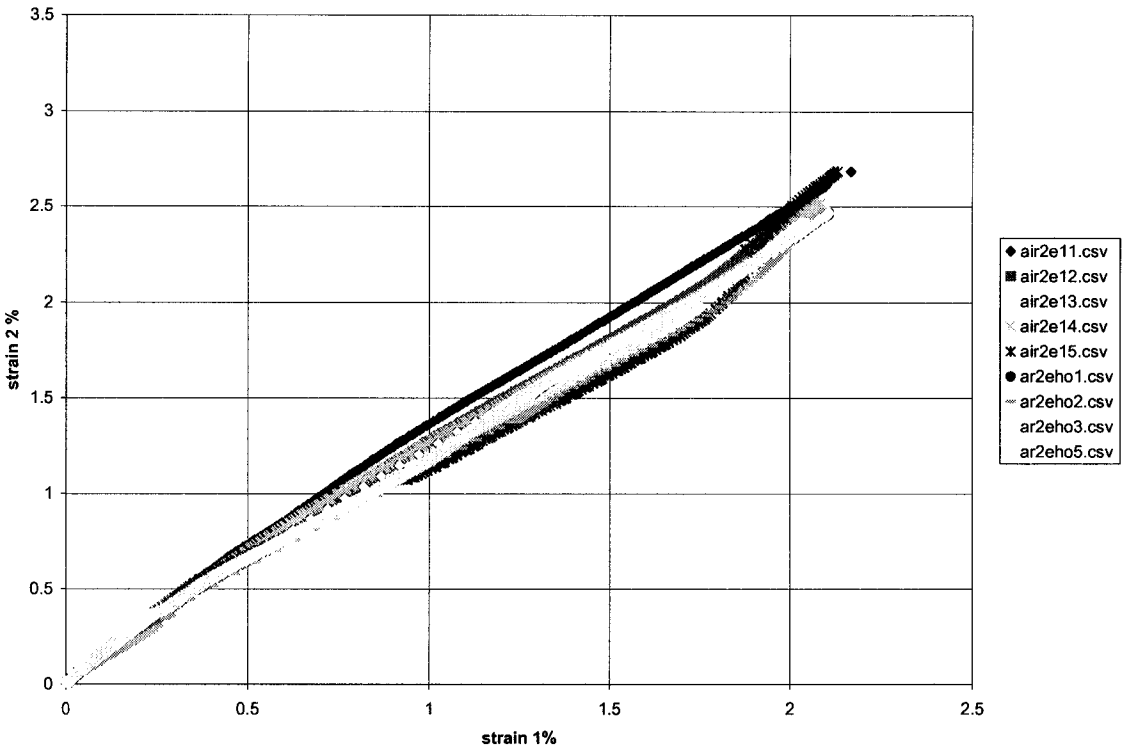

Figure 1 Strain 1 vs Strain 2 calibration for X65

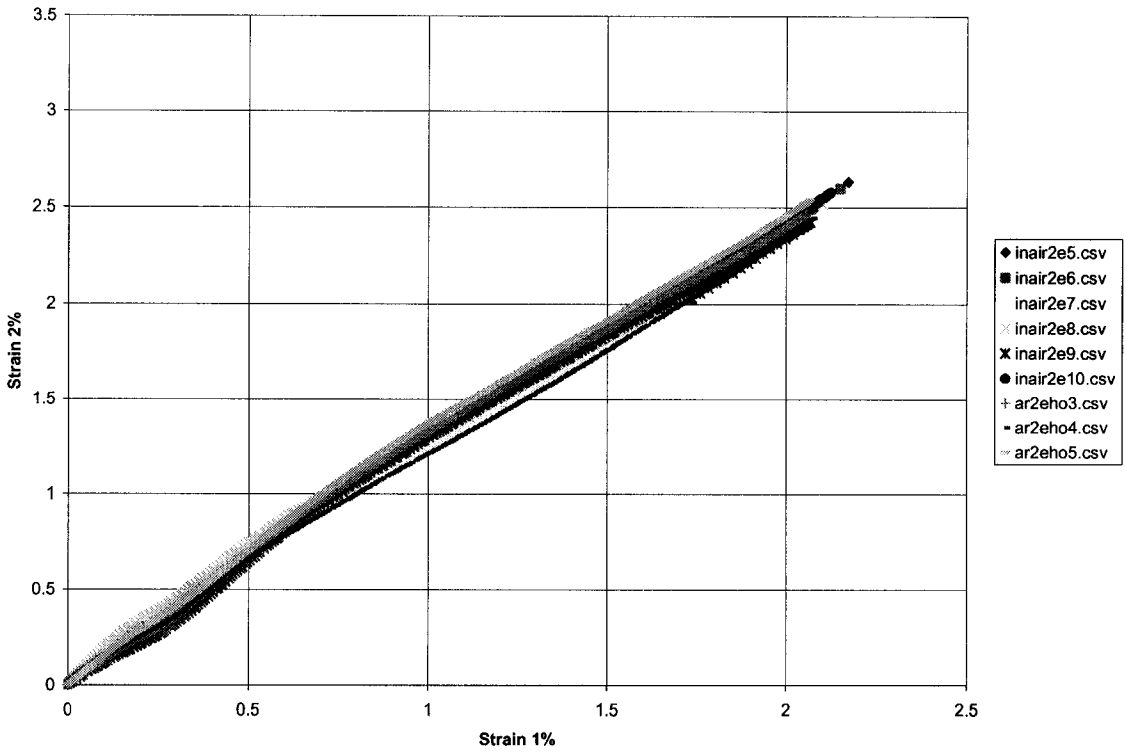

Figure 2 Strain 1 vs Strain 2 calibration for X80

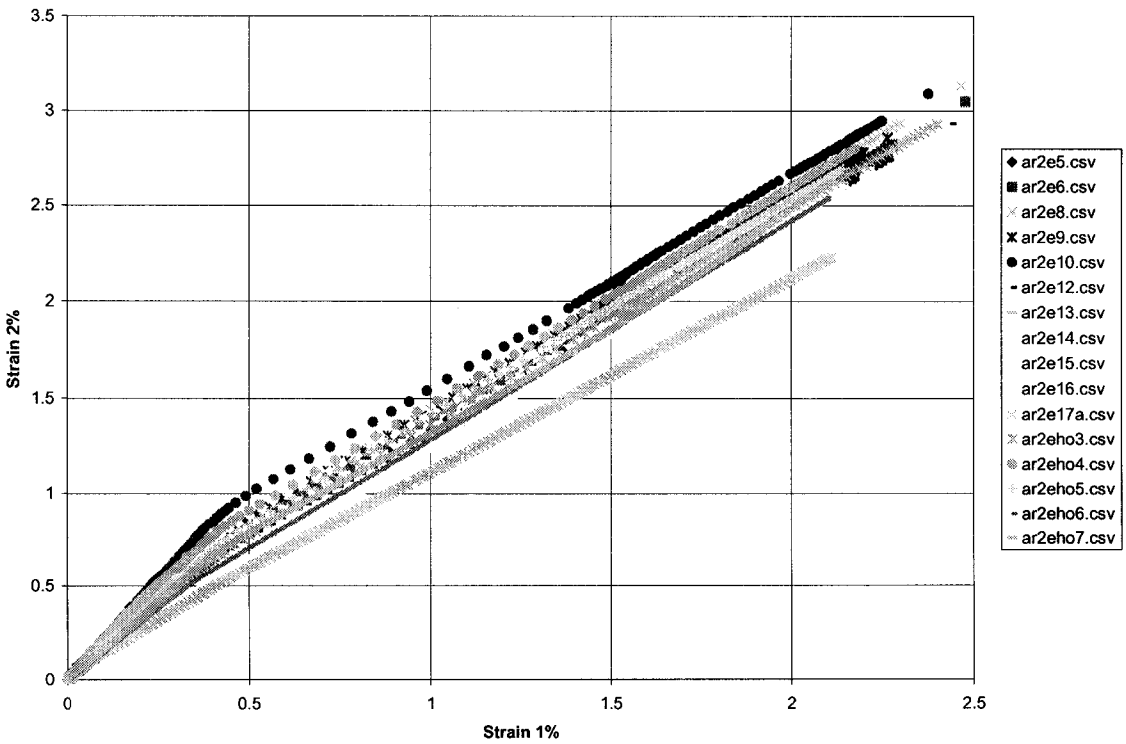

Figure 3 Strain 1 vs Strain 2 calibration for X100

As can be seen from the above figures, calibration was performed on all three steels used in this study. From the calibration curves, it is seen that 2% strain measured at the sample corresponds to slightly less 2.5% strain measured on the extension arms away from the sample for almost all cases. Thus, for tests used in the study, 2.4% strain measured at the extension arms was taken to be 2% strain at the sample. From the above examples, this was taken to be well within experimental scatter.

APPENDIX II

Heat treated X100

Experimental

The X100 steel was heat-treated for 24hours at various temperatures in order to decompose the banded microstructure; the subsequent micrographs and hardness were taken. As is clear from Figure 1, the hardness is very constant until the heat treating temperature reaches 650°C, at which point the hardness drops off significantly.

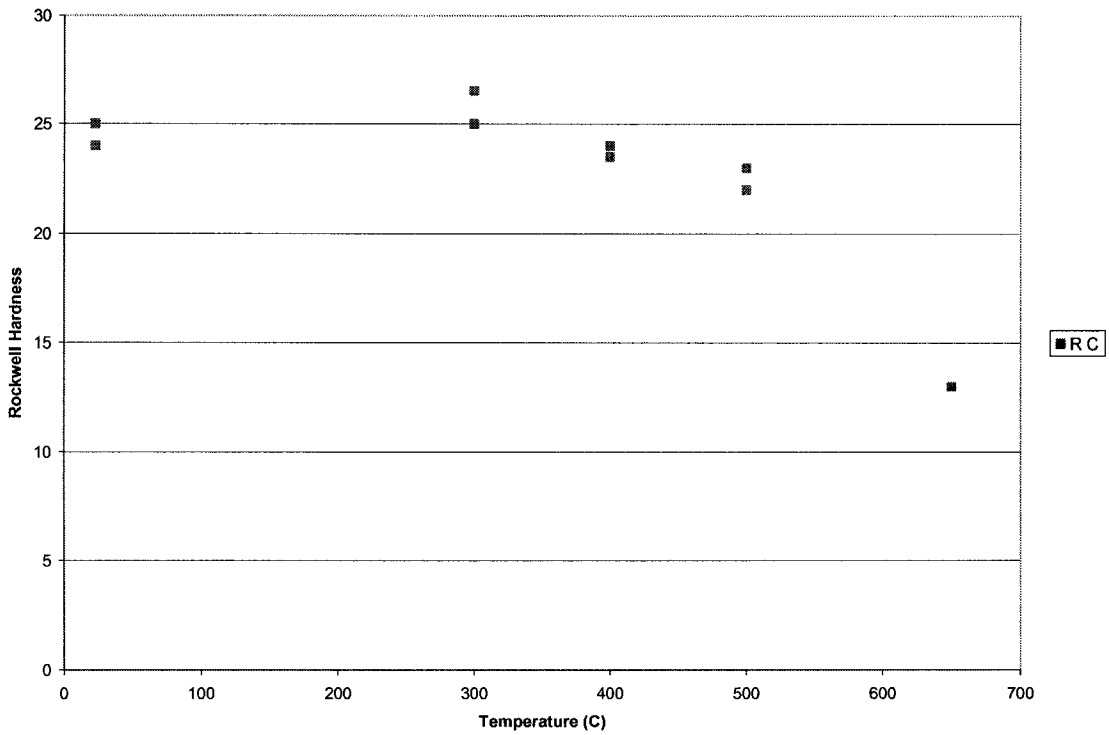

Figure 1 Hardness of X100 after heat-treated at various temperatures

The hardness variation, and therefore related properties such as yield strength, can be attributed to the microstructural variations that are seen on heat treating. As is seen from the microstructures, the heat-treated steel closely resemble the banded structure of the 'as-received' X100 material until heated to 650°C at which point the microstructure collapses, and recrystallization occurs.

Figure 2 Microstructure of X100 heat-treated at 300°C

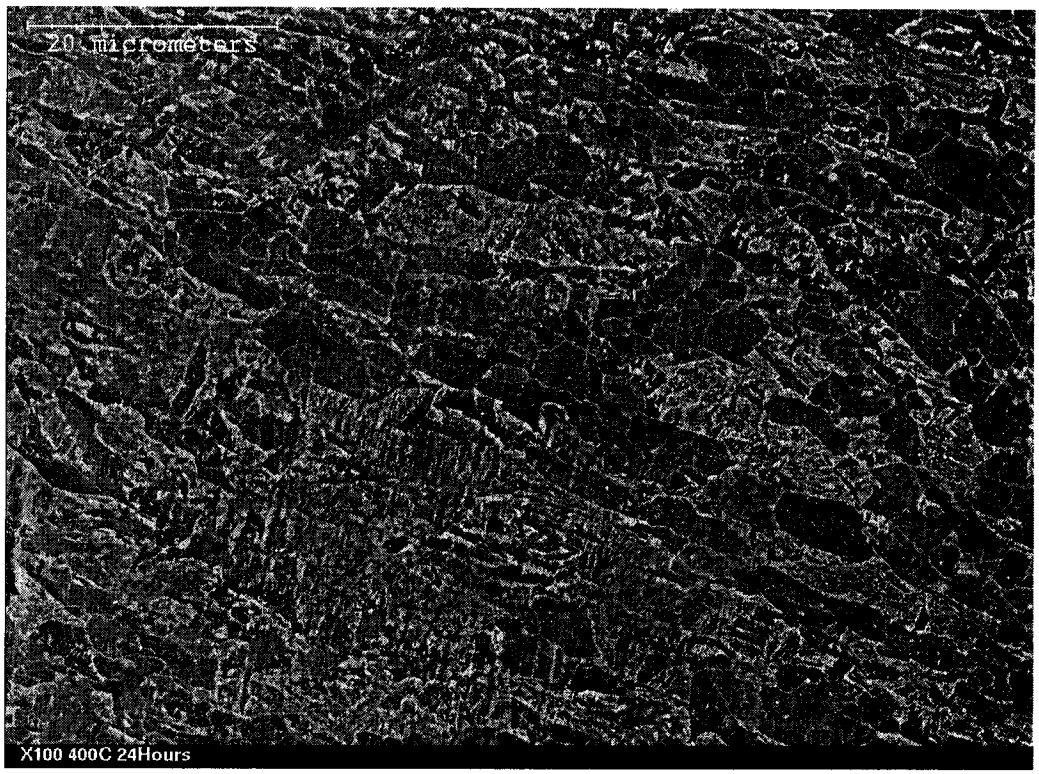

Figure 3 Microstructure of X100 heat-treated at 400°C

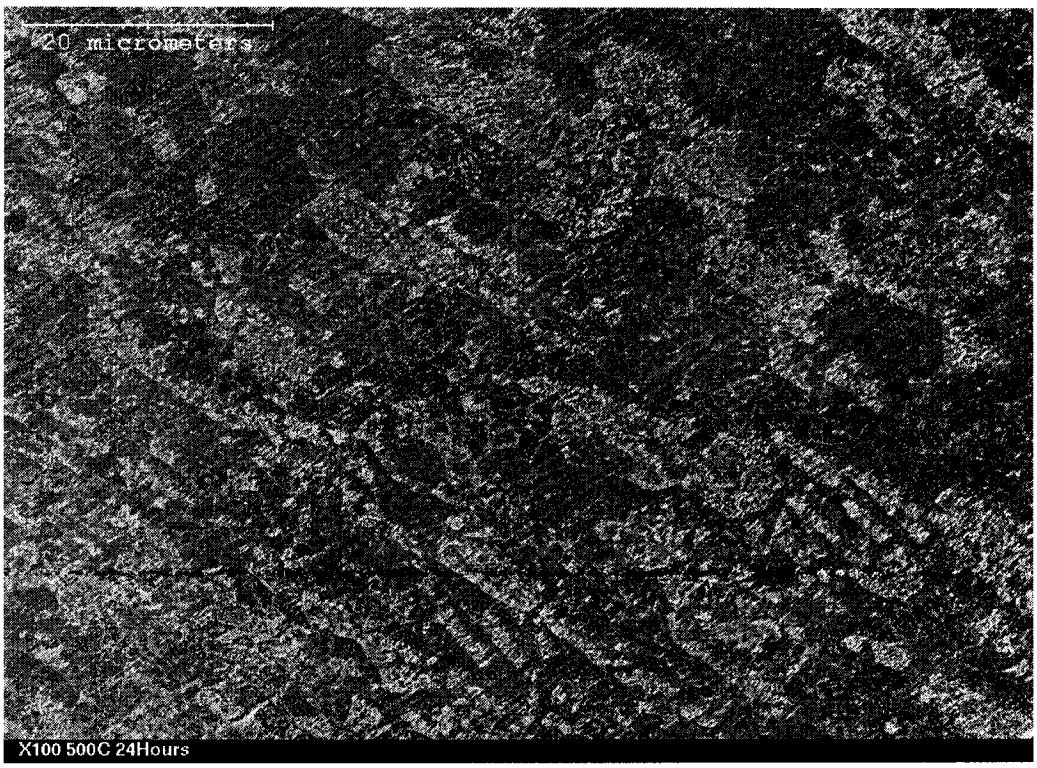

Figure 4 Microstructure of X100 heat-treated at 500°C

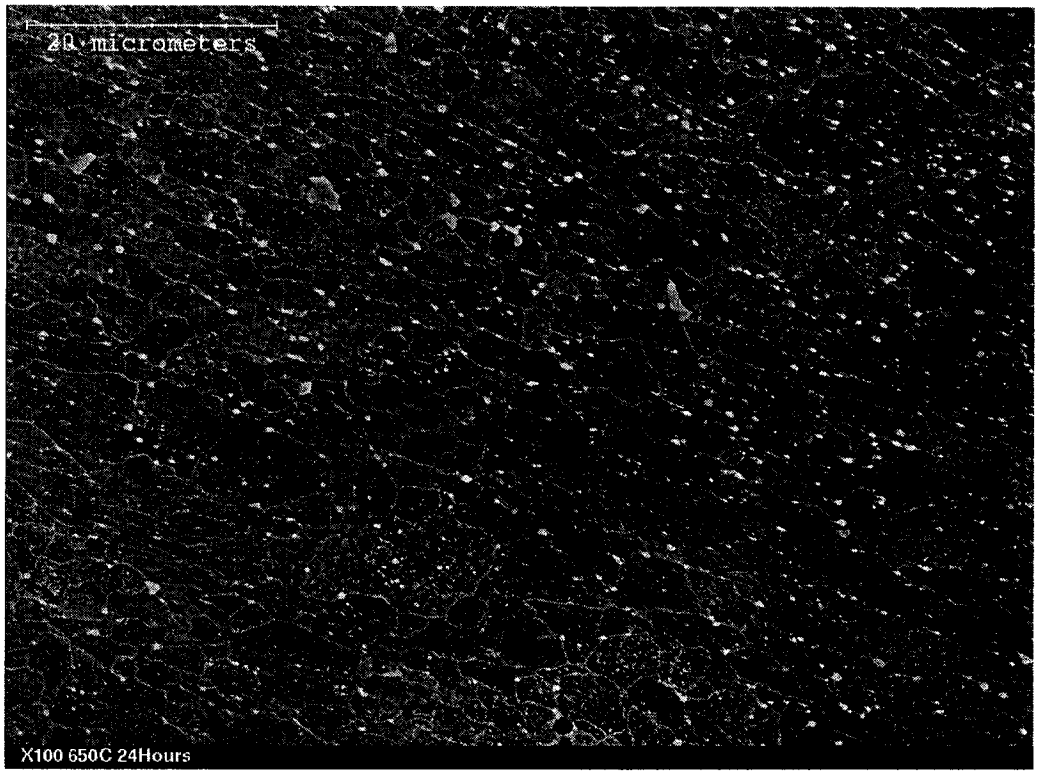

Figure 5 Microstructure of X100 heat-treated at 650°C

Two sets of 'bar'-type samples were prepared from X100; one was heat-treated at 450°C and the other at 650°C. Once again these 'bar'-type samples were used to determine the hydrogen behavior for various charging times. The diffusible and trapped hydrogen contents of the X100 material, in the 'as-received' condition and the subsequent to the heat-treated samples are shown in Figure 6 and Figure 7 respectively. As with the hardness and microstructure, no large difference in the diffusible hydrogen contents between the 'as-received' and 450°C samples, but the 650°C samples had a much lower hydrogen content. Once again the trapped hydrogen content does not significantly increase with charging time.

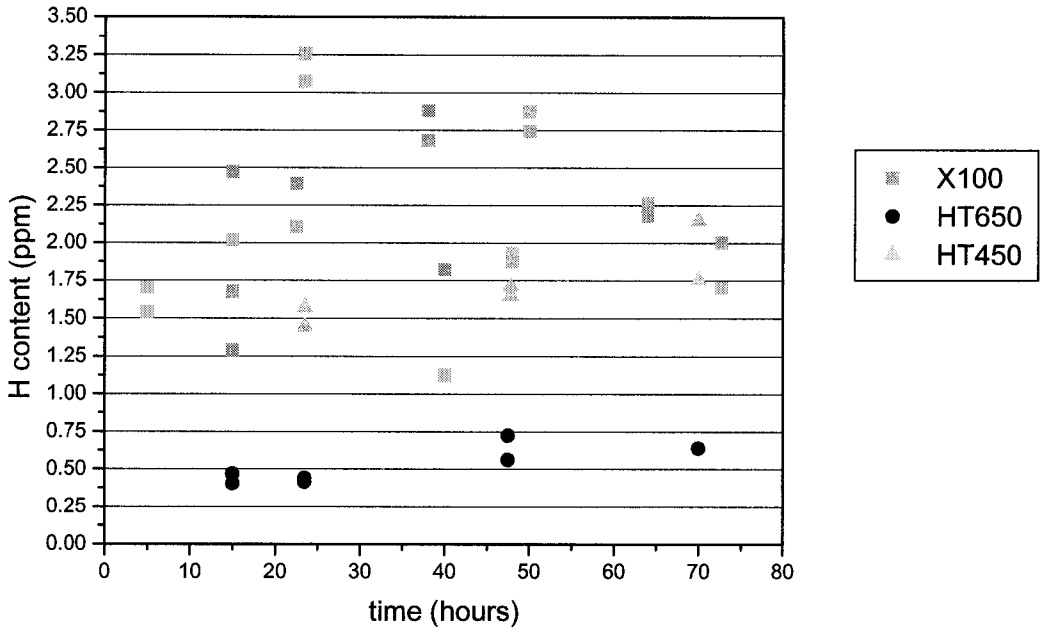

Figure 6 Diffusible hydrogen contents

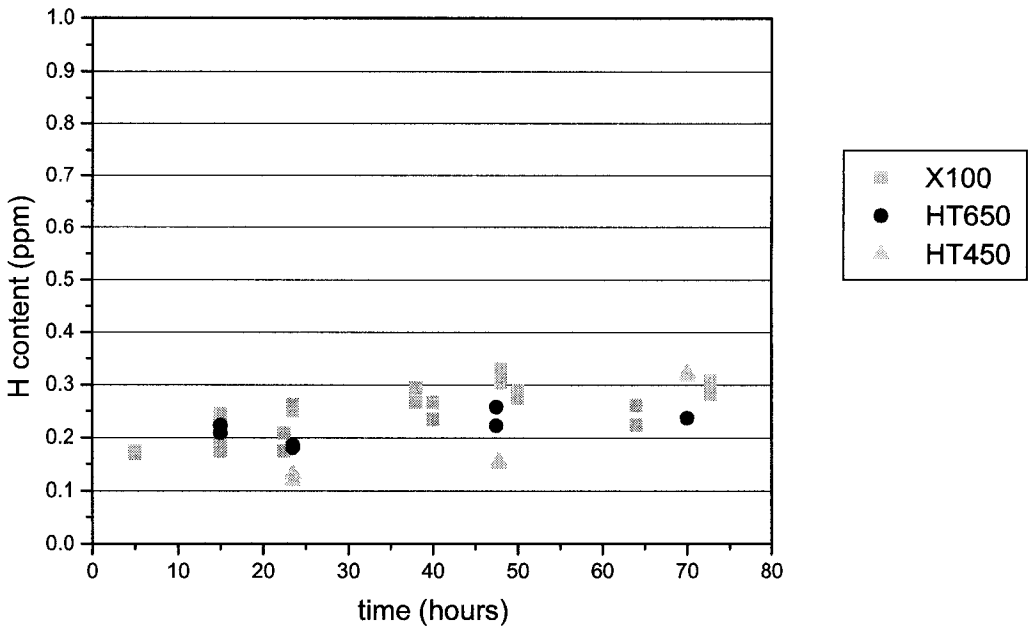

Figure 7 Trapped hydrogen contents

It is interesting to note from Figure 6 that there is a delay in the 450°C reaching the same "normal" value as the "as-received" X100; the 650°C sample never reached the same

value as the "as-received" X100 steel. This was most likely because at 650°C the microstructure of the steel collapsed as was seen in Figure 5, and was indicated by the large drop in hardness and therefore yield strength. The microstructures of the samples that were heated from 300°C to 500°C were very similar to the microstructure of the "as-received" X100 indicating that there were other more microscopic changes happening to the microstructures, such as collapsing of the dislocation structure in the material. Though these changes were happening, they were not readily observable in the SEM. Further understanding of the trap sites could be performed by transmission electron microscopy, however, the scope of the present research was restricted.

APPENDIX III

MICROGRAPHS

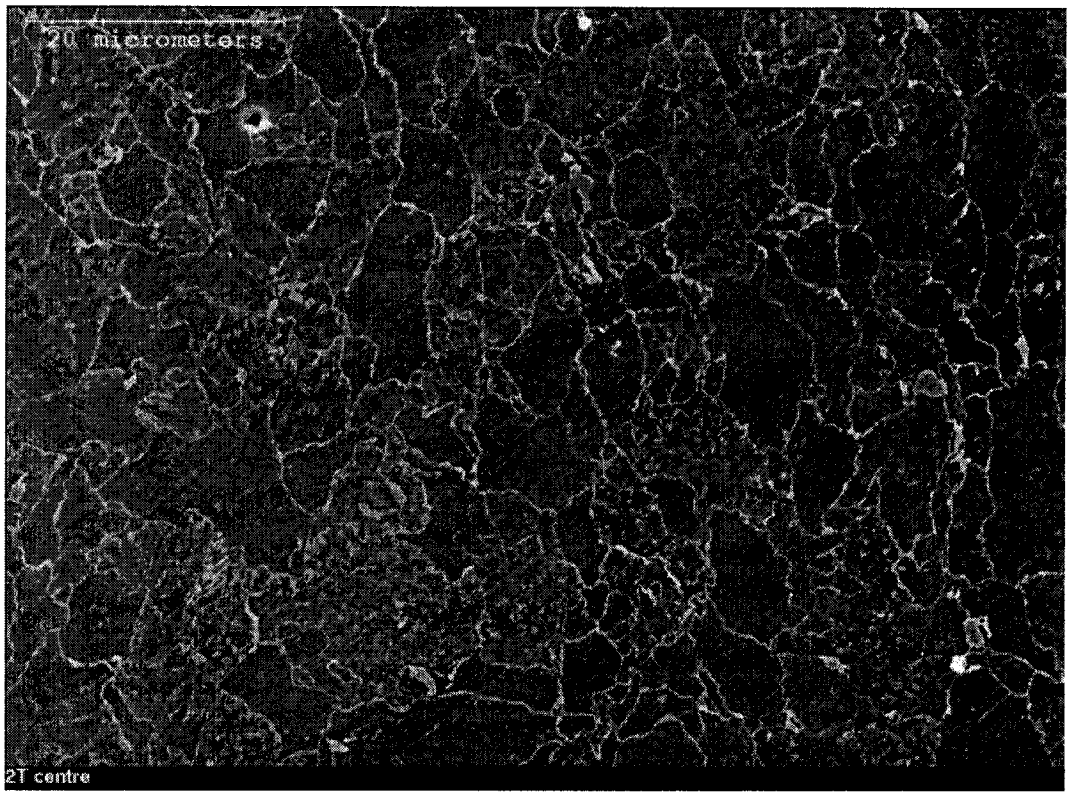

Figure 1 X65 as received

Figure 2 X65 no load, charged at 0.05mA/cm^2 for 15 hours

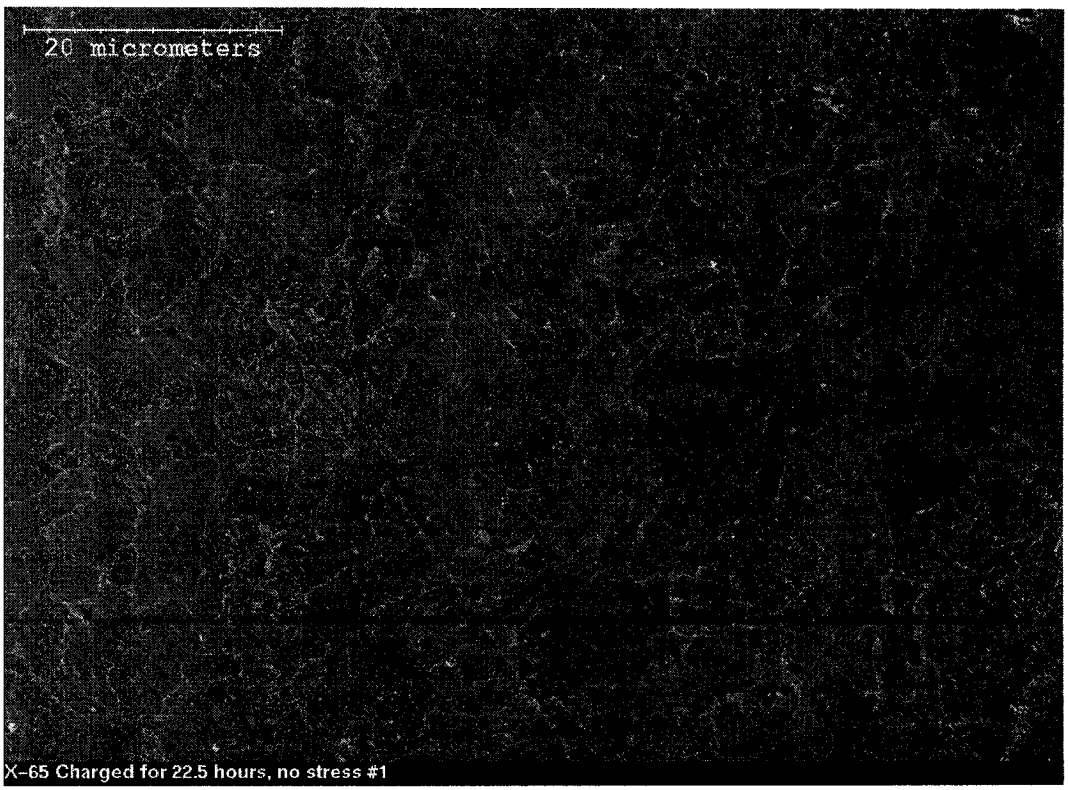

Figure 3 X65 no load, charged for 22.5 mA/cm^2 for 22.5 hours (stain is an etching artifact)

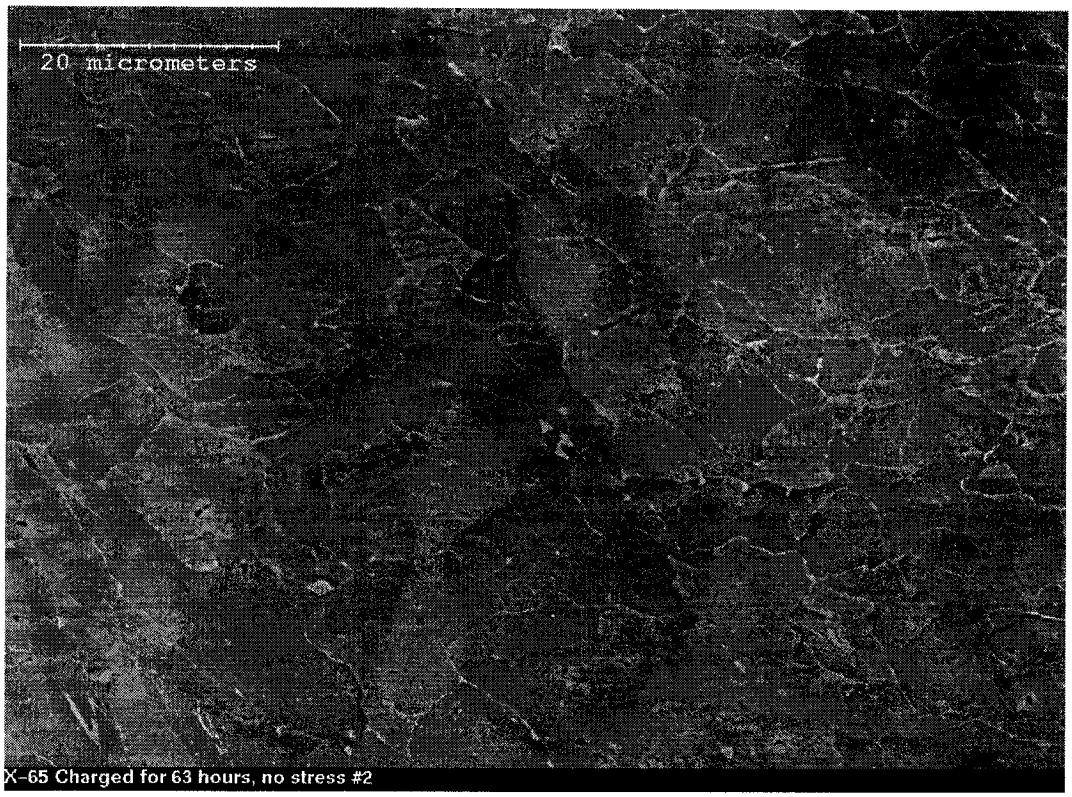

Figure 4 X65 no load, charged at 0.05mA/cm^2 for 63 hours (discoloration is etching artifact)

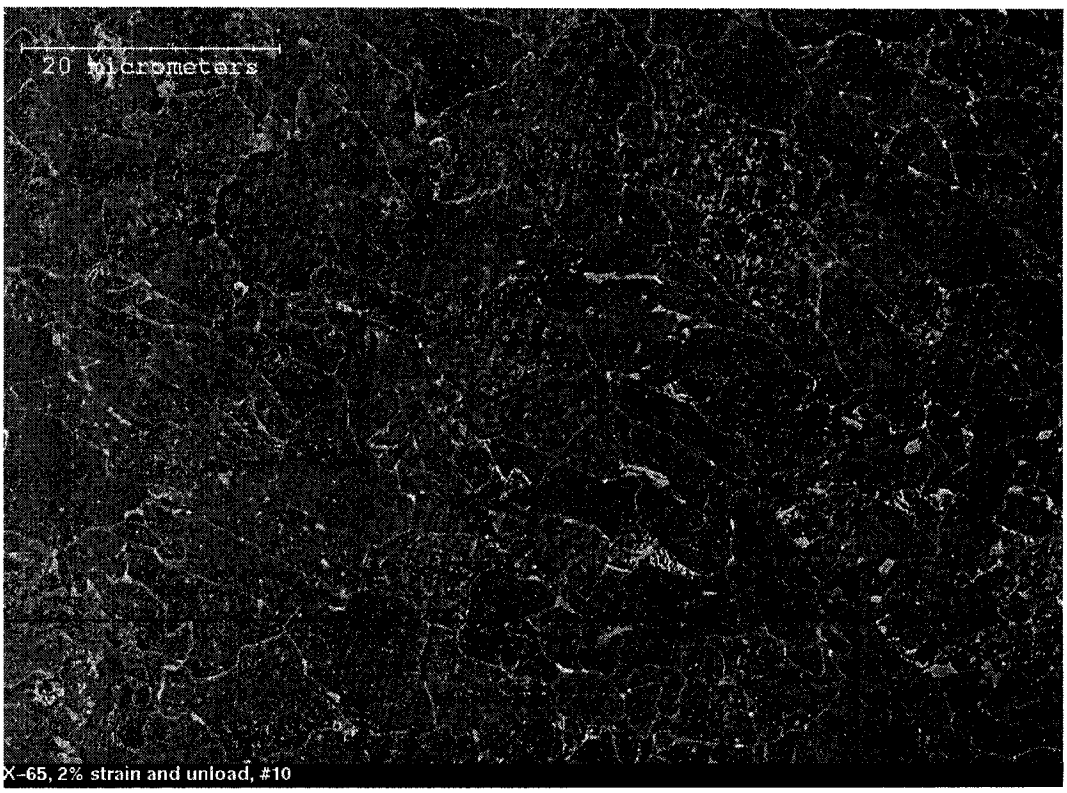

Figure 5 X65 2% strain and unload then charged at 0.05mA/cm^2 for 23.5 hours

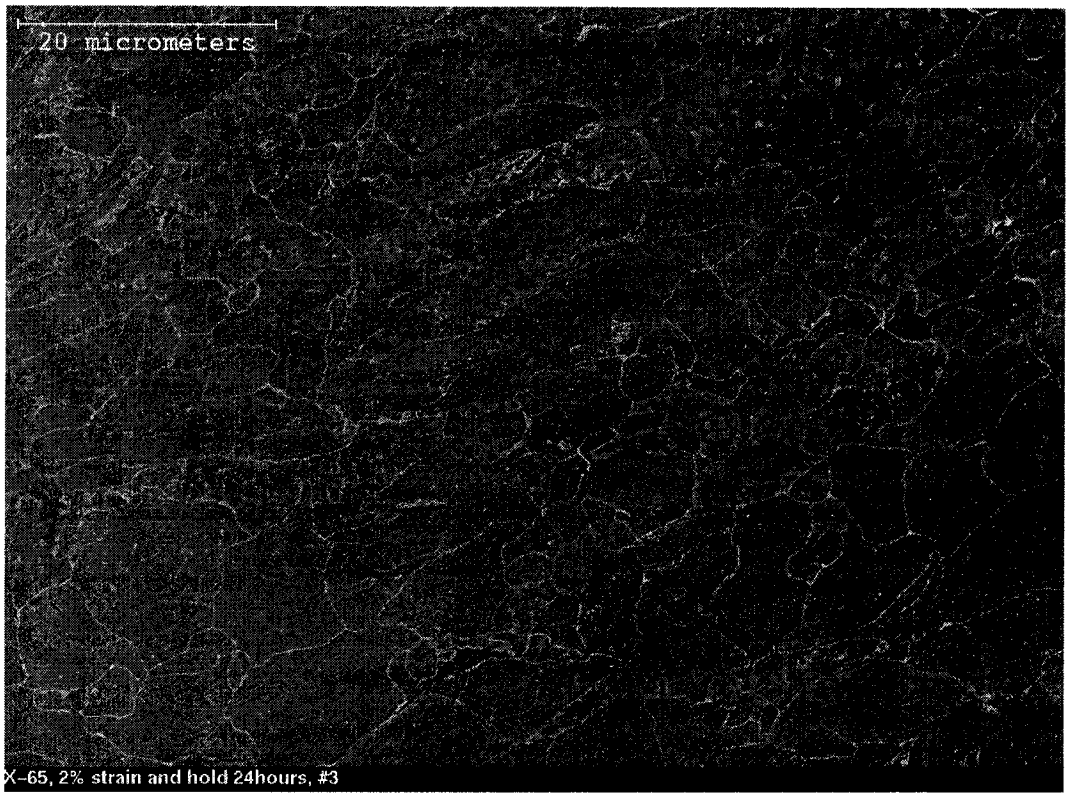

Figure 6 X65 2% strain and hold max load for 24hours then charged at 0.05mA/cm^2 for 23.5 hours

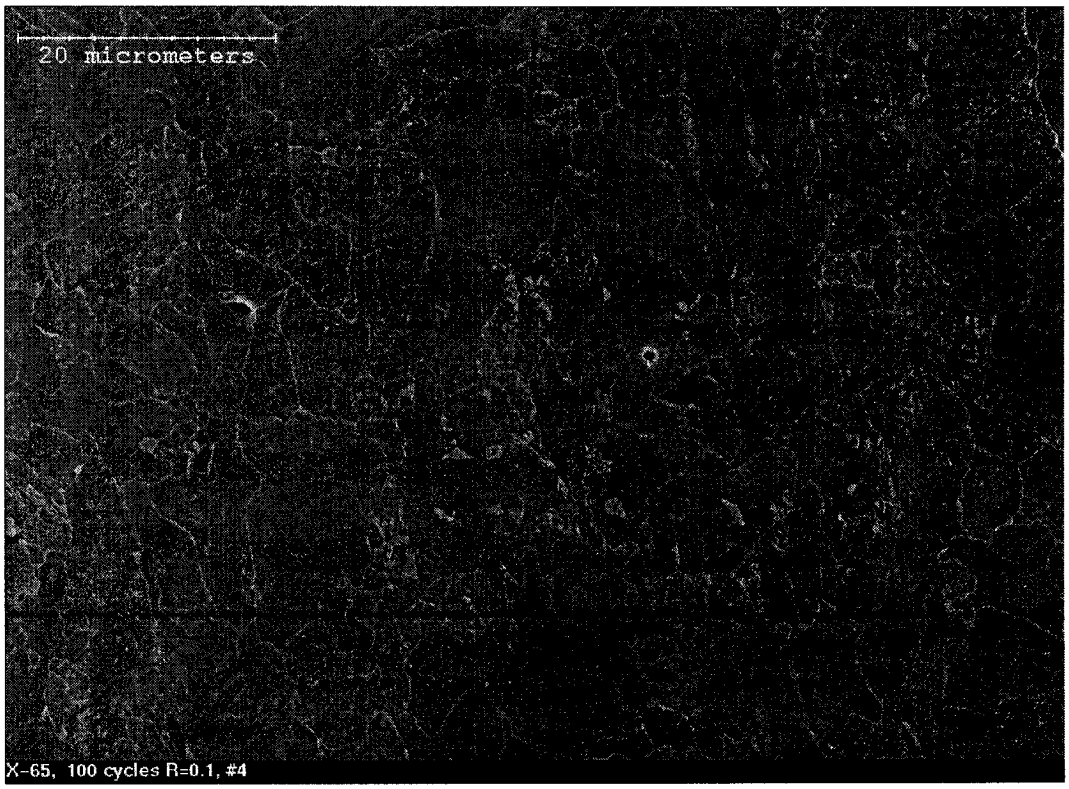

Figure 7 X65 2% strain, 100 cycles at R=0.1 then charged at 0.05mA/cm^2 for 23.5 hours

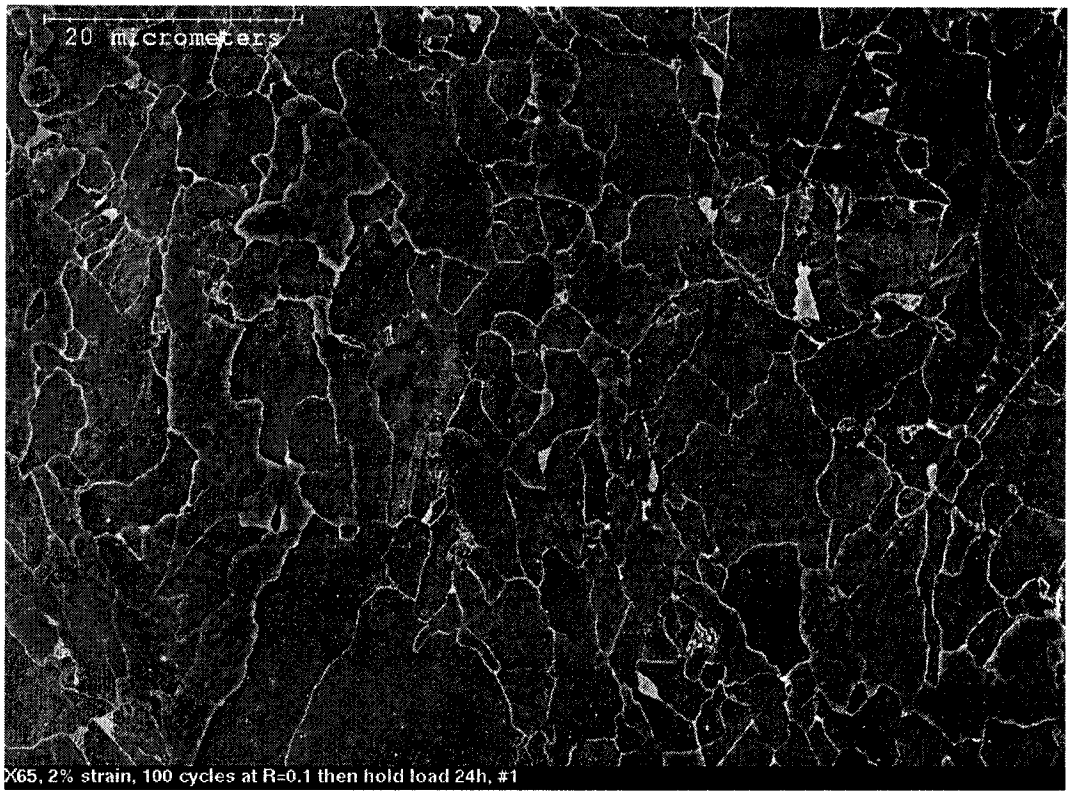

Figure 8 X65 2% strain, 100 cycles at R=0.1 and hold max load 24 hours then charged at 0.05mA/cm^2 for 23.5 hours

Figure 9 X65 90% YS 100 cycles at R=0.1 then charged at 0.05mA/cm^2 for 23.5 hours

Figure 10 X65 90%YS 100 cycles at R=0.1 and hold max load 24 hours then charged at 0.05mA/cm^2 for 23.5 hours

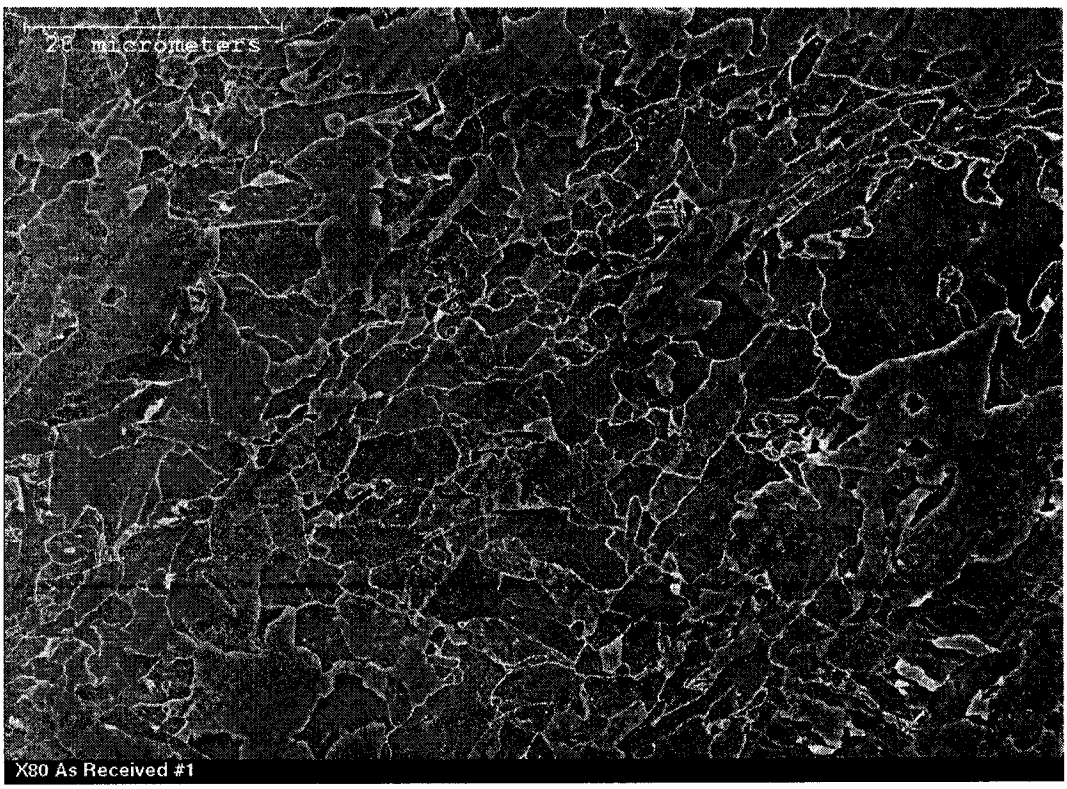

Figure 11 X80 as received

Figure 12 X80 no load charged at 0.05mA/cm^2 for 15 hours

Figure 13 X80 no load charged at 0.05mA/cm^2 for 40 hours

Figure 14 X80 no load charged at 0.05mA/cm^2 for 60 hours

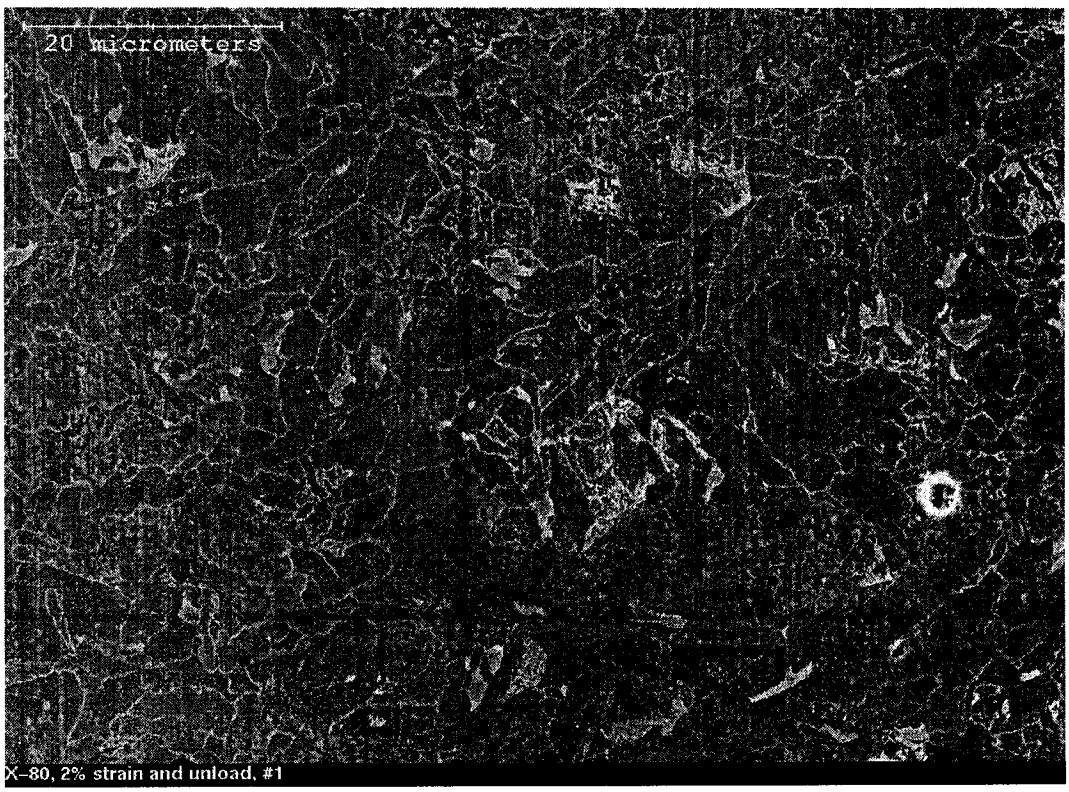

Figure 15 X80 2% strain and unload then charged at 0.05mA/cm^2 for 23.5 hours

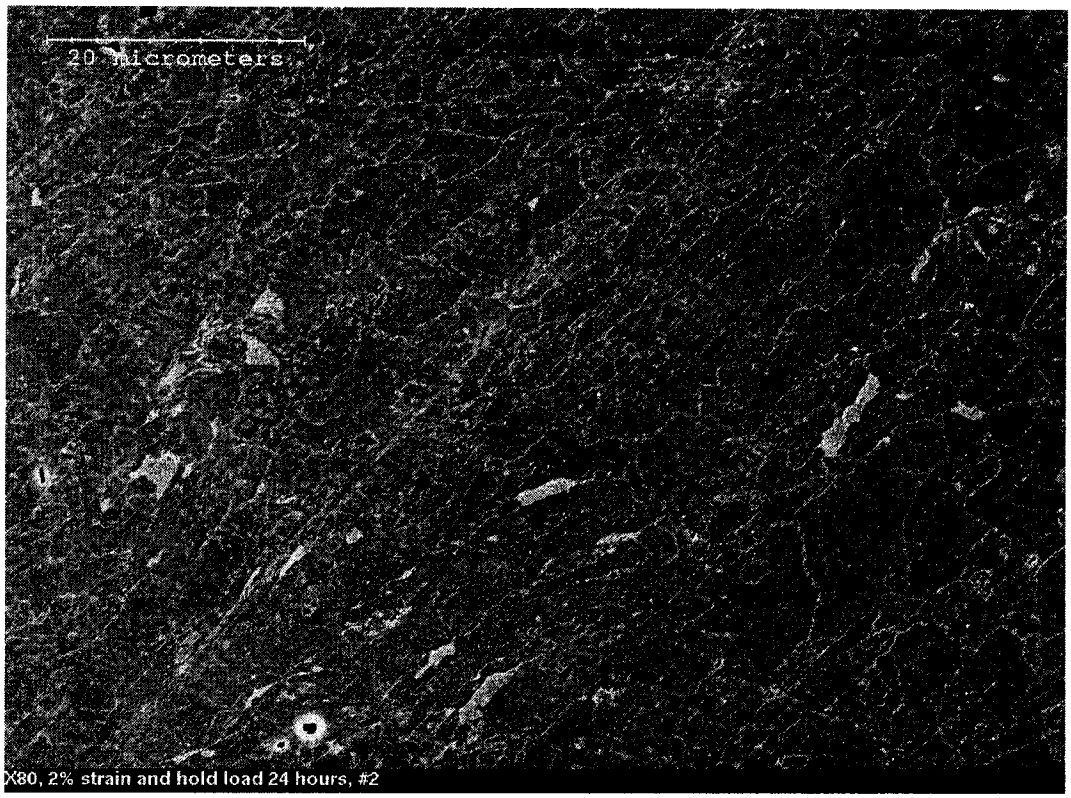

Figure 16 X80 2% strain and hold max load for 24 hours then charged at 0.05mA/cm^2 for 23.5 hours

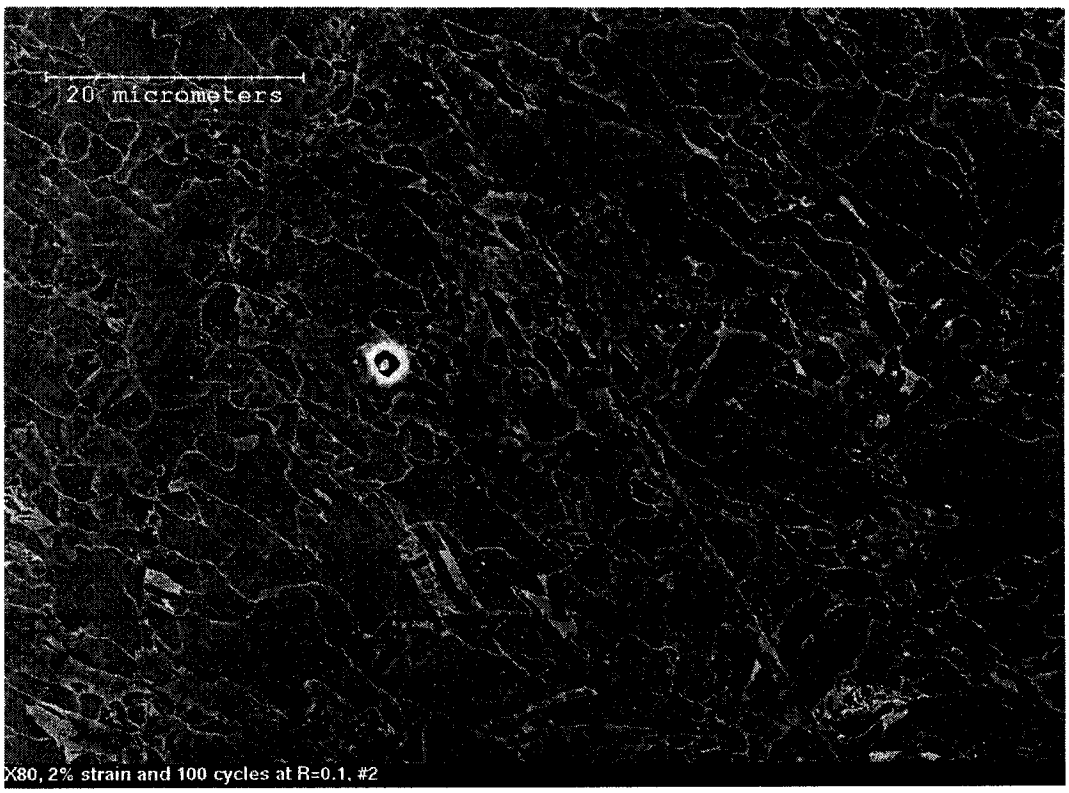

Figure 17 X80 2% strain, 100 cycles at R=0.1 then charged at 0.05mA/cm^2 for 23.5 hours

Figure 18 X80 2% strain, 100 cycles at R=0.1 and hold max load 24 hours then charged at 0.05mA/cm^2 for 23.5 hours

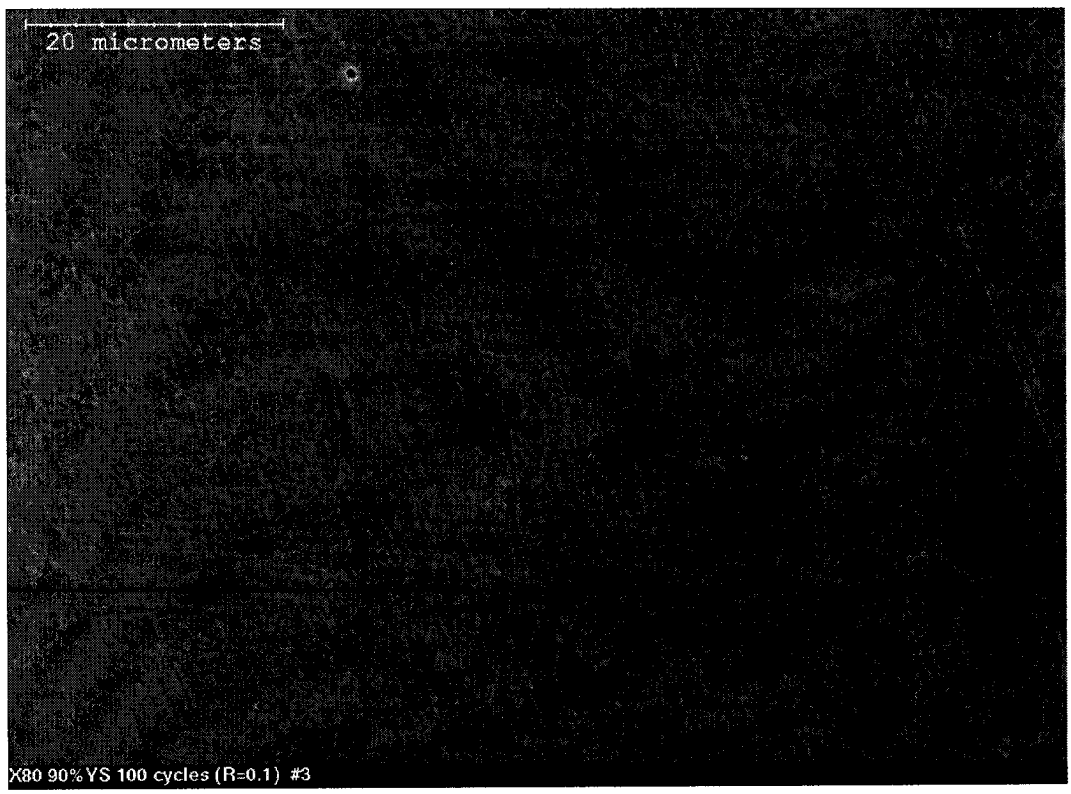

Figure 19 X80 90% YS 100 cycles at R=0.1 then charged at 0.05mA/cm^2 for 23.5 hours

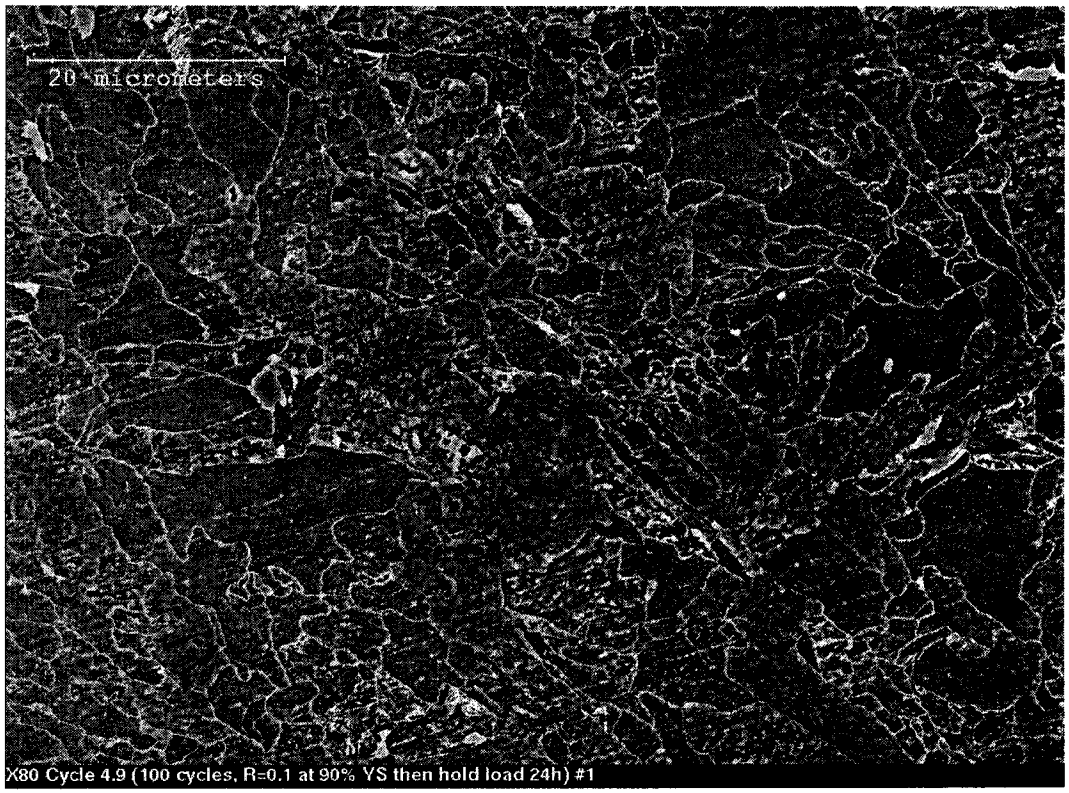

Figure 20 X80 90%YS 100 cycles at R=0.1 and hold max load 24 hours then charged at 0.05mA/cm^2 for 23.5 hours

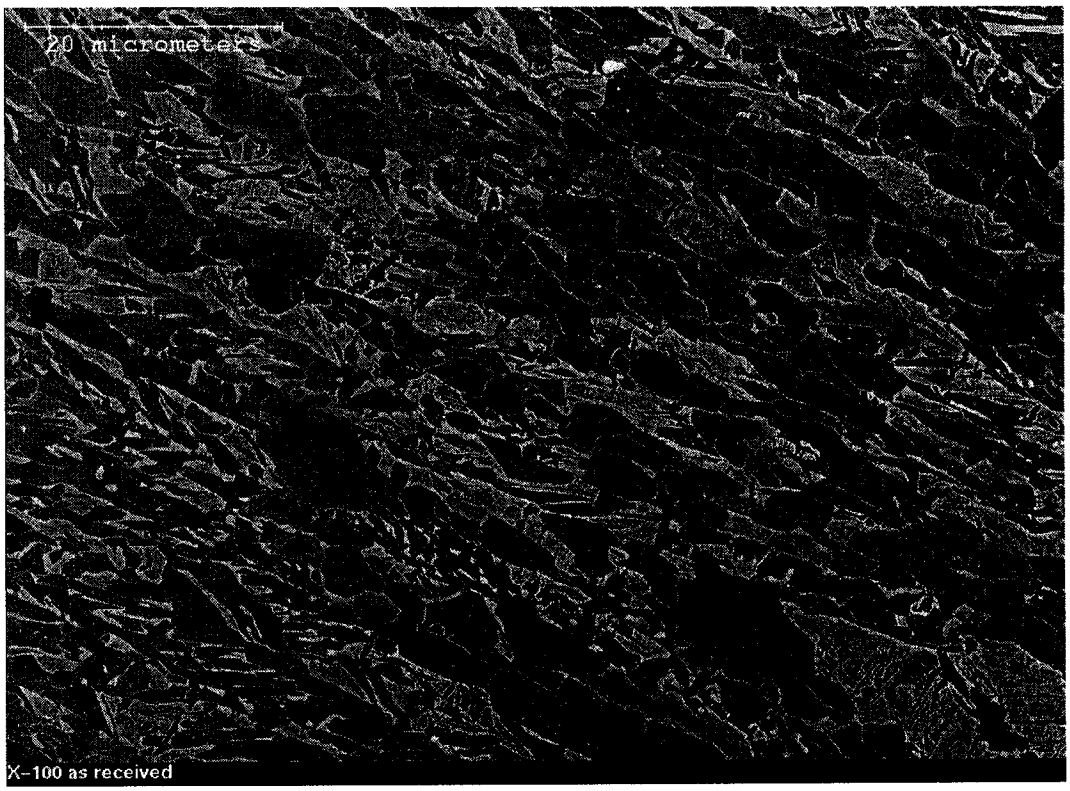

Figure 21 X100 as received

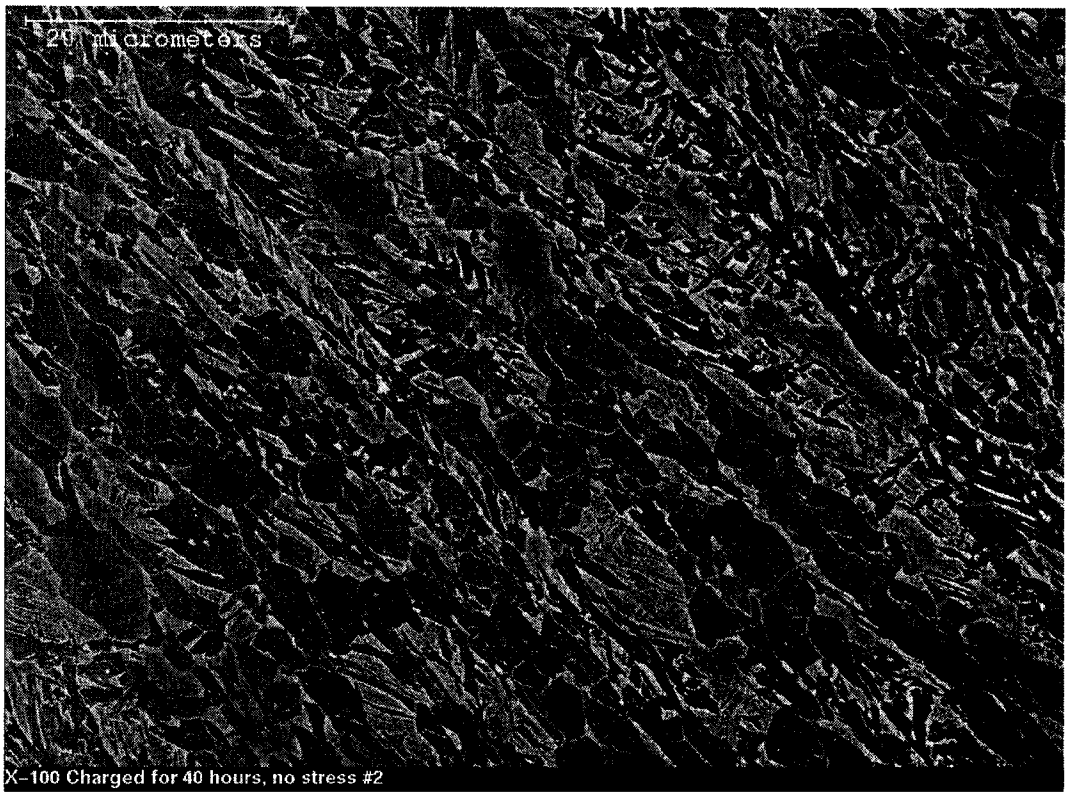

Figure 22 X100 no load, charged at 0.05mA/cm^2 for 40 hours

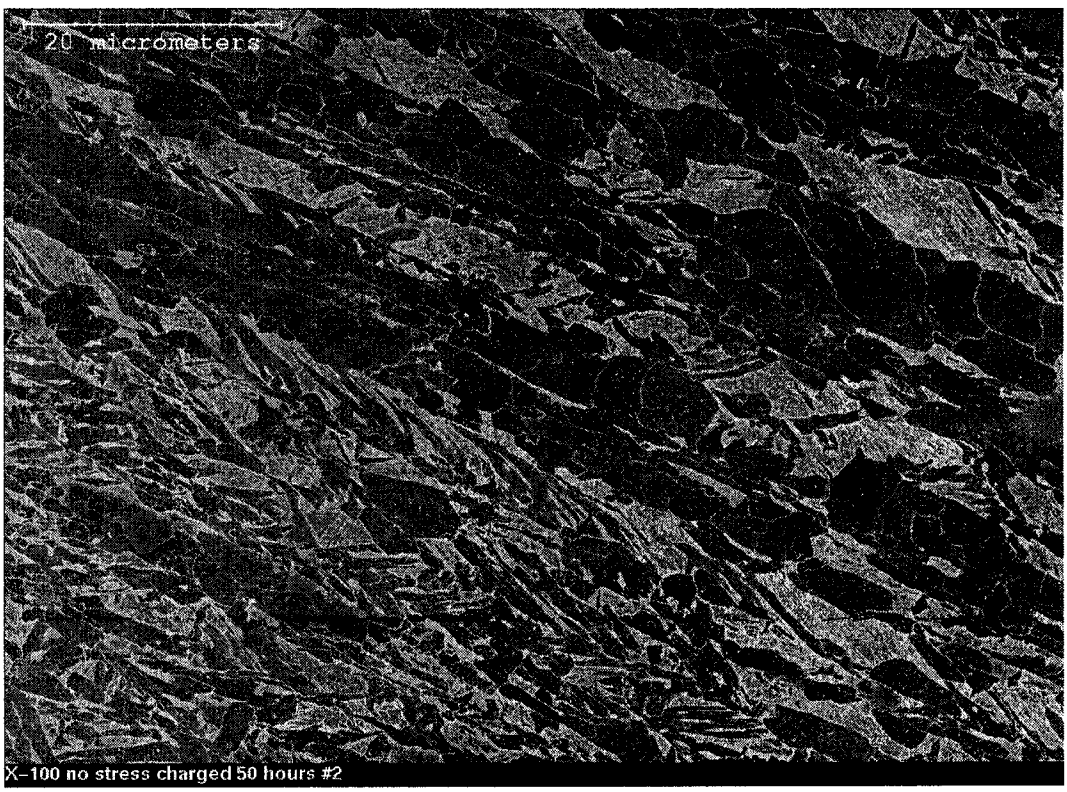

Figure 23 X100 no load, charged at 0.05mA/cm^2 for 50 hours

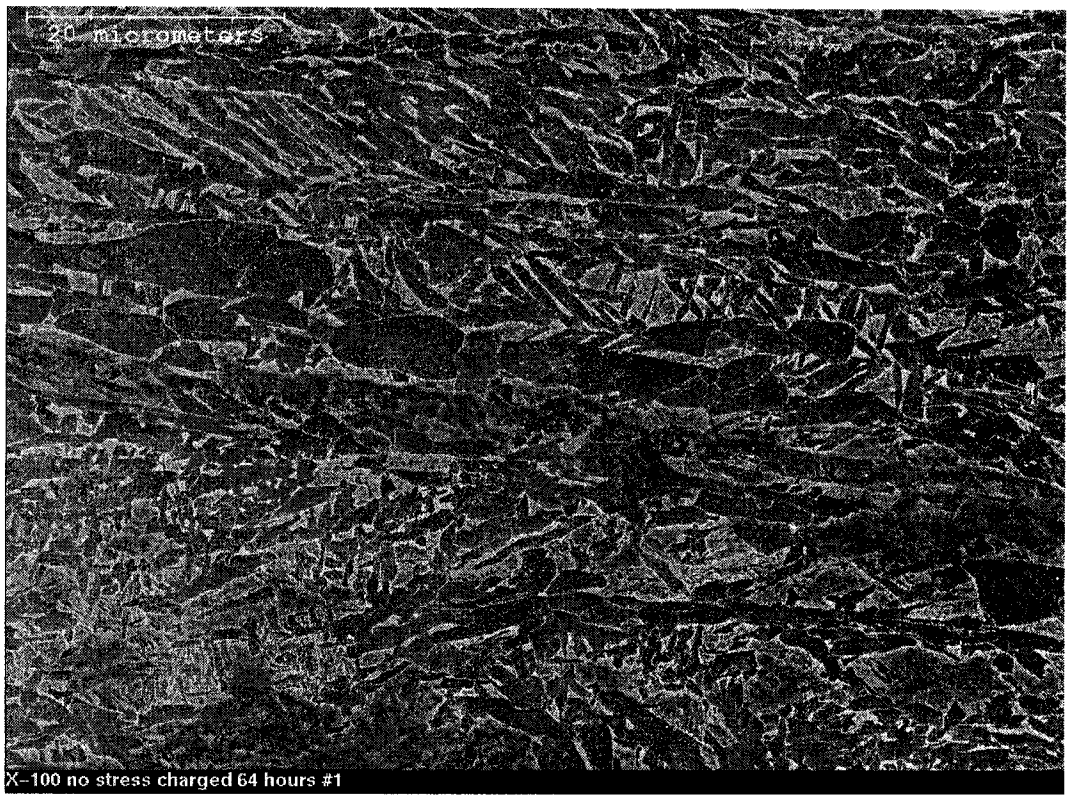

Figure 24 X100 no load, charged at 0.05mA/cm^2 for 64 hours

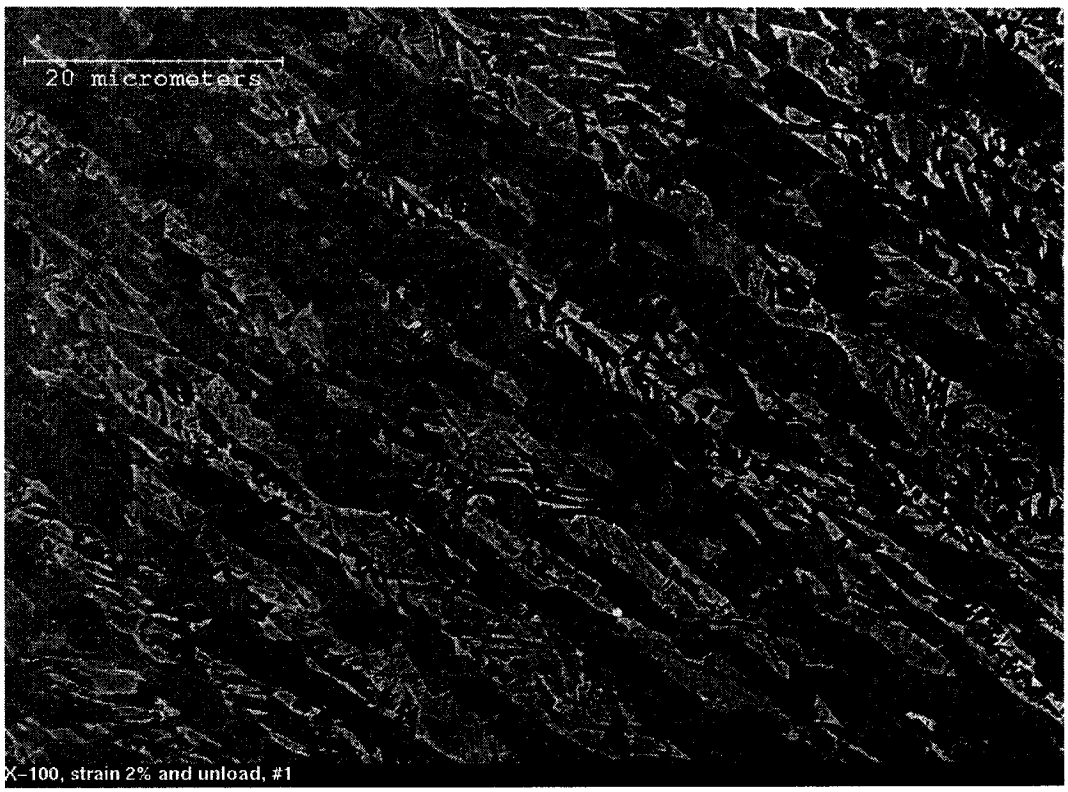

Figure 25 X100 2% strain and unload then charged at 0.05mA/cm^2 for 23.5 hours

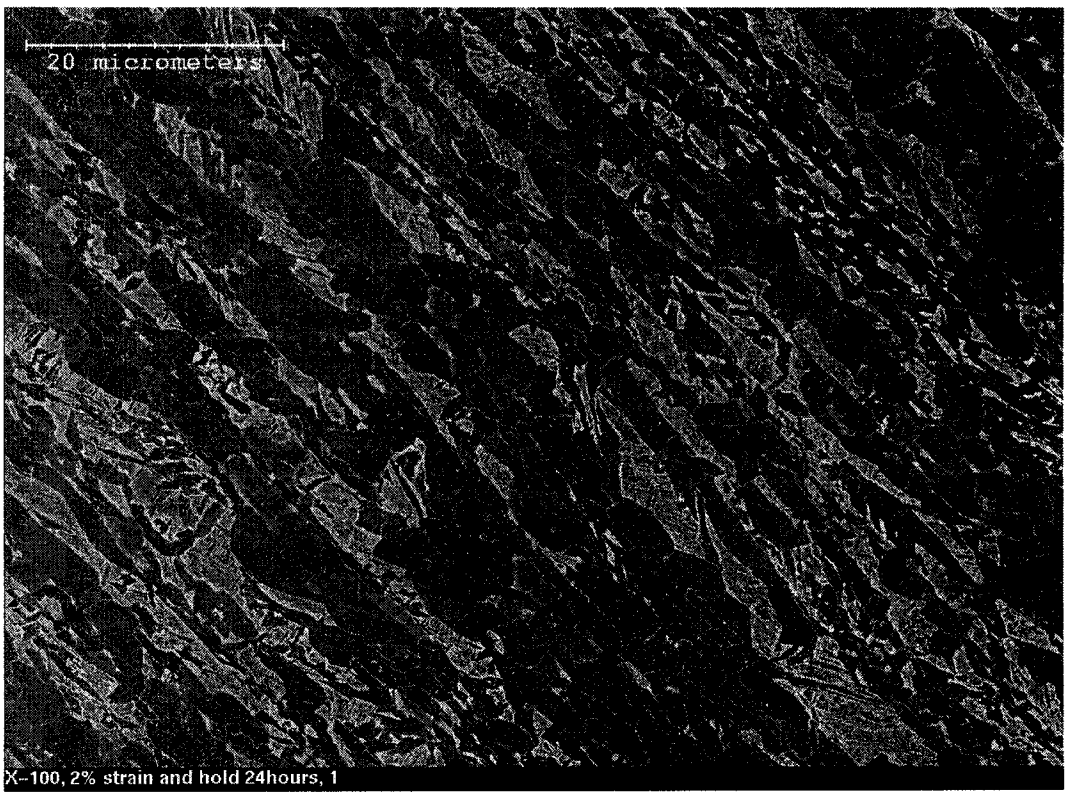

Figure 26 X100 2% strain and hold max load for 24 hours then charged at 0.05mA/cm^2 for 23.5 hours

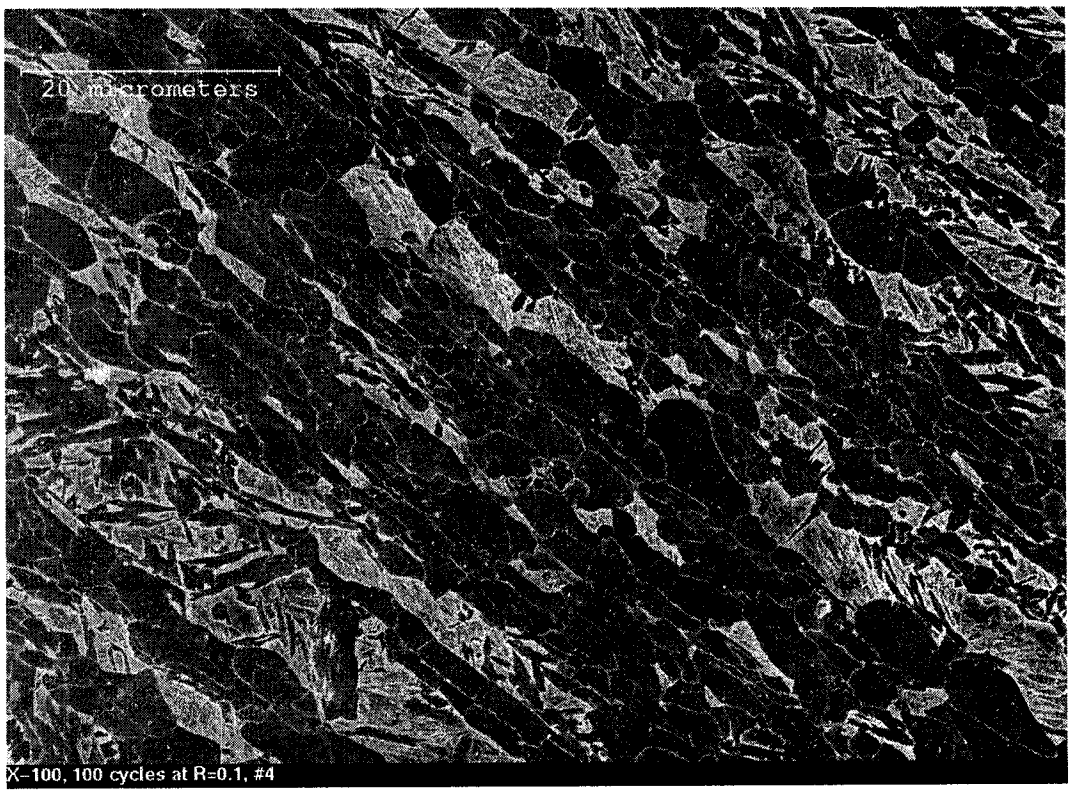

Figure 27 X100 2% strain, 100 cycles at R=0.1 then charged at 0.05mA/cm^2 for 23.5 hours

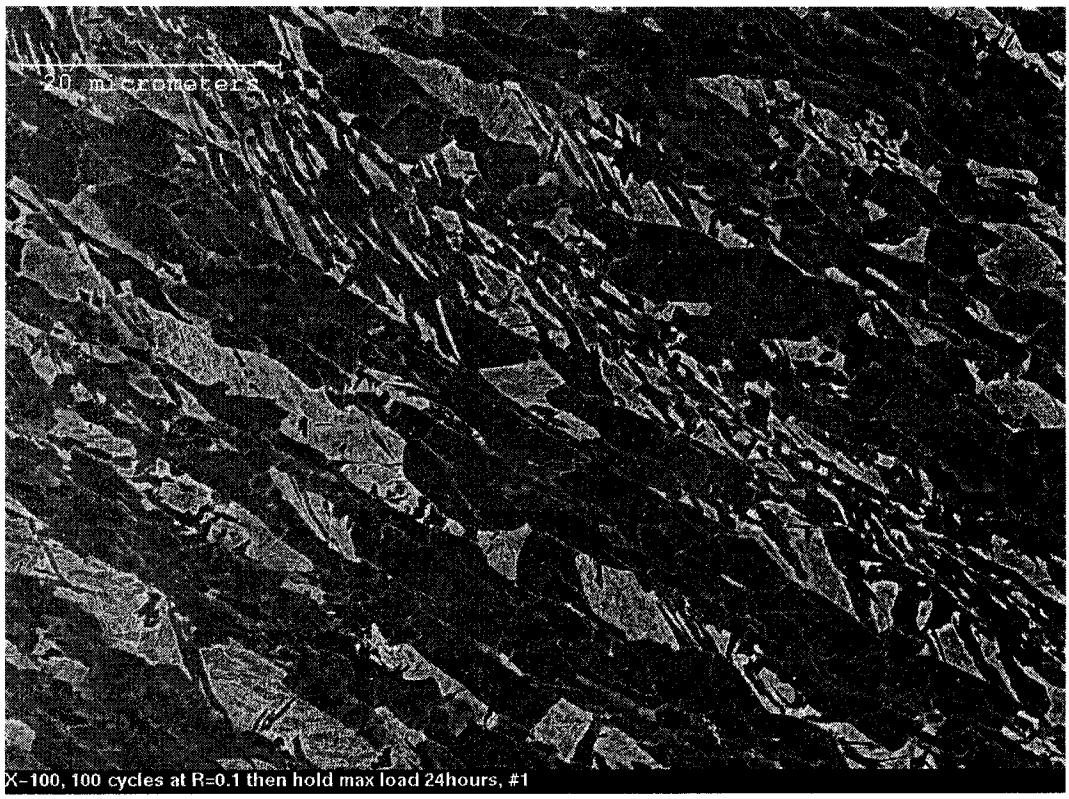

Figure 28 X100 2% strain, 100 cycles at R=0.1 and hold max load 24 hours then charged at 0.05mA/cm^2 for 23.5 hours

Figure 29 X100 90% YS 100 cycles at R=0.1 then charged at 0.05mA/cm^2 for 23.5 hours

Figure 30 X100 90%YS 100 cycles at R=0.1 and hold max load 24 hours then charged at 0.05mA/cm^2 for 23.5 hours

Figure 31 X100 fracture surface of tensile sample tested in air (low mag)

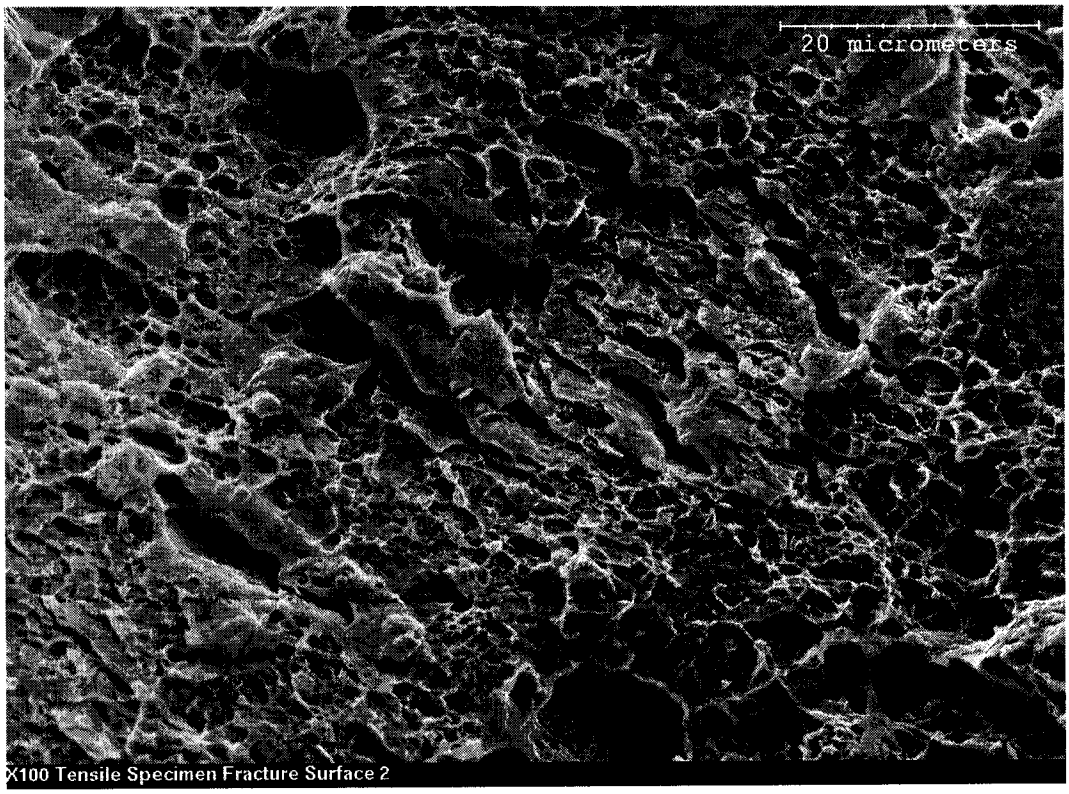

Figure 32 X100 fracture surface of tensile sample tested in air (high mag)

Figure 33 X100 fracture surface of tensile sample tested in air (low mag)

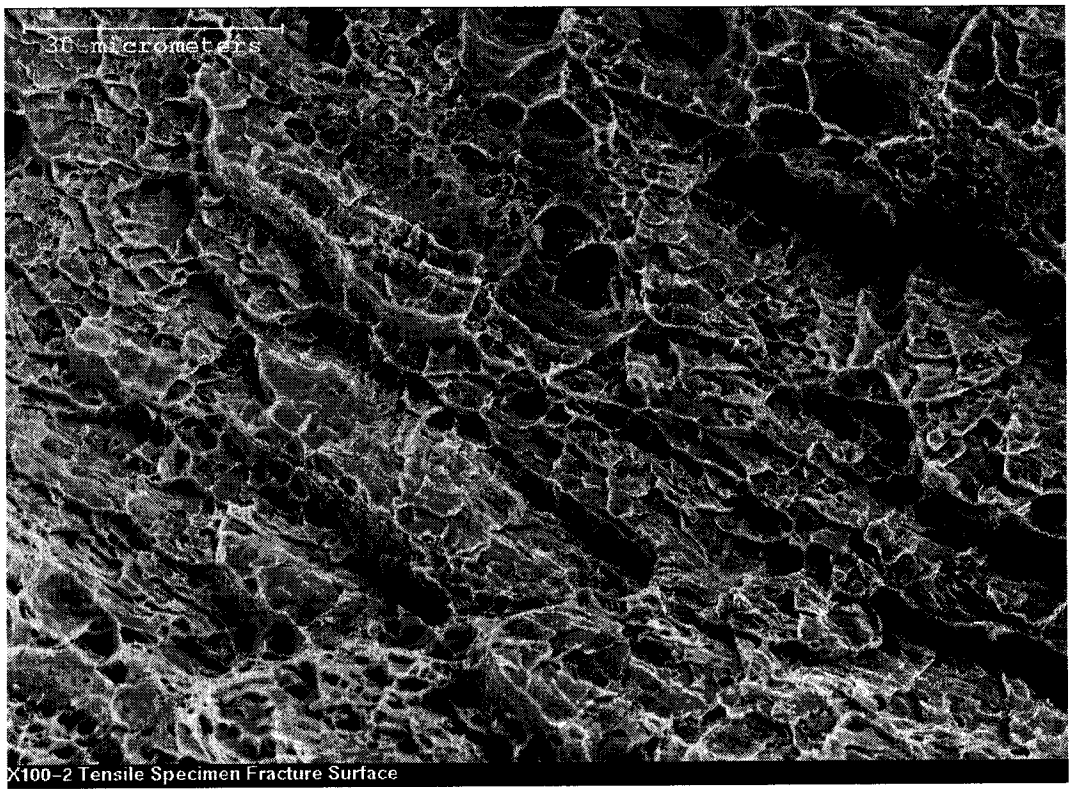

Figure 34 X100 fracture surface of tensile sample tested in air (high mag)

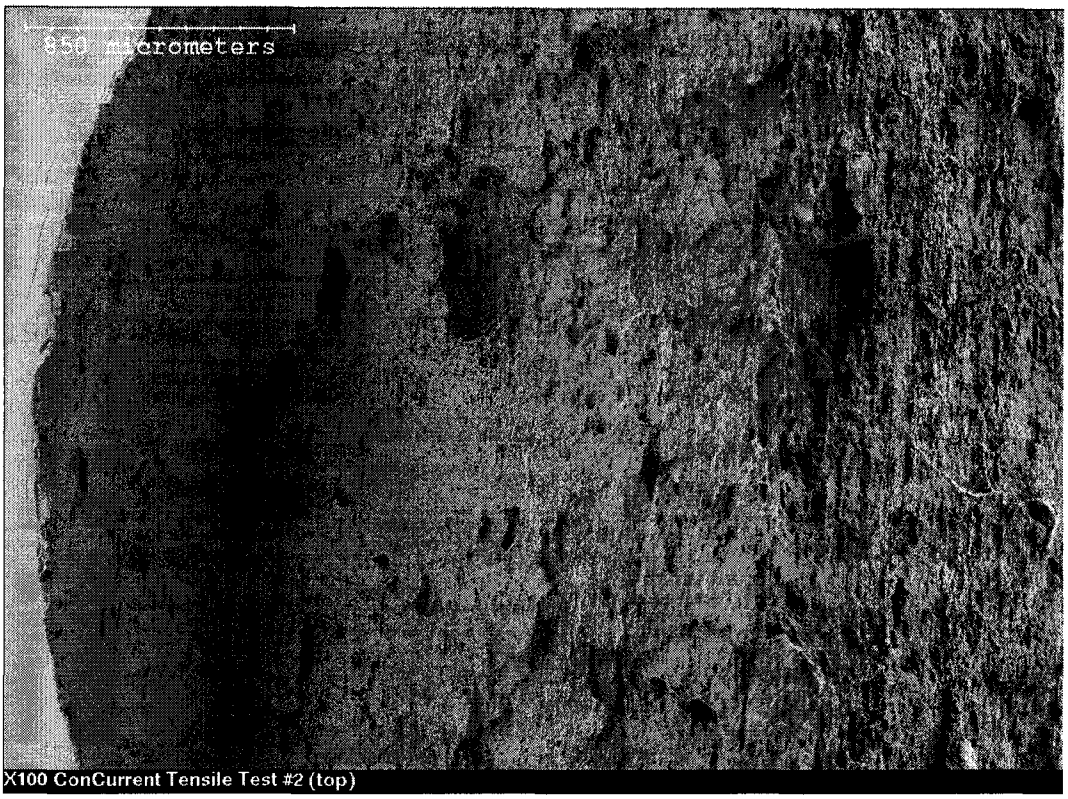

Figure 35 X100 fracture surface of tensile sample tested in solution (low mag)

Figure 36 X100 fracture surface of tensile surface tested in solution, cleavage (high mag)

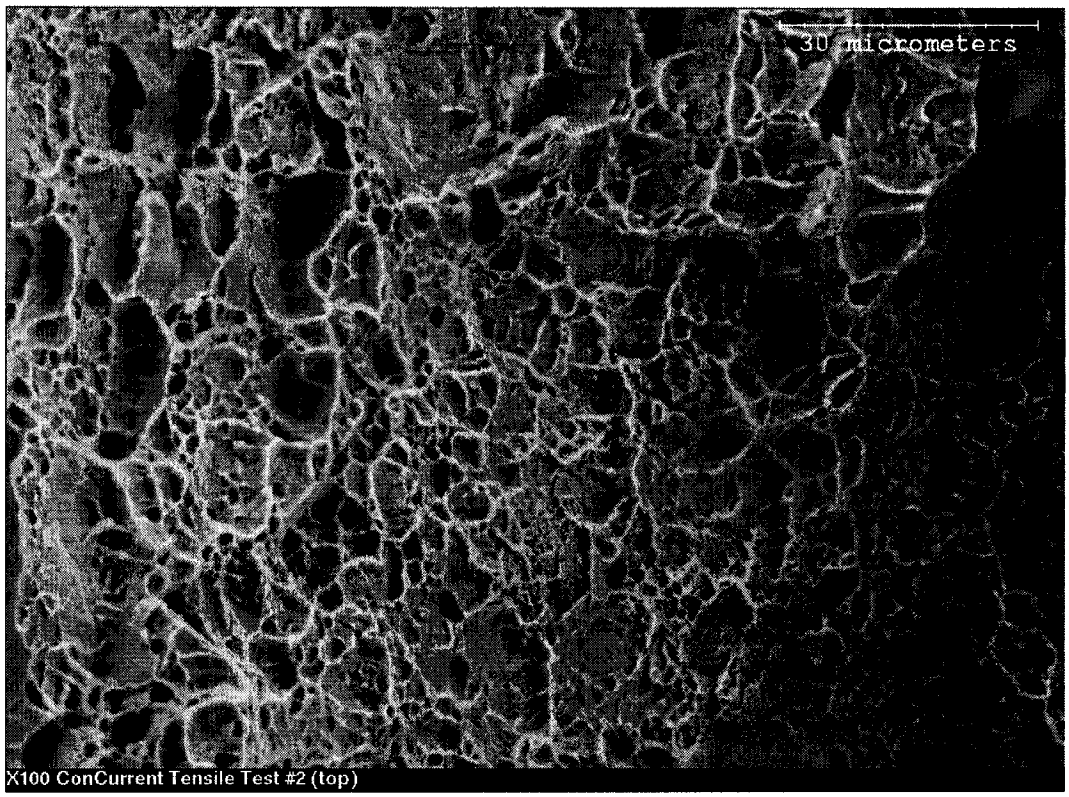

Figure 37 X100 fracture surface of tensile sample tested in solution, dimples (high mag)

Figure 38 X100 fracture surface of precharged 4th cycle (low mag)

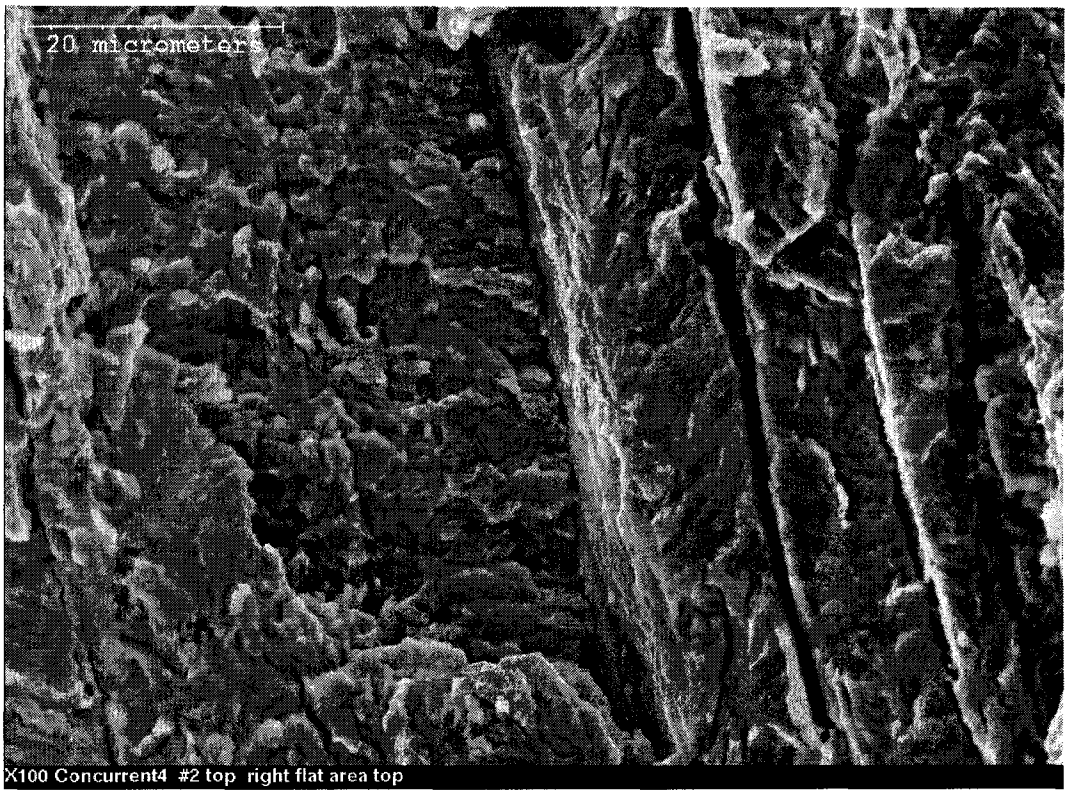

Figure 39 X100 fracture surface of precharged 4th cycle, cleavage (high mag)

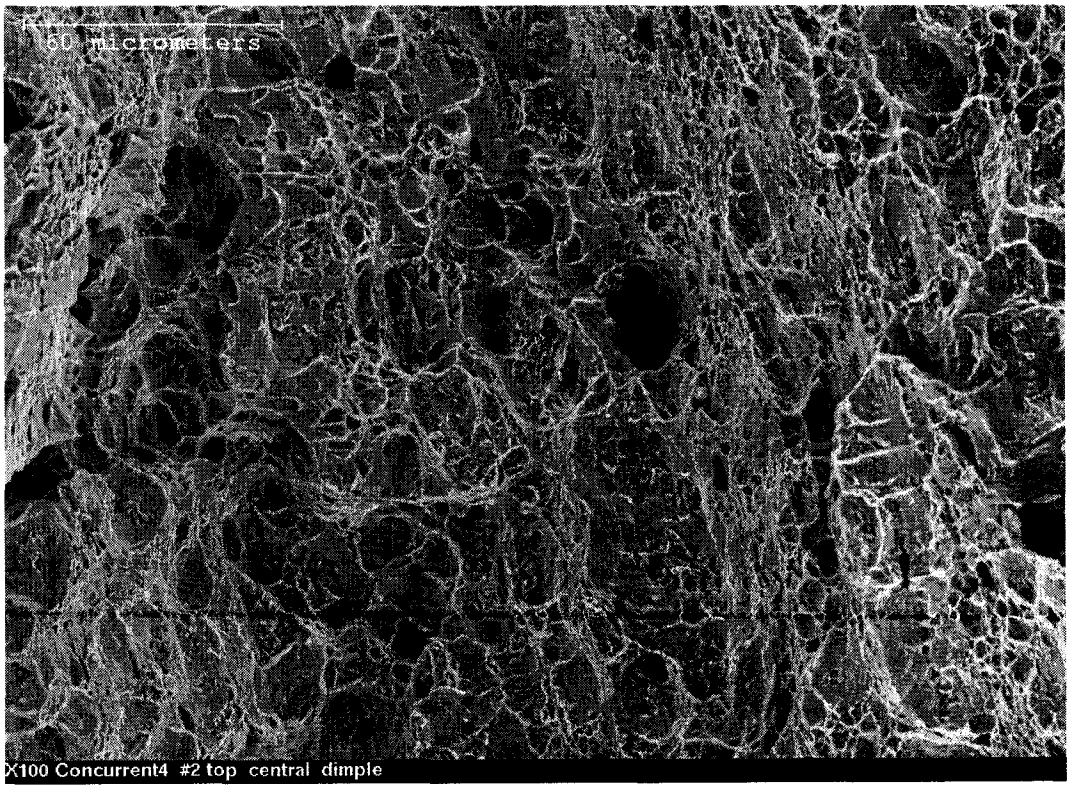

Figure 10 X100 fracture surface of precharged 4th cycle, dimples (high mag)

Figure 11 X100 fracture surface of precharged 4th cycle (low mag)

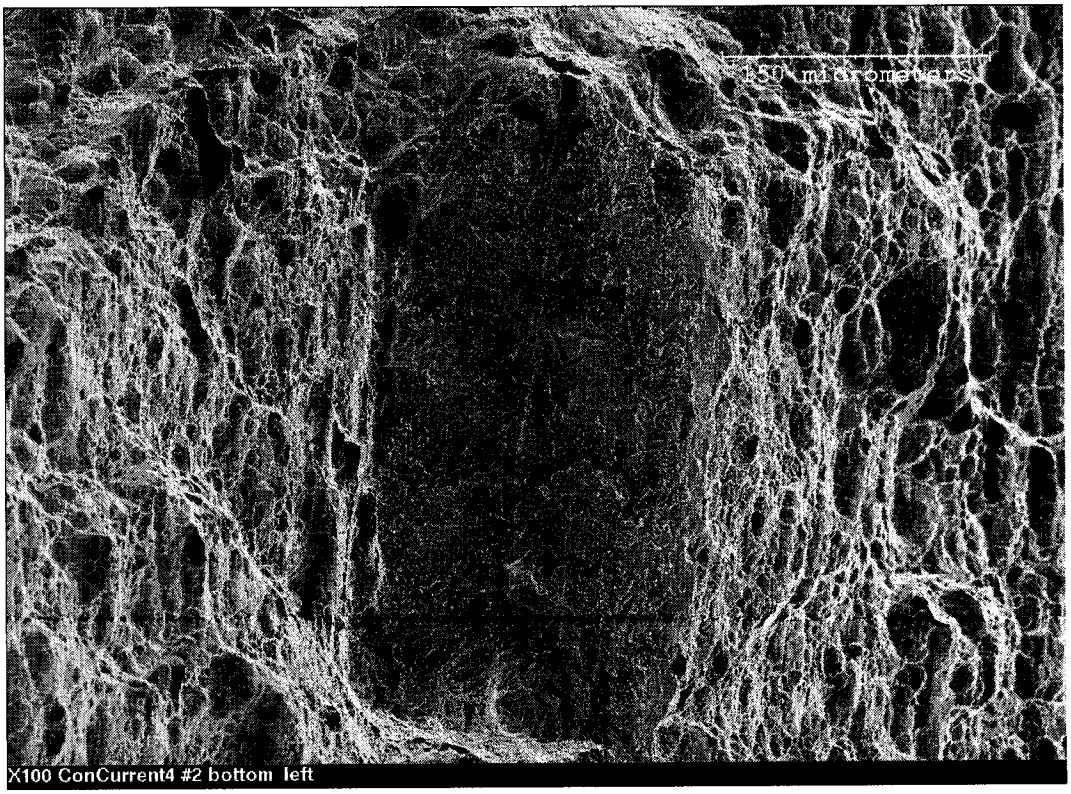

Figure 12 X100 fracture surface of precharged 4th cycle, cleavage and dimples (high mag)